Digital Image Processing Techniques in Static and Dynamic Clinical Radioisotope Studies

Nanette Maria Theresa Freedman

Ph.D. Thesis

Royal Postgraduate Medical School

CORRECTIONS

P.6 Second line from bottom should read "Initialization procedures"

P.16 10th line from bottom; symbol in equation should be *

P.20 Line 5; Insert) at end of line

Line 13; Substitute "is" for "if"

P.21 Line 1; Substitute "is" for "if"

P.24 Line 2; Substitute psf $(x - x^1, y - y^1)$ for psf $(x, y^1, y - y^1)$

P.41 Line 16; Insert "amplitude" before "modulation"

P.47 Second line from bottom; insert $|Q''(\underline{W})|$ at end of line

P.48 Line 3; Substitute "Graph IIIA" for "Graph IIA"

6 lines from bottom; delete paragraph "From Table ..... is varied."

P.49 Line 5; Insert } at end of line

P.52 Line 4; Insert F after Σ

P.59 Line 4; Substitute B(ix) for B(x)

P.68 Bottom line; Substitute "also" for "again"

P.70 Line 6; Substitute "incident on" for "present to charge"

P.72 Line 7; Insert at end of line "because it is not simply additive. It is"

Line 8; Delete "this"

Line 9; Substitute "therefore" for "obviously"

P.73 Line 13; "This choice of sampling interval also conforms to the criterion (ref. 7) that sampling distance must be less than 0.8 of the half width at half maximum of the system line spread function, since this half width is typically of the order of 1.5 cells here".

P.85 Line 4; Substitute "response to a periodic object" for "frequency response"

P.108 Lines 1-2; Delete "not statistically significant"

Line 3; Substitute "very apparent" for "significant"

P.119 Insert after line 21, "Results are only presented here for one patient, because the data for other patients was stored on magnetic tape and accidentally deleted during my absence, leaving only the qualitative scan images from these studies."

P.123 Line 16; Insert after "scans", "This basically requires an assumption of zero depth in the object which is being imaged."

P.158 Line 12; Insert at end of line, "Examination of the results in Tables VA-D reveals this consistently."

Nanette Maria Theresa Freedman

Digital Image Processing Techniques in Static and Dynamic Clinical Radioisotope Studies

Abstract

A review is given of the literature of image processing methods used on radioisotope scan images. The techniques used, their modes of application, and degree of success in improving images are outlined. The derivation of the Metz filter and its application are then discussed in detail, with particular emphasis of those problems relevant to the application of the filter to process images from the gamma-camera-computer system used for the work described in this thesis. An attempt is made to devise rules for the selection of the optimum order of Metz filter, using images of a Siemens' star phantom. Approximate criteria are obtained for choosing the optimum order of Metz filter for processing images according to the level of noise present in the images.

The Metz filter is applied to a study of changes in bone metastases and the resulting improvement in the visual quality of the images and the quantitative information obtained from them is discussed. Application of the Metz filter to a dynamic study of lung function in infants is then described. Here too the visual quality of the images is improved and the changes produced by Metz filtering on the quantitative information derived from the dynamic part of the study are discussed. Application of the criteria for selection of the optimum order of Metz filter to the images obtained in both these clinical studies is discussed, and the criterion is seen to be promising, though further work on its application is required.

Table of Contents

Table of Contents

Table of Contents

Table of Contents

Table of Contents

Table of Contents

List of Tables

List of Illustrations

List of Illustrations

List of Illustrations

CHAPTER I

Introduction and Review of the Literature

Abstract

The types of image degradation which occur in radioisotope scan images, the aims and limitations of the Metz filter and other comparable image processing methods are outlined. Some of these techniques for improving images both by smoothing to reduce noise and by resolution enhancement are described in brief. The Metz filter is seen to be one of several filters with similar theoretical justification; it is easier to use than many because its computation is relatively straightforward and it does not require subsequent use of a smoothing method. Assessment of processed images and methods suggested to overcome the difficulties which arise in this are also mentioned.

CHAPTER I

Intrcduction and Review of the Literature

A. Definitions and classification of image processing methods

(i) Aims of image processing

All the image processing methods considered here attempt to recover or reveal in the image, features of the object which may be obscured and lost as a result of the imaging process. One method of digital image processing, the Metz filter, will be described in detail in this thesis. It is interesting to see how this method differs in its aims, its practical applications and its achievements from other methods in use in the same field. This chapter contains a general review of several such methods. Only digital methods are discussed here (although some of these methods may also be applied by analogue means), and it is not intended to give an exhaustive list of all techniques used, but to describe how several basic principles have been applied to this problem. The methods considered are all limited in that they make no attempt to resolve the distortions arising from the fact that in general a three-dimensional object distribution is to be mapped onto a two-dimensional image.

Degradation of the image occurs at every stage in its formation; in the object and the medium between it and the collimator, in the collimator, the detector, the processing system and the display, though in a given practical situation, only the errors introduced at one or two stages may be significant. Image processing methods

may aim to correct for the failure of the recording of a finite number of discrete events to represent the continuous activity distribution of the object, for the geometric degradation by the imaging system, or for defects in the display system. The methods which will be described each correct for one or more of these forms of error; sometimes two or three methods may be applied consecutively to achieve a satisfactory final result. Defects in the display system and their significance will not be discussed.

(ii) Definitions

Particularly when comparing or combining several image processing methods, it is of interest to know something about the mathematical formulation and properties of the various techniques, and so the notation and definitions which are applied to the systems and methods discussed are given here.

The definitions and notation used to describe the object, image, imaging system and processing methods in this thesis are given in Table IA. The cartesian coordinates $(x,y) \equiv \underline{r}$ are used to describe the two dimensional representation of the object and the image, and the coordinates $(\omega_x,\omega_y) \equiv \underline{\omega}$ are used to describe the object and the image in the spatial frequency domain. All the functions are given in the spatial frequency domain as well as in the space domain, since transformations into the frequency domain are useful for the Metz filter and some of the other techniques described here.

A processing method is defined as being linear in the usual mathematical way[1]: if $f(x,y)$ is the unprocessed image, and $g(x,y)$

is the corresponding processed image, and if h(x,y), i(x,y) are, respectively, the unprocessed and processed forms of another image, then the processing method is linear if the processed version of (f + h) is equal to (g + i), for all images f and h.

A method is defined as being stationary if it applied in the same way, independently of the position in the image plane[2].

(iii) Image degradation - geometric factors

Any practical imaging system has a point spread function of finite width; consequently, each point in the object is represented in the image not just by a single point but by a blur extending into neighbouring points in a form described by the point spread function. Provided that certain assumptions (discussed in detail as they apply to the derivation of the Metz filter, in Chapter II) hold for the imaging system, this can be expressed mathematically as follows:

$$f(x,y) = \iint psf(x',y')\phi(x-x',y-y')dx'dy'$$

i.e. $$f(x,y) = psf(x,y) \ast \phi(x,y)$$

This equation describes the formation of the image from the object in the absence of noise. The integral equation can be solved in various ways; in general the point spread function and the image distribution are complicated and only an approximate solution may be obtained, g(x,y) say, which is an approximation to the required object distribution $\phi(x,y)$. The assumptions made in obtaining the approximate solution must be valid and suitable for the object, image and point spread function considered, both in view of the shapes of these distributions and with reference to the effects of

noise which are discussed in the next section. Several of the image processing techniques described here make use of various methods of approximation to find a solution for this equation and so correct for geometric degradation.

(iv) Degradation due to noise and statistical fluctuations

This degradation occurs as a result of the nature of the radio-active decay process, which can only be described in terms of the probability of decay, and because of further statistical factors inherent in processes of detecting and registering its position. In such a situation the more counts which are recorded the less significant the noise becomes in relation to the overall number of counts[3], so that the degradation resulting from this effect will be most serious when the image count density is low.

However though the degree of degradation due to noise depends on the counts recorded, at any particular count density, when the statistical fluctuations in an image are analyzed in the frequency domain, the noise level is fairly constant though it rises slightly at high frequencies[4]. As mentioned in Section A(ii) above, the point spread function of any real imaging system has a finite width, resulting in blurring of small features in the image. Thus the modulation transfer function gradually decreases at high spatial frequencies; in fact it decreases to zero above a certain frequency, since the collimator has zero response above this frequency. Consequently the signal-to-noise ratio decreases with the modulation transfer function, finally decreasing to zero at high frequencies, so that features of the image which may appear as fine detail may

be mostly due to noise and may therefore be completely spurious in relation to the "true" image. "Smoothing" methods of image processing eliminate this high frequency noise.

The noise and statistical fluctuation interact with the geometric degradation inherent in the formation of the image, and effect the corrections which may be made for it. Both the image and the point spread function are recorded in the presence of random statistical noise. The point spread function may be recorded with many counts so that the effects of noise are not significant, but the number of counts in a clinical image may be limited, for example, by the dose of radioactivity which may safely be administered to the patient, and the length of time the patient can reasonably remain in front of the scanning device. Consequently the noise in the image may be very significant. In this case the recorded image distribution is effectively only an estimate of the "true" image which would be obtained in the absence of noise (e.g. by recording for an infinitely long period of time). As described above, the image will approximate more closely to the "true" image distribution in the lower part of the spatial frequency spectrum than at higher frequencies, and the severity of the effects of noise will depend on the number of counts recorded. The recovery of a good estimate of the object distribution from a noisy image distribution is naturally complicated by the presence of the noise, and methods for correcting geometric degradation must all take this into account.

B. Smoothing Procedures

(i) Fixed Spatial Averaging

As mentioned above, the principle of smoothing methods is to remove

from the image those high spatial frequencies for which the collimator has no response, since these must be due only to noise and their presence in the image may obscure genuine image features. When considering the problem of smoothing out noise, it is necessary to decide where in the frequency spectrum useful information ends and noise begins, and so how much one should smooth. One possible criterion is merely to choose to eliminate all frequencies for which the collimator has no response and retain the lower frequencies in full[5]. Another method is to choose a smoothing function adapted to the shape and extent of the measured point spread function[5]. However most workers have chosen arbitrary smoothing functions which are often of similar form to the point spread function but are selected primarily for their simple formulation.

In images with low count densities, the signal-to-noise ratio may decrease rapidly at relatively low frequencies because the noise due to the quantum statistics of the source can give rise to large fluctuations. Consequently it is sometimes desirable to use a smoothing function that is much wider than the point spread function when overall improvement in visualization is more important than loss of some small detail.

Many smoothing methods can be applied very simply by selecting a sampling area centred on a given spot and replacing the counts at that spot by a weighted average (depending on the smoothing function) of the counts at all the spots within the sampling area; this is then repeated for all spots in the image. Smoothing functions can be constructed from the point spread function of the individual system.

However the following simple functions are frequently used[5].

5 point smoothing - The processed image g(x,y) is obtained from the unprocessed image f(x,y) by:

$$g(x,y) = 1/6\{f(x,y-\varepsilon) + f(x-\varepsilon,y) + 2f(x,y) + f(x+\varepsilon,y) + f(x,y+\varepsilon)\}$$

where ε is the sample size in both x and y directions. (see Fig. IA). The equivalent operator in the frequency domain $Q(\underline{\omega}) = G(\underline{\omega})/F(\underline{\omega})$ can be calculated simply:

$$Q(\omega_x,\omega_y) = 1/3\{\cos 2\pi\omega_x\varepsilon + \cos 2\pi\omega_y\varepsilon + 1\}$$

Values of this operator are tabulated in Table IB below, and it can be seen that it decreases rapidly at high frequencies.

9 point, 13 point, 25 point etc. schemes can also be used, and examples of these are shown in Table IB and Fig. IA.

In practice 5 or 9 point smoothing if generally sufficient to remove most statistical variation, and smoothing over larger areas may obscure important structures[5]. The table below (Table IB) shows, as expected, that averaging over larger areas is equivalent to substantially reducing lower spatial frequency components of the image as well as high frequency ones; this is only desirable if the image has so much statistical variation that the signal-to-noise ratio is low at these lower frequencies. Whichever smoothing function is used, the method is linear and stationary.

Many authors report that they remove improbable values before smoothing, to avoid introducing local distortions as a result of unlikely values[5]. This process may be carried out by comparing each element to the mean of the eight surrounding ones and rejecting the element if it does not fall within one standard deviation of the

mean. If it is too low, the rejected element if replaced by the (mean-s.d.), or if too high, by the (mean+s.d.).

(ii) Variable spatial averaging

When performing fixed spatial averaging noise may sometimes only be eliminated at the expense of loss of image detail. This detail may not be significant in regions where there is much noise, but there may be parts of an image where the count density and therefore the signal-to-noise ratio are high so that the small detail contains useful information. The information in these regions may be lost if the same smoothing procedures are used throughout the image thus losing the useful as well as the spurious small structures. In fact Pizer and Vetter have shown formally[6] that the greater the density of the surrounding population of counts, the smaller the area needed to obtain a good estimate of density.

On the basis of this, a non-stationary method of variable spatial averaging was developed in which the sampling area decreases as the local count density increases. In practice this is done by choosing a sampling area centred on the point of interest such that the number of counts in this sampling area is some selected value N - thus a sampling area of large radius will be required if the count density is low. The number of counts to be reached, N, is chosen by a combination of theory and experiment to give the best compromise between statistical accuracy and geometrical blurring. If N is suitably chosen, Pizer and Vetter found that, as expected, variable spatial averaging will give better results than fixed spatial averaging.

(iii) "Adaptive" smoothing

The problem of smoothing to eliminate noise may be approached

from another point of view, by investigating the behaviour of noise within the image. Brown et al.[7] have done this by Fourier transforming the image into the spatial frequency domain and then estimating its average random noise level. This was done by averaging the coefficients of the Fourier transformed image for all spatial frequencies above the intrinsic resolution of the collimator, since the contributions to these frequencies must be due only to noise. The average random noise level obtained in this way is assumed to be a good estimate of the noise level throughout the frequency spectrum, and so spatial frequency components which are within the resolution of the collimator but which are only present in the image spectrum at a level as low as the noise level are expected to have little statistical significance. The smoothing procedure is therefore carried out by testing all the transform coefficients against the average random noise level; the coefficients are set to zero if they are less than this value, and retained if they are higher. If greater statistical significance is desired in spite of the consequent lack of resolution, a higher factored value of the average noise level may be used instead as a standard for comparison.

This method is equivalent to using a smoothing function in the spatial domain, but the function may be very irregular and non-circular in shape, because of the way it is constructed. This method of smoothing involves Fourier transforms, and so may take considerably more computer time than the simpler methods described above. However smoothing is often used in combination with other processing methods where Fourier transforms are required anyway, and then there is no disadvantage in using a method such as this which is applied to the spatial frequency domain. (Brown et al. used this method in combination with a filtering technique in the frequency domain.)

C. Methods for Improvement of Geometric Degradation

(i) Simple uses of the modulation transfer function

The philosophy behind this method and all the others in this section is in part exactly opposite to that behind the smoothing methods. The modulation transfer function decreases with increasing frequency and consequently the higher frequency features of the object are poorly transferred to the image. The high frequencies in the image therefore have low signal-to-noise ratios and are not accurately defined; by smoothing procedures these uncertain contributions to the image are eliminated, or at least decreased. In most smoothing methods frequency components are gradually decreased more and more, low frequency components being only slightly diminished while higher frequencies may be eliminated completely.

However, it may be argued that for "reasonable" count densities, although the modulation transfer function and so the signal-to-noise ratio begins to decrease at relatively low frequencies, this decrease is not sufficient to prevent object features from being transferred to the image with acceptable accuracy, and it is only at the very high frequency end of the spectrum that noise really predominates. In a situation where this is so, smoothing procedures needlessly alter the relationship between the amplitudes of the contributions to the image from the various frequency components, thus distorting the image. In fact the imaging process itself distorts this relationship; this is the geometrical degradation described by the modulation transfer function. The methods described here all seek to reduce this geometric degradation inherent in the imaging process.

As mentioned in Section IA(ii), in the absence of noise, this

distortion can be described mathematically by the following equation:

$$f(x,y) = \iint psf(x-x',y-y')\phi(x',y')dx'dy' \qquad \text{I}$$

or in other words f(x,y) is the convolution of the object distribution, $\phi(x,y)$, with the point spread function. One method of performing this deconvolution is by transforming the equation into the spatial frequency domain:

$$F(\omega_x,\omega_y) = M(\omega_x,\omega_y)\Phi(\omega_x,\omega_y) \qquad \text{II}$$

According to this, a corrected image can be obtained from the initial image, if the modulation transfer function is known:

$$\phi(x,y) = \text{F.T.}^{-1}\{\Phi(\omega_x,\omega_y)\} = \text{F.T.}^{-1}\{F(\omega_x,\omega_y)/M(\omega_x,\omega_y)\} \qquad \text{III}$$

This expression can be evaluated provided that $M(\omega_x,\omega_y)$ is never zero.

However there are drawbacks in this simple method of attempting resolution recovery. Clearly noise does predominate over the signal at high frequencies, and even if $M(\underline{\omega})$ does not become zero at high frequencies, it will always decrease to small values. Consequently division by $M(\underline{\omega})$ at high frequencies will give rise to amplification of noise, and this will subsequently have to be smoothed out if the resulting image is not to be totally obscured by noise. However if this is done, the smoothing may once again distort the low end of the frequency spectrum as well as eliminating high frequency noise.

One problem which occurs when using this procedure, as well as some of the other methods described in this chapter, is that it may be very difficult in practice to determine the modulation transfer function of an imaging system accurately, particularly for higher frequencies. Use of an incorrect modulation transfer function can

obviously lead to distortions; in particular if the modulation transfer function is not smooth. this can lead to the production of artifacts. Because of this, some workers resorted to using instead of the modulation transfer function a so-called equivalent Gaussian function, generally with the same full-width at half maximum as the measured modulation transfer function. Others have used a narrower function instead of the modulation transfer function since improved results have been observed if the filter rises more sharply than the inverse of the modulation transfer function at low frequencies.

Since convolution is a linear operation, this is a linear method of image processing, and provided that the same modulation transfer function is used all over the image, it is also a stationary one.

(ii) Metz filter

To avoid the problems involved in dividing the Fourier transform of the image by the modulation transfer function and then smoothing to eliminate high frequency components, several authors[7,4] have invented functions which approximate to $1/M(\underline{\omega})$ at low frequencies but do not amplify the high frequency part of the spectrum as $1/M(\underline{\omega})$ does. The Metz filter[8] is such a function; it will only be described briefly here since it is described in great detail in the next chapter. It is given by:

$$Q^n(\underline{\omega}) = \{1 - [\, 1-|M(\underline{\omega})|^2 \,]^{n+1}\}/M(\underline{\omega})$$

or it can be expressed by an equivalent function in the space domain.

This function approximates to $1/M(\underline{\omega})$ for $|M(\underline{\omega})| \to 1$, which holds true at low frequencies, but it decreases to zero for $|M(\underline{\omega})| \to 0$, at high frequencies so that it is not necessary to use

an additional smoothing procedure as well as the Metz filter. Also for $n \to \infty$, since $|M(\underline{\omega})| < 1$ always, $Q^n(\underline{\omega}) \to 1/M(\underline{\omega})$, and by plotting out $Q^n(\underline{\omega})$ for some $M(\underline{\omega})$ obtained in practice, it can be seen that by increasing n, one can raise the frequency to which $Q^n(\underline{\omega})$ continues to approximate to $1/M(\underline{\omega})$ before decreasing.

This approximation converges if and only if $|M(\underline{\omega})| < \sqrt{2}$; it does converge for negative $M(\underline{\omega})$. Once again this is a linear stationary method, although it can be applied in a non-stationary manner by varying the function used for $M(\underline{\omega})$ or the order of the processor over the image plane.

The flexibility achieved by changing n, the order of the filter, is very useful when dealing with images with differing noise levels. More resolution enhancement is obtained the higher the order of filter used, but to avoid producing artifacts due to amplification of noise, processors with high values of n should only be used when the image is relatively free from noise, whereas lower orders of the filter may be used on very noisy images. Thus if suitable values of n can be chosen, images with differing levels of noise can be processed without producing artifacts, though more resolution enhancement will be achieved in the less noisy images for which higher order filters may be used.

However the choice of the optimal order of filter for processing a given image is not an easy one. The selection is generally made visually by an observer who looks at several images processed with different orders of the filter and selects the "best". This procedure is time-consuming and subjective and only particularly appropriate when the images are processed to enhance their visual quality rather than the quantitative accuracy with which they represent the object

distribution. As a result, although the method is very flexible, the absence of rules for utilizing this flexibility when processing images limits it use at present. In Chapter III attempts are made to devise such rules for the Metz filter and so to increase its usefulness.

(iii) Iinuma-Nagai method - iterative approximation

This linear, stationary method is also based on an attempt to obtain a deconvolution of the recorded image with the point spread function without the amplification of noise:

$$f(x,y) = \iint \phi(x-x',y-y')psf(x',y')dx'dy'$$

Instead of solving this equation by taking Fourier transforms, Iinuma and Nagai[9] considered this as an integral equation, and used an iterative method to obtain successively closer approximations to $\phi(x,y)$.

The first approximation is given by:

$$f^1(x,y) = f^o(x,y) + \{f(x,y) - \int_{-\infty}^{\infty}\int f^o(x-x',y-y')psf(x',y')dx'dy'\}$$

where $f^o(x,y)$ is an arbitrary function which is used as an initial guess at $\phi(x,y)$. In practice it is easiest to use $f(x,y)$ as $f^o(x,y)$. The use of this approximation implies the assumption that the change induced by degrading the observed image with the system spread function will be roughly equal to the change in the object distribution caused by the system spread function in forming the image. The validity of this assumption under all conditions has not been proved.

Subsequent estimates are given by

$$f^n(x,y) = f^{n-1}(x,y) + \{f(x,y) - \int_{-\infty}^{\infty}\int f^{n-1}(x-x',y-y')psf(x',y')dx'dy'\}$$

The rationale once again is that the changes caused by degrading the estimated object distribution by the system spread function will approximate to the change in the object distribution in forming the image. In the limit if the estimated distribution converges to the object distribution, this will certainly hold true, but otherwise its validity is not plain.

In this limit, if $f^n(x)$ converges to $\phi(x)$,

$\{f(x,y) - H^n(x,y)\} \to 0$

where $H^n(x,y) = \int\int_{-\infty}^{\infty} f^n(x-x',y-y')psf(x',y')dx'dy'$

However because of noise in f(x,y) and psf(x,y), iteration must be stopped earlier, at a certain point determined by the magnitude of the noise. A criterion for stopping iteration may be expressed by

$|f(x,y) - H^n(x,y)| \leq A$

where A is a function of the noise level in f and psf. In practical situations, only one or two iterations may be possible, but even the first approximation should be closer to the ideal image than the original image is.

Metz[10] has examined this filtering method by considering the corresponding expressions in the frequency domain. The nth estimate of the image is given in the frequency domain by

$F^n(\underline{\omega}) = F(\underline{\omega}) - F^{n-1}(\underline{\omega})\{1 - M(\underline{\omega})\}$

or $F^n(\underline{\omega}) = F(\underline{\omega})\{1 - [1 - M(\underline{\omega})]^{n+1}\}/M(\underline{\omega})$

Thus the processor is given in the frequency domain by:

$\{1 - [1 - M(\underline{\omega})]^{n+1}\}/M(\underline{\omega}) \equiv Q^n(\underline{\omega})$

It can be seen that for $M(\underline{\omega}) \to 1$, this will be approximately $1/M(\underline{\omega})$, so that the correct frequency relationships will be restored at low frequencies. However, as $M(\underline{\omega}) \to 0$, $Q^n(\underline{\omega}) \to n+1$; thus the processor levels off to a plateau at high frequencies instead of increasing

rapidly with $1/M(\underline{\omega})$. By plotting out the processor frequency response for a Gaussian point spread function, it can be seen that as for the Metz filter, $Q^n(\underline{\omega})$ for the Iinuma-Nagai technique continues to adhere closely to the $1/M(\underline{\omega})$ curve to higher frequencies for higher values of n. However it is unlike the Metz technique in that the frequency response levels off to a plateau rather than decreasing to zero at high frequencies, and consequently if high frequency noise is to be eliminated this must be done by an independent smoothing method applied either before or after the iterative approximation.

Thus the Iinuma-Nagai method and the Metz filter both approximate to $1/M(\underline{\omega})$ at low frequencies but not at high frequencies. The Iinuma-Nagai method has a rationale behind it, but the assumption involved may not be valid under all conditions, particularly in the presence of noise. Like the Metz filter, this method is flexible, and furthermore a criterion is proposed for deciding on the best order of approximation to be used; however this criterion is neither clearly defined nor easy to use. Since the Iinuma-Nagai method does not eliminate high spatial frequencies, a smoothing procedure must also be applied; this distorts the relationship between the spatial frequency components and requires an arbitrary decision as to which smoothing method is most suitable. Processing by the Metz filter requires less computer time than the Iinuma-Nagai method as described here. However Iinuma and Nagai have developed another method, the differential operator method[11], for evaluating the deconvolution integral, and while it gives similar results to the iterative approximate method, it requires much less computer time.

(iv) Dot shifting

This method was first used by Pizer and Vetter[12], and its derivation

is also described by Metz[13]. It is a non-stationary, non-linear method whereby the dots in the image are reassigned to their most probable origins, calculated a posteriori from the observed count density data. Knowledge of the point spread function and use of Bayes' theorem enable one to obtain an estimate of the origin $\underline{r}'$ of a photon detected at some position r.

Bayes' theorem enables one to relate the unknown probability that a photon detected at $\underline{r}$ was emitted at $\underline{r}'$ to the known probability distribution, given by the point spread function, of a photon emitted at $\underline{r}'$ being detected at $\underline{r}$. From these probabilities one can obtain an estimate of the most probable origin $\hat{r}'$ of the observed counts:

$$\hat{\underline{r}}' \approx \underline{r} - \{ \sum_{\underline{\eta}} \underline{\eta}\, s(\underline{r}-\underline{\eta})psf(\underline{\eta})d\underline{\eta}\}/\{ \sum_{\underline{\eta}} s(\underline{r}-\underline{\eta})psf(\underline{\eta})d\underline{\eta}\}$$

where s(r) is an estimate of the count density distribution.

This method has been used successfully by Pizer and Vetter, and intuitively it is clear that use of the point spread function in this way should enhance the image. Pizer and Vetter use as their estimated activity distribution $s(\underline{r})$, the observed image after processing by variable smoothing, and obviously distortions could arise if this estimate is poor. In such cases there seems to be no theoretical way of demonstrating that dot shifting will give a better representation of the image.

D. Assessment and Intercomparison of Image Processing Methods

(i) Problems in the assessment and comparison of images.

There are obviously many ways of comparing digital images, and many sorts of images that could be compared, and it is very difficult to judge which will be most relevant to the application of image

processing methods to clinical situations. Digital images may be examined visually, in which case the result may be highly dependent on the display mode, and on the observer himself; on the other hand they may be assessed statistically, for example by testing for areas of raised or lowered count density.

All approaches to the problem must involve assessing in some way, how near the observed count distribution is to the distribution of activity in the object. This is not straightforward since the image is a two-dimensional representation of a three-dimensional object, and the mapping of the object onto the image is complicated by scattering, which will vary according to the object structure. Furthermore in a clinical situation, the true activity distribution can only be ascertained in the rare cases where surgery or a post-mortem is performed shortly after the radioisotope scan was carried out, and also the structural complexity of a clinical scan may make simple quantitative comparisons difficult. The alternative is to scan a phantom object, or mathematically to construct some form of phantom image. Such procedures can be made very flexible, but it is necessary to consider very carefully if they are relevant to any clinical situations.

However, even when a scan corresponding to some known object has been obtained, problems of how to assess it remain. One possibility is direct point-by-point comparison of how closely the variation in image count density reflects changes in activity in the object. This would be a complex procedure; it would require modification in situations where only some regions of the image are of interest and it would not be relevant to cases where overall accuracy in representing structures is less important than detection of some

particular lesions. Thus it is apparent that the assessment of images, unprocessed or processed, must be considered with a view to the applications for which the images are required.

(ii) Assessment and comparison of image processing methods

Image processing methods may be examined for the theoretical justification of their use and by comparison of the processed images with unprocessed ones, and if appropriate, with images processed by other methods. The characteristics of the image and the application for which it is required are highly relevant, and so factors which must be considered include the signal-to-noise ratio of the image, the extent of the regions of interest, and whether small scale fluctuations or larger features or both are required.

The theoretical bases of some image processing methods have been discussed in Sections B and C of this chapter, and the assumptions made in deriving these methods hold, at least approximately, in most clinical situations. In devising image processing methods, some workers have concentrated on studying image noise and attempting to eliminate it. Others on the other hand have tried to manipulate the lower part of the spatial frequency spectrum to enhance resolution, while using fairly arbitrary methods to reduce image noise to visually acceptable levels. The noise characteristics of the image and the purpose for which the image is processed may determine whether elimination of noise alone is required, or if resolution enhancement is also desirable. However to decide between image processing methods it is generally necessary to study the behaviour of the techniques under various conditions and devise performance indices to describe this behaviour. The definition of the indices and their relative importance will depend on the application for which the image is intended.

Although detailed study is desirable before any method or group of methods is adopted, discarded or replaced by another, few processing techniques have been given such consideration, and definitive performance indices have not been devised. The International Atomic Energy Agency has carried out international intercomparisons of image processing methods[14,15]. Mathematical phantoms were set up consisting of circular lesions of various sizes in a hemispherical count density distribution, with statistical variation superimposed. Processed images were compared for their reliability in detecting these lesions, and for their tendency to give rise to artifacts i.e. "false positive" lesions. Another detailed comparison of image processing methods is that of Kirch and Brown[16]. Their aim too is to assess these methods in terms of their abilities to detect small circular defects on a broad uniform background, and they have chosen performance indices accordingly. They attempt to measure the degree of resolution enhancement, the amount of smoothing and the tendency to produce artifacts, since all these influence the detectability of lesions. Although these qualities of filters are all related to their ability to improve images which are structurally more complex, the significance of the performance indices is no longer clear outside the context of "detection" processing. It appears that no quantitative assessments have been made of the behaviour of image processing methods on images of complex structure, and the applicability of performance indices referring to detection processing in other situations has not been discussed. In fact even in the context of detection processing no single method has been established as being superior to all others, and any method which produces clinically useful images, such as the Metz filter, seems worthy of detailed investigation.

Table IA

Definitions and Notation

$\underline{r} \equiv (x,y)$ (Cartesian coordinates)

$\underline{\omega} \equiv (\omega_x, \omega_y)$

	Function in space domain	Function in spatial frequency domain
Object distribution (represented in 2 dimensions)	$\phi(\underline{r})$	$\Phi(\underline{\omega})$
Image distribution	$f(\underline{r})$	$F(\underline{\omega})$
Point spread function	$psf(\underline{r})$	$[M(\underline{\omega})$ usually$]$
Modulation transfer function	$psf(\underline{r})$ usually	$M(\underline{\omega})$
Processed image	$g(\underline{r})$	$G(\underline{\omega})$
Processor	$q(\underline{r})$	$Q(\underline{\omega}) \equiv G(\underline{\omega})/F(\underline{\omega})$
Processed frequency response	$psf(\underline{r}) * q(\underline{r})$	$M(\underline{\omega})Q(\underline{\omega})$

Table IB

Processor Frequency Responses for Smoothing Procedures

ω_x	ω_x.1/64ε	5-point	9-point(a)	9-point(b)	13-point
0	0	1.00	1.00	1.00	1.00
1/12ε	5.3	0.96	0.94	0.93	0.90
1/8 ε	8	0.90	0.86	0.83	0.78
1/6 ε	10.7	0.83	0.75	0.70	0.65
1/4 ε	16	0.67	0.50	0.40	0.40
1/3 ε	21.3	0.50	0.25	0.10	0.25
3/8 ε	24	0.43	0.15	-0.03	0.22
5/12ε	26.7	0.37	0.06	-0.13	0.20
1/2 ε	32	0.33	0.00	-0.20	0.20

Figure IA

Diagrammatic Representations of Smoothing Procedures

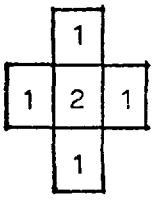

5-point

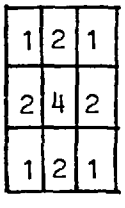

9-point(a)

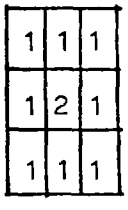

9-point(b)

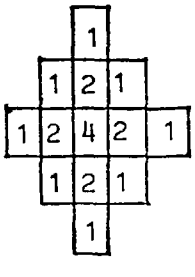

13-point

CHAPTER II

The Metz Filter

Abstract

The derivation of the Metz filter and the rationale behind it are discussed in detail. The derivation follows Metz, but in addition the assumptions made are considered throughout as they apply to a real system and points which are of special relevance to the applications of Chapters IV and V, such as the validity of the derivation for a non-spherically symmetric point spread function, are stressed. Discussion of the numerical computation of the filters, which likewise follows Metz, includes comments made in the light of following Metz's suggestions for carrying out these calculations. The properties of the filters are described with reference to the theory and to the filters calculated.

CHAPTER II

The Metz Filter[1]

A. Formulation of the Metz Filter

(i) Purpose of the Metz filter

The purpose of an imaging system is to produce some image from an object! In the case of a gamma camera, for example, the object is, in general, a three-dimensional distribution of radioactivity, and the image is some more or less distorted two-dimensional mapping of this.

Consider an object distribution $\phi(\underline{r},z)$ where z is the perpendicular distance from the collimator plane, and $\underline{r}$ defines the position in the plane perpendicular to z.

Now the ideal image should be $f'(\underline{r},z)$ where $f'(R,Z) = \phi(\underline{R},Z)$ for any specified values of $\underline{R}$, Z. However, in view of the inevitable limitation of the image to two dimensions, the best one could hope for is some two-dimensional image $f(\underline{r})$, with $f(\underline{r}) = \int_0^\infty f'(\underline{r},z)dz$ for each $\underline{r}$.

The aim of the Metz filter, as it is applied here, is to recover from the real image something more like the best two-dimensional image and so a truer representation of the original object.

(ii) Point spread function of an imaging system

The aim of a gamma camera system is to transfer the variations in activity in the object to the image; obviously major variations in radioactivity or size will be transferred more effectively, and small features or small differences in radioactivity may only be

distinguished with difficulty, depending, among other factors, on the quality of the gamma camera.

The performance of a particular gamma camera under some specified conditions can be described in terms of its point spread function. Consider an object which consists only of a single point source of unit intensity at some position ($\underline{r}$,z), the resulting image will, by definition, be the point spread function psf($\underline{r}$,z; $\underline{r}'$) where $\underline{r}'$ is the position in the image plane. This function describes the behaviour of the gamma camera under the particular operating and physical conditions, e.g. for that collimator, radioisotope energy, thickness and nature of scattering medium, distance from the collimator face z etc. There is no reason to assume that the point spread function will remain constant if any of these parameters were changed.

The "ideal" image of a point source object would be a point image at a corresponding position in the image field, but for any real system the point spread function will not have the form of this "ideal" image with psf($\underline{r}$,z; $\underline{r}'$) = $\phi(\underline{r},z)$ for r = $\underline{r}'$ and psf($\underline{r}$,z; r') = 0 for $\underline{r} \neq \underline{r}'$, but there will also be some counts scattered around this central point. Thus the point spread function is in effect a probability distribution describing the probabilities that counts originating from a point source of activity will arrive at a corresponding point in the image or at surrounding points. The shape of this distribution will depend on the detection device used and the recording conditions, as will be described in detail for the gamma camera in Chapter III. The point spread function is therefore a constant property of a given system as long as the conditions of recording remain fixed, but it may alter if any factors relating to the detection system or the recording conditions vary.

The full width at half maximum (FWHM) of the point spread function can be used as an indication of the resolution of a detection system. Mallard[2], discussing this in terms of line sources and the FWHM of the line spread function, states that two line sources are only likely to be distinguishable from one another if the distance between them is greater than the FWHM. A similar conclusion would presumably hold for point sources. However although the FWHM is useful as a rough guide to the performance of a scanning system, the complete point spread function contains much more information, and indeed two quite differently shaped point spread functions could have the same FWHM.

(iii) Stationarity and linearity

Any composite object distribution $\phi(\underline{r},z)$ could be considered to be made up of many point sources of intensity $\phi(r,z)$ placed at all points $(\underline{r},z)$. The contribution to the image at a point $\underline{r}'$ from the point source $\phi(\underline{R},Z)$ placed at the point $(\underline{R},Z)$ will be $\phi(\underline{R},Z)psf(\underline{R},Z;\underline{r}')$ by definition. So if the system is linear i.e. if the image resulting from two or more objects recorded together is equal to the sum of the images formed when the objects are viewed separately, then the image of any composite object may be written as the sum of the images produced by each point in the object separately. In other words, the composite image is built up of the sum of point spread functions for all points on the image, weighted by the activities at each point.

$$\text{Image } f(\underline{r}') = \iint \phi(\underline{r},z)psf(\underline{r},z;\underline{r}')d\underline{r}dz \qquad \text{II A.1}$$

In Chapter III the validity of this linear assumption is examined in detail for the case of a gamma camera system.

If the response of a detection system to a radioactive source is independent of the position of the source in the object plane,

the system is said to be stationary. If a point source is placed at various positions in the object field and point spread functions are recorded, a system can be tested for stationarity. For example, for a well-tuned gamma camera, the shape of the point spread function (after correction for non-uniformity) is found to be independent of the position of the source in an object plane at a fixed distance from the collimator i.e. with z fixed.[3] If, as in this case, the system is stationary, at least for specified parts of the object field, one can write

$$psf(\underline{r},z;\ r') = psf(r-r',z)$$

and if the system is also linear, the form of any image of a 2-dimensional object in a plane where z is a constant is described by

$$f(\underline{r}') = \iint \phi(\underline{r},z)psf(\underline{r}-\underline{r}',z)d\underline{r}dz \qquad \text{II A.2}$$

For a 2-dimensional object, since z is constant this may be written more simply:

let $\phi(\underline{r},z)_{z\ \text{fixed}} = \phi(\underline{r})$ and $psf(\underline{r}-\underline{r}',z)_{z\ \text{fixed}} = psf(\underline{r}-\underline{r}')$

Now $f(\underline{r}') = \int \phi(\underline{r})psf(\underline{r}-\underline{r}')d\underline{r}$ for that value of z. II A.3

(iv) Modulation transfer function

The above equation II A.3 describes the relationship which holds between a two-dimensional object and its image provided that the system is linear and stationary. The right hand side of equation II A.3 has the form of a convolution integral; therefore on taking Fourier transforms and so transforming the equation into the domain of spatial frequency, it has the simple form:

$$F(\underline{\omega}) = \Phi(\underline{\omega})M(\underline{\omega}) \qquad \text{II A.4}$$

This transformation will be possible provided that $F(\underline{\omega}), \Phi(\underline{\omega})$

and $M(\underline{\omega})$, which are the Fourier transforms of $f(\underline{r})$, $\phi(\underline{r})$ and $psf(\underline{r})$ respectively, exist. According to Margenau and Murphy[4] the Fourier transform of a function $f(x)$ will exist if $f(x)$ is at least piecewise continuous and such that $\int_{-\infty}^{\infty} |f(x)|dx$ exists. This should hold for the functions $f(\underline{r})$, $\phi(\underline{r})$ and $psf(r)$ encountered in practice.

The Fourier transforms $F(\underline{\omega})$, $\Phi(\underline{\omega})$ describe the image and the object respectively in terms of their distributions in the spatial frequency domain. Examination of the equation II A.4 shows that when the system views some object whose spatial activity distribution is sinusoidal, with frequency $\underline{\omega}$, the image will also be sinusoidal, with the same frequency $\underline{\omega}$, but the amplitude may be altered. The ratio of amplitudes of modulation in the object to that in the image for any frequency $\underline{\omega}$, is given by $M(\underline{\omega})$, thus $M(\underline{\omega})$ is by definition the modulation transfer function (MTF) for the system. It can be seen that this function describes the performance of the system by describing the way in which it transfers modulation from object to image. It must be emphasized that equation II A.4 will not necessarily be valid unless the conditions of linearity and stationarity hold; otherwise modulation of a given frequency in the object may not be transferred to the image as a single sinusoidal variation of the same frequency merely with a change in amplitude.

It should be noted that this definition of $M(\underline{\omega})$ does not disregard the fact that $\underline{\omega}$ is a vector quantity. $M(\underline{\omega})$ is the factor by which frequencies of magnitude and direction given by this vector $\underline{\omega}$ are transferred from object to image. Since $psf(\underline{r})$ and hence $M(\underline{\omega})$ may not be spherically symmetric in practice, such a general definition of $M(\underline{\omega})$ is useful.

Now, if the assumptions of stationarity and linearity of the detector system hold, the modulation transfer function is given simply

by the Fourier transform of the point spread function, and the "smearing" effect of the point spread function can be described equivalently in terms of the modulation transfer function. If the point spread function is wide, small objects will not be distinguishable from each other while larger objects will. These larger objects correspond to low spatial frequencies where the MTF is close to 1 and there is good efficiency of transfer, while the smaller objects correspond to higher frequencies where the MTF drops. The wider the point spread function, the lower the frequency at which the MTF drops, and the poorer the small detail in the image, as one would imagine. In practice image quality is of course determined by factors such as counting statistics, as well as by the shape of the point spread function and the MTF. Examples of some point spread functions and the corresponding MTFs are shown in the following chapters.

(v) $1/M(\omega)$ as a frequency filter

In theory, using the above equation, II A.4, it would be possible to obtain $\Phi(\underline{\omega})$, the spatial frequency distribution of the original object, from $F(\underline{\omega})$, the observed distorted spatial frequency distribution, and so to calculate the required $\phi(\underline{r})$.

From above $\Phi(\underline{\omega}) = F(\underline{\omega})/M(\underline{\omega})$

$$\phi(\underline{r}) = \text{F.T.}^{-1}\{F(\underline{\omega})/M(\underline{\omega})\} \qquad \text{II A.5}$$

where F.T.^{-1} means the inverse Fourier transform.

Thus $1/M(\underline{\omega})$ acts as a frequency filter amplifying frequency components in the observed image distribution at various levels, to give the processed image $\phi(\underline{r})$ with a frequency spectrum restored to that of the original object.

If $M(\underline{\omega})$ exists and is known exactly, and if it is never zero except where $F(\underline{\omega})$ is zero, $\phi(r)$ could be calculated from this expression. In practice these conditions are not always fulfilled; $M(\underline{\omega})$ is often zero for some high frequencies, but even in such a case these frequencies could be omitted and a bandwidth limited version of $\phi(r)$ could be calculated. However, $M(\underline{\omega})$ is also not usually known everywhere with sufficient accuracy; in particular, at higher frequencies where $M(\underline{\omega})$ is small it is difficult to determine it exactly, and when $M(\underline{\omega})$ is low, small errors in the values of $M(\underline{\omega})$ may give rise to large errors in the frequency filter $1/M(\underline{\omega})$ which is applied to the image distribution. In view of this and of the problems of image noise discussed in the next section, it becomes desirable to apply equation II A.5 in a modified form.

(vi) Statistical noise

The nature of statistical noise in radioisotope scan images has been described briefly in Chapter I Section A(iii), and its effects on the validity of equations II A.2, 3 and 4 will now be considered. Statistical noise arises because the rate of radioactive decay can only be described in terms of the probability of decay occuring within a given time interval, and also because the positions at which counts originating from a given point in the object are recorded in the image are determined by a probability distribution - the point spread function.

Since the radioactive decay process is defined in terms of probabilities, the number of counts recorded is not related directly to the radioactivity in the object, but only gives an estimate of this activity. The numbers of decays occuring within fixed time

intervals make up a Poisson distribution[5]. For such a distribution, the variance is equal to the mean, and so the standard deviation in the number of decays, which is equal to the square root of the variance, decreases as a proportion of the mean, as the mean increases[5]. As a consequence of this, the relative statistical variation in the number of counts recorded and so the probable magnitude of the proportional error in the estimate of activity will be less the greater the number of counts recorded.

In deriving equations II A.2, 3 and 4 it is assumed that each point in the object is represented by a point spread function centred at the corresponding position in the image and with its amplitude depending on the radioactivity at that point in the object. Clearly if many counts from a given point on the object are recorded in the image, the corresponding point spread function will be well-defined, whereas if only a few counts are recorded, the function will be poorly estimated and so the equation will not hold exactly.

Thus both these sources of statistical variation may affect the validity of equations II A.2, 3 and 4 so that they only hold approximately. The noise will be lower in relation to the count density when the count density is high, but whatever the count density, the noise level is fairly constant throughout the spatial frequency spectrum[6]. The signal-to-noise ratio, however, will decrease considerably at high frequencies since, as described by the modulation transfer function, the signal is much lower there. Consequently, in the presence of noise the relationship defined in equations II A.2, 3 and 4 will be valid at low spatial frequencies, but particularly for images with few counts, it will only hold approximately at higher frequencies.

Therefore although it would be reasonable and hopefully beneficial to image quality to use the frequency filter $1/M(\underline{\omega})$ at low frequencies, it could be very misleading at high frequencies where the noise level is significant. The danger of using this filter at high frequencies becomes particularly apparent if one considers the form of the filter. Firstly, for large $\underline{\omega}$, where the noise level is high, the relationship defined in equations II A.2, 3 and 4 is only approximately valid. Secondly $M(\underline{\omega})$ is small for large $\underline{\omega}$ and it may therefore be difficult to determine it accurately; consequently $1/M(\underline{\omega})$ will be ill-defined but very large. These large and uncertain values of $1/M(\underline{\omega})$ will then be used to amplify greatly $F(\underline{\omega})$, which has a low signal-to-noise ratio for large $\underline{\omega}$ when there is noise in the image.

One could try, as suggested above, to apply the filter $1/M(\underline{\omega})$ in the regions where noise is not significant and set $\Phi(\underline{\omega})$ to zero for all other frequencies to obtain a bandwidth limited version of $\phi(r)$. However, apart from the difficulty of defining some frequency at which the useful part of the image ends and noise begins, such a procedure would give rise to sharp discontinuities in $\Phi(\underline{\omega})$ and so to severe undulations in the inverse transform $\phi(\underline{r})$. Brown et al.[7] have tried this method and found that the presence of these undulations in the processed image can give rise to the appearance of artifacts and the obscuring of image features.

A more sophisticated approach is therefore required. It is useful to look for some function which approximates to $1/M(\underline{\omega})$ for lower frequencies where signal-to-noise ratio is high, but decreases gradually to zero at high frequencies to avoid amplifying the noisy part of the image spectrum and to avoid sharp discontinuities in $\Phi(\underline{\omega})$. The frequency range over which the filter response should approximate

to $1/M(\underline{\omega})$ will depend on the circumstances. If the image is very noisy, for instance if the count rate is poor, then only a very low range of frequencies will be sufficiently noise-free to amplify them without risking serious distortion. Similarly the shape of $M(\underline{\omega})$ may limit the range of frequencies at which amplification is desirable; if $M(\underline{\omega})$ falls to zero at quite a low frequency (this corresponds to a system with a wide point spread function) then at higher frequencies $M(\underline{\omega})$ will not be accurately known as mentioned above, and also the high frequency part of the object spectrum will be poorly transferred to the image and the signal-to-noise ratio in this part of the image spectrum will be very low. Consequently contributions to the image at these frequencies will not be significant so that their amplification is pointless.

So one is searching for an approximation $Q(\underline{\omega})$ say, to $1/M(\underline{\omega})$ with the following properties.

$Q(\underline{\omega}) \sim 1/M(\underline{\omega})$ for $\underline{\omega}$ small $\leq \omega_n$

$Q(\underline{\omega}) \to 0$ gradually for $\underline{\omega}$ large $\geq \omega_n$

where ω_n is some frequency which depends on the shape of $M(\underline{\omega})$ but can also be varied to allow for the possibility of filtering more or less noisy images collected under the same conditions (i.e. with the same $M(\underline{\omega})$). An approximation which has these properties will have automatic suppression of high frequency noise, in contrast to other filtering techniques where it is necessary to use separate procedures such as smoothing to eliminate noise.

There is no unique result to this search for a suitable approximation, but only one such filter, the Metz filter, will be described in detail here.

(vii) The Metz filter

Consider the following expansion for $1/M(\underline{\omega})$

$$1/M(\underline{\omega}) = \frac{M^*(\underline{\omega})}{|M(\underline{\omega})|^2} = \frac{M^*(\underline{\omega})}{1 - [1 - |M(\underline{\omega})|\ ]^2} = M^*(\underline{\omega}) \sum_{k=0}^{\infty} [1 - |M(\underline{\omega})|^2\ ]^k$$

This expansion converges to $1/M(\underline{\omega})$ for $|M(\underline{\omega})| < \sqrt{2}$; this requirement is satisfied in all the practical situations encountered in our clinical work.

Consider approximations to this expression by defining an nth order approximation

$$Q^n(\underline{\omega}) \equiv M^*(\underline{\omega}) \sum_{k=0}^{n} [\ 1 - |M(\underline{\omega})|^2\ ]^k$$

$$= M^*(\underline{\omega}) \frac{1 - [1 - |M(\underline{\omega})|^2\ ]^{n+1}}{|M(\underline{\omega})|^2} = \frac{1 - [1 - |M(\underline{\omega})|^2\ ]^{n+1}}{M(\underline{\omega})}$$

This function clearly approximates to $1/M(\underline{\omega})$ for $|M(\underline{\omega})| \to 1$, but decreases to zero as $|M(\underline{\omega})| \to 0$. Plotting this function, for $n = 6$ say, for typical values of $M(\underline{\omega})$, it can be seen (see Graph IIIA) that it approximates to $1/M(\underline{\omega})$ where $|M(\underline{\omega})|$ is large (for small $\underline{\omega}$), but decreases to zero for large $\underline{\omega}$ where $|M(\underline{\omega})|$ tends to zero. This function could therefore be used instead of $1/M(\underline{\omega})$ as a frequency filter to give some nth order approximation to the object distribution in the realistic situation where noise is present.

Processor response amplitude $|Q^n(\underline{\omega})|$ is maximum if $\frac{d|Q^n(\underline{\omega})|}{d|M(\underline{\omega})|} = 0$

i.e. $[1 - |M(\underline{\omega})|^2\ ]^n\{(2n+1)|M(\underline{\omega})|^2 + 1\} = 1$

For large n, this implies $|M(\underline{\omega})| \simeq 1.121/\sqrt{n}$ at maximum. It can be seen in practice that this approximation holds fairly well for $n \gtrsim 10$. It shows that as n increases, the values of $|M(\underline{\omega})|$ for maximum $|Q^n(\underline{\omega})|$ decreases, and consequently the maximum values themselves of $|Q^n(\omega)|$ will become higher. Thus for any realistic modulation transfer function,

which decreases at higher frequencies, the maximum will occur at higher frequencies for greater n. These general conclusions are also true for n <10, where the above approximation does not hold (see GraphIIIA).

Plotting $Q^n(\underline{\omega})$ for various values of n, again for example for a typical $M(\underline{\omega})$ (it is also true for any similar shaped function), it can be seen that the range of frequencies amplified increases as n increases (see Graph IIIA) eventually as $n \to \infty$, $Q^n(\underline{\omega}) \to 1/M(\underline{\omega})$, and then clearly the higher frequencies too are amplified. However, for lower values of n, it is clear that the range of frequencies amplified can be altered, as demanded by the amount of noise in the image, by varying n. The frequency at the maximum $Q^n(\underline{\omega})$ will depend on the detailed shape of $M(\underline{\omega})$ and so the optimal value of n which should be selected for processing a particular image is likely to depend on this shape as well as on the noise in the image. The performance of the Metz filters may also be seen by considering the processed frequency response functions $S^n(\underline{\omega}) = Q^n(\underline{\omega})M(\underline{\omega})$ (see Graph IIIB). The ideal processed frequency response would be 1 throughout the spatial frequency spectrum. This is approached as $n \to \infty$. For lower n the processed frequency response is near 1 at low frequencies but decreases to 0 at the high frequency end of the spectrum, showing that if low order Metz filters are applied, high frequency components of the image, where noise is greatest, may be eliminated.

[From Table II A the sensitivity of the Metz filter approximation to the shape of the MTF can be seen; this table also shows how flexible the method is when n is varied.]

(viii) Algorithms for the Metz filter $Q^n(\omega)$[8]

As described in Section A(v) above, if there were no problem of non-additive noise, one might attempt to recover the object distribution

from the measured image by estimating

$\phi(\underline{r}) = F.T.^{-1}\{F(\underline{\omega})/M(\underline{\omega})\}$

Here one can only hope to obtain some approximation $p^n(\underline{r})$ to $\phi(\underline{r})$ by using $Q^n(\underline{\omega})$, the nth order approximation to $1/M(\underline{\omega})$.

Now $p^n(\underline{r}) = F.T.^{-1}\{F(\underline{\omega})Q^n(\underline{\omega})\}$

or $p^n(\underline{r}) = f(\underline{r}) * q^n(\underline{r})$ where $q^n(\underline{r}) = F.T.^{-1}\{Q^n(\underline{\omega})\}$

One can derive an algorithm for calculating $Q^n(\underline{\omega})$ or its inverse Fourier transform $q^n(\underline{r})$ from $M(\underline{\omega})$ or psf(r) using the expressions above for $Q^n(\underline{\omega})$.

$$Q^n(\underline{\omega}) = M^*(\underline{\omega}) \sum_{k=o}^{n} \left[1 - |M(\underline{\omega})|^2\right]^k = \frac{1 - \left[1 - |M(\underline{\omega})|^2\right]^{n+1}}{M(\underline{\omega})}$$

$$\therefore Q^n(\underline{\omega}) = M^*(\underline{\omega}) \sum_{k=o}^{n-1} \left[1 - |M(\underline{\omega})|^2\right]^k + M^*(\underline{\omega})\left[1 - |M(\underline{\omega})|^2\right]^n$$

$$Q^n(\underline{\omega}) = M^*(\underline{\omega}) + Q^{n-1}(\underline{\omega}) - M^*(\underline{\omega})M(\underline{\omega})Q^{n-1}(\underline{\omega})$$

where $Q^1(\underline{\omega}) = 2M^*(\underline{\omega}) - M^*(\underline{\omega})M^*(\underline{\omega})M(\underline{\omega})$

Inverse Fourier transforms of these expressions give the algorithms for $q^n(\underline{r})$.

$F.T.[psf(-\underline{r})] = M^*(\underline{\omega})$

$$\therefore q^1(\underline{r}) = 2psf(-\underline{r}) - psf(-\underline{r}) * psf(-\underline{r}) * psf(\underline{r})$$

$$q^n(\underline{r}) = psf(-\underline{r}) + q^{n-1}(-\underline{r}) - psf(-\underline{r}) * psf(\underline{r}) * q^{n-1}(\underline{r})$$

One can also calculate $p^n(\underline{r})$ directly:

$$p^1(\underline{r}) = 2psf(-\underline{r}) * f(\underline{r}) - psf(-\underline{r}) * psf(-\underline{r}) * psf(\underline{r}) * f(\underline{r})$$

$$p^n(\underline{r}) = psf(-\underline{r}) * f(\underline{r}) + p^{n-1}(\underline{r}) - psf(-\underline{r}) * psf(\underline{r}) * p^{n-1}(\underline{r})$$

B. Digital Computation Methods for the Metz filter

(i) Problems in digital calculation of Metz filtered images

The Metz filter could be applied to images by analogue or digital methods, however, digital methods are more flexible and so

more practical while the benefits of the filter and the method of best using it are not yet established. In any event, when a system for sampling and digitizing the image data is already in operation, and when other digital processing is required e.g. correction for non-uniformity in the case of gamma camera data, it may be simpler to use digitized data.

The problems of obtaining suitably sampled digitized data and the use of the algorithms described above (see Section A(viii)) to evaluate the Metz filters and the corresponding filtered images from digitized images and point spread function data will be discussed in this section.

The object is continuous and the image is formed by the gamma camera as a continuous function of the position coordinates. The equations describing the imaging system are therefore written in terms of continuous functions and so are the algorithms for calculating the Metz filter. Under certain conditions, accurate approximations to Metz filtered images may be obtained by substituting discretely sampled digitized point spread functions and images for the continuous ones and similarly using discrete Fourier transforms and convolutions instead of continuous ones. On the other hand if the required conditions do not apply, discrete transforms, both forward and inverse, and discrete convolutions may differ from the corresponding continuous versions, giving rise to distortion of the processed image.

Problems also arise in the digital calculations because of the large arrays and hence the large amount of computer time required. When calculating convolutions in the space domain, it may therefore be necessary to truncate the functions involved in order to reduce computer time; however, this may introduce distortions. Alternatively the convolutions can be calculated by transforming to the spatial

frequency domain, multiplying and then doing an inverse transform. Since Fast Fourier Transform (FFT) programs are available for computing discrete Fourier transforms of large arrays, this method can be quicker.

(ii) Discrete Fourier transforms

When calculating a continuous Fourier transform, or in other words analysing a function into sinusoidal frequency components, there is no limiting frequency above which no components of higher frequencies may be found. However, for a discrete Fourier transform of a function sampled at a finite sampling distance ε, clearly no frequency higher than $2\pi/\varepsilon$ or 1 cycle per unit sampling distance can be distinguished. Any frequency of the form $\omega + 2\pi n/\varepsilon$ will be indistinguishable from the frequency ω itself and the spectrum from $\omega = -\pi/2$ to π/ε is repeated throughout the frequency range with period $2\pi/\varepsilon$. Also when "searching" for components with frequency ω, all frequencies $\omega + 2\pi n/\varepsilon$, $n = 0,1,2....\infty$ will be selected together.

The description here of the relationship between continuous and discrete Fourier transforms, as this effects the digital calculation of the Metz filter, follows that given by Metz[9].

The continuous 2-dimensional Fourier transform is given by

$$F(\omega_x,\omega_y) = \iint_{-\infty}^{\infty} f(x,y)e^{-i(\omega_x x + \omega_y y)}dxdy$$

the discrete approximation to it is

$$F_D(\omega_x,\omega_y) = \sum_{m,n=-\infty}^{\infty} \varepsilon^2 f(m\varepsilon,n\varepsilon)e^{-i(\omega_x m + \omega_y n)}$$

It can be seen immediately from this expression, that $F_D(\omega_x,\omega_y)$ is periodic on the ω_x and ω_y axes with period $2\pi/\varepsilon$:

$$F_D\left(\omega_x + \frac{2\pi k}{\varepsilon}, \omega_y + \frac{2\pi l}{\varepsilon}\right) = \sum_{m,n=-\infty}^{\infty} \varepsilon^2 f(m\varepsilon,n\varepsilon)e^{-i(\omega_x m + \omega_y n)-i(2\pi km + 2\pi ln)}$$

$$= F_D(\omega_x,\omega_y)$$

since $e^{-i(2\pi km + 2\pi ln)} = 1$ for k,l,m,n integers.

The relationship between the discrete and continuous transforms is given by

$$F_D(\omega_x,\omega_y) = \sum_{m,n=-\infty}^{\infty} F\left(\omega_x + \frac{2\pi m}{\varepsilon}\ \omega_y + \frac{2\pi n}{\varepsilon}\right)$$

This equation described the phenomenon of summing all frequencies $\omega + 2\pi/n\varepsilon$ mentioned above - the effect is known as aliasing, and the frequency $2\pi/\varepsilon$ is the aliasing frequency. The frequency π/ε, half the aliasing frequency, is known as the Nyquist frequency.

As a result of this aliasing any components with frequencies outside the range $|\omega_x| < \pi/\varepsilon$ and $|\omega_y| < \pi/\varepsilon$ will appear in the discrete spectrum added on to the "true" components of the continuous spectrum within this range, so that the discrete spectrum may differ considerably from the continuous one. In order to avoid this, and so to be able to estimate continuous transforms by calculating discrete approximations to them, it is necessary to choose ε sufficiently small that all frequency components outside the range $|\omega_x| < \pi/\varepsilon$ and $|\omega_y| < \pi/\varepsilon$ are negligible.

When calculating the Fourier transform of an array such as the radioisotope scan image f(x,y) which is undefined (set to zero probably) outside an array e.g. 64 x 64 or 128 x 128 cells in dimension, the continuous transform cannot be completely band-limited in frequency space. However aliasing can be minimized by choosing small enough sampling distance ε.

In the case of a system point spread function for example, the frequency spectrum i.e. the modulation transfer function, gradually decreases to zero for increasing frequencies. If it has become negligible at frequencies below the Nyquist frequency, and

remains so, then the discrete approximation of the Fourier transform will be an accurate representation of the continuous one within the range $|\omega_x| \leq \pi/\varepsilon$ and $|\omega_y| \leq \pi/\varepsilon$, e.g. the MTF for ^{133}Xe approaches zero before the Nyquist frequency (see Graph IIIA). On the other hand, if ε is too large, and the MTF is not negligible at the Nyquist frequency, then the discrete transform will rise before the Nyquist frequency since distortion occurs as a consequence of aliasing. Similar considerations must be made for all arrays which are to be Fourier transformed.

(iii) Inverse Fourier transforms

The sample array $f(m\varepsilon,n\varepsilon)$ can be calculated from $F_D(\omega_x,\omega_y)$ by the inverse transform

$$f(m\varepsilon,n\varepsilon) = \frac{1}{(2\pi)^2} \int_{-\pi/\varepsilon}^{\pi/\varepsilon}\int F_D(\omega_x,\omega_y)e^{+i(\omega_x m + \omega_y n)}\, d\omega_x d\omega_y$$

This sampled array is completely and uniquely specified by the portion of $F_D(\omega_x,\omega_y)$ in the square region $|\omega_x| \leq \pi/\varepsilon$ and $|\omega_y| \leq \pi/\varepsilon$; obviously the remainder of $F_D(\omega_x,\omega_y)$ adds no more information since it is just a repetition of the values in this region. The function $f(x,y)$ is not however uniquely specified by $F_D(\omega_x,\omega_y)$ since a whole family of functions with equal values at $(\pm m\varepsilon, \pm n\varepsilon)$ yield the same sample array $f(m\varepsilon,n\varepsilon)$ and therefore the same discrete transform.

If the inverse transform too is to be calculated digitally, then the integrals must be approximated by a double sum:

$$f(m\varepsilon,n\varepsilon) \simeq \frac{1}{(2\pi)^2} \sum_{k=-k}^{+k} \sum_{\ell=-L}^{+L} F_D(k\Delta\omega_x,l\Delta\omega_y)e^{+i(km\Delta\omega_x + ln\Delta\omega_y)}\Delta\omega_x\Delta\omega_y$$

where $k = \pi/\varepsilon\ \Delta\omega_x$ and $l = \pi/\varepsilon\ \Delta\omega_y$.

This discrete approximation of the inverse Fourier transform applicable when $F_D(\omega_x,\omega_y)$ is evaluated at $(2K + 1).(2L + 1)$ points in a rectangular periodically spaced array in frequency space i.e. F_D is sampled using a rectangular array with "sampling distances" $\Delta\omega_x$, $\Delta\omega_y$ in the ω_x and ω_y directions respectively.

The problems involved in this discrete transform are exactly analogous to those for the forward discrete transform, and so an exact periodic verion of $(m\varepsilon, n\varepsilon)$ is given by the above equation of $f(x,y) = 0$ for $|x| \geq \pi/\Delta\omega_x$ and $|y| \geq \pi/\Delta\omega_y$; otherwise an aliased version is obtained.

This doubly discrete transform pair gives rise to certain problems. As mentioned above, if $f(x,y)$ is "region limited" in image space, then $F(\omega_x,\omega_y)$, the continuous transform, cannot be band-limited in frequency space. Similarly, if $F(\omega_x,\omega_y)$ is band-limited, its inverse transform $f(x,y)$ cannot be zero outside a finite region of image space. So in the situation where $f(x,y)$ is a gamma camera image, which is region limited, then $F(\omega_x,\omega_y)$ will not be band-limited in frequency space so that a discrete approximation to it $F_D(\omega_x,\omega_y)$ will be distorted by aliasing, though this may be minimized by choosing ε so small that $F(\omega_x,\omega_y)$ is small for $|\omega_x| \geq \pi/\varepsilon$ and $|\omega_y| \geq \pi/\varepsilon$. $F_D(\omega_x,\omega_y)$ is therefore a verion of $F(\omega_x,\omega_y)$ which is band-limited and also distorted by aliasing. Its inverse transform $f'(x,y)$ will therefore also not be region limited, so that the discrete approximation to it $f_D(x,y)$ will once again be distorted by aliasing to an extent depending on the choice of the sampling interval $\Delta\omega$.

Consider the implementation of this for a digitized radioisotope scan image where $f(m\varepsilon,n\varepsilon) = 0$ for $|m| \geq M$ and $|n| \geq N$ - in other

words where f(x,y) can be represented by a square array of samples with (2M + 1) samples on each side and the border equal to zero. Then a discrete Fourier transform array $F_D(k\Delta\omega_x, l\Delta\omega_y)$ can be calculated.

From above we have seen that no aliasing will occur on the inverse transform if $f(x) = 0$ for $|x| \geq \pi/\Delta\omega$. Here $f(x) = 0$ for $|x| \geq M\varepsilon$, so if $\Delta\omega_x \leq \pi/M\varepsilon$, then the discrete inverse Fourier transform will yield an exact periodic version of the truncated array $f(m\varepsilon,n\varepsilon)$. No aliasing will occur if $\Delta\omega = \pi/M\varepsilon$ because the points $f(\pm M\varepsilon,\pm M\varepsilon)$ on the border of the defined array were set equal to zero. If $\Delta\omega$ is chosen equal to $\pi/M\varepsilon$, then $K = \pi/\varepsilon\Delta\omega = M$, and the arrays in image space and frequency space have equal dimensions, which can be very convenient for computation. In any case such a choice is sensible because if f(x) is limited to the region $2M\varepsilon$ long, then the smallest differences in frequency which will be significant are $2\pi/2M\varepsilon$ i.e. $\Delta\omega = \pi/M\varepsilon$ as above.

(iv) Fast Fourier transforms (FFT)

The Fast Fourier transform alogrithm by Cooley and Tukey calculates discrete forward and inverse transforms with K = M, as defined above.

Calculation of a one-dimensional Fourier transform using the FFT requires approximately $N/2\log_2 N$ complex additions, $N/2\log_2 N$ complex subtractions and $N/2\log_2 N$ complex multiplications. Therefore for the two-dimensional Fourier transform of a N x N array, approximately $N^2\log_2 N$ complex additions, $N^2\log_2 N$ complex subtractions and $N^2\log_2 N$ complex multiplications are required. The spectrum calculated will be a N x N array in frequency space, the inverse transform of which is periodic in image space with period N.

(v) Discrete and continuous convolutions

The convolution-multiplication theorem holds for both discrete and continuous convolutions[9] i.e. if $g_1(x,y)$ is defined by

$$g_1(x,y) = f(x,y) * h(x,y) = \int\int_{-\infty}^{\infty} f(x-\xi, y-\eta)h(\xi,\eta)d\xi d\eta$$

then its continuous Fourier transform $G_1(\omega_x,\omega_y)$ is given by

$$G_1(\omega_x,\omega_y) = F(\omega_x,\omega_y)H(\omega_x,\omega_y)$$

where $F(\omega_x,\omega_y)$, $H(\omega_x,\omega_y)$ are the continuous Fourier transforms of $f(x,y)$, $h(x,y)$ respectively, and if $g(m\varepsilon,n\varepsilon)$ is defined by

$$g(m\varepsilon,n\varepsilon) = f(m\varepsilon,n\varepsilon) * h(m\varepsilon,n\varepsilon) = \sum_{k,\ell=-\infty}^{\infty} \varepsilon^2 f\left[(m-k)\varepsilon,(n-1)\varepsilon\right]h(k\varepsilon,l\varepsilon)$$

then the discrete Fourier transform of $g(m\varepsilon,n\varepsilon)$ is given by

$$G_D(\omega_x,\omega_y) = F_D(\omega_x,\omega_y)H_D(\omega_x,\omega_y)$$

where $F_D(\omega_x,\omega_y)$ $H_D(\omega_x,\omega_y)$ are the discrete Fourier transforms of $f(m\varepsilon,n\varepsilon)$, $h(m\varepsilon,n\varepsilon)$ respectively.

However in general $g_1(m\varepsilon,n\varepsilon) \neq g(m\varepsilon,n\varepsilon)$

$$\text{and } G_{1D}(\omega_x,\omega_y) \neq G_D(\omega_x,\omega_y)$$

where G_{1D} is the discrete Fourier transform of $g_1(m\varepsilon,n\varepsilon)$ i.e. sampling and convolution are not commutative.

Here in evaluating the Metz filters it is necessary to use discrete convolutions to obtain estimates of the corresponding continuous convolutions. Therefore one must consider under what conditions such approximations can be made, and what distortions are introduced as a result.

It is clear from the equations above and the discussion of discrete Fourier transforms in Section (ii), that if both functions $h(x,y)$ and $f(x,y)$ are such that their Fourier transforms are identically zero outside the square region $|\omega_x| < \pi/\varepsilon$ and $|\omega_y| < \pi/\varepsilon$, aliasing

will not occur. However if this condition does not hold $G_D(\omega_x,\omega_y)$ will be distorted so that it will not be equal to $G_1(\omega_x,\omega_y)$ and so $g_1(x,y)$ will not be equal to $g(x,y)$.

Thus, in order to minimize distortions when calculating Metz filters and processing images using discretely sampled data, the above conditions must apply, as nearly as possible, to the point spread function, the unprocessed image and the processed image.

(vi) Estimation of discrete convolutions in space domain

Consider a square matrix of dimensions a x a to be convoluted with another square matrix of dimensions N x N. For each point in the N x N result, a^2 real multiplications and a^2 real additions will be required, or a total of $2a^2N^2$ real operations for the entire convolution. When calculating convolutions of any functions, discrete or continuous, which are only defined within a limited region, edge effects may introduce distortions. Here, points closer than a/2 elements to the edge of the matrix obviously involve the use of points outside the matrix for their calculation, and so they will not be well-defined. This problem can be dealt with by reflecting the N x N matrix about its edges. This is equivalent to convoluting a periodic version of the N x N matrix with the a x a array, and it will at least give some estimate of the edge elements. (In the case of gamma camera data where the image is in fact only defined within a circular region inside the N x N matrix, edge effects may not be eliminated well by this procedure.)

(vii) Estimation of discrete convolutions using FFT

Alternatively this convolution could be performed by transforming both arrays to the frequency domain, multiplying them, and doing an inverse transform. The result is required to be the same as that

calculated by convoluting the a x a matrix with the periodic version of the N x N matrix in the space domain. Since the doubly discrete Fourier transform of the a x a array is equivalent to the transform of the periodic version of the a x a matrix with period equal to the dimensions of the array, the a x a array must be supplemented by enough zeros around its edges to prevent its periodic nature from affecting the region of interest in the convolution result. This can be done by adding zeros round the edges of the a x a matrix expanding it to a 2N x 2N matrix.

Total computational time is made up of time for the initial forward Fourier transforms, the complex multiplication of the two arrays and for the inverse Fourier transform.

In all, approximately

$2N^2(3\log_2 N + 2)$ complex additions

$2N^2(3\log_2 N + 2)$ complex subtractions

$N^2(6\log_2 N + 5)$ complex multiplications

are required. Obviously this compares favourably with a^2N^2 real additions and a^2n^2 real multiplications for reasonable values of a. Assuming that complex additions and subtractions take twice as long as real ones and that complex multiplications take four times as long as real ones, and if multiplications are the chief time-limiting factor, then the Fast Fourier Transform method will perform convolutions faster for

$4(6\log_2 N + 5) < a^2$

Thus for a 64 x 64 image the FFT will be quicker for $a \geq 13$.

(viii) Computation of discrete Metz filtered images

For the calculation of the Metz filters, Algorithm II (see

Section II A(viii)) was used:

$q^1(\underline{r}) = 2psf(-\underline{r}) - psf(-\underline{r}) * psf(-\underline{r}) * psf(\underline{r})$

$q^n(\underline{r}) = psf(-\underline{r}) + q^{n-1}(\underline{r}) - psf(-\underline{r}) * psf(\underline{r}) * q^{n-1}(\underline{r})$

A program was available (see Section II B(ix)) to compute the filters by this method, calculating the convolutions in the space domain, using truncated versions of the point spread function. Considerations in Section II B(vii) indicate that for the array sizes used, time might be saved by using FFT and performing the convolutions in the spatial frequency domain. However this was not done because of the convenience of using the program which was available. In any case time considerations are not so important here since this part of the computation is only performed once to calculate filters which can then be used to process many images.

The computer time can be kept low by truncating the initial 64 x 64 image matrix of the point spread function. This function is often narrow so that only elements near to its centre have significant counts, so that no significant error is introduced by using a much smaller matrix for the calculations.

Further truncation is also necessary during the calculation since with each convolution, the size of the matrix will increase so that after n iterations the side of the matrix will be $[(2n+1)a - 2n]$ elements, where a is the side of the initially truncated point spread function array. For a = 21, after 6 iterations, this would give a 261 x 261 matrix. Apart from requiring large amounts of core space to store them, these enlarged matrices will demand increased calculation time in each subsequent convolution involving them. However if even after truncation of the point spread function from a N x N matrix to an a x a one, the elements near the edges of the a x a matrix are small, then after convoluting one of these

matrices with another, they will become even smaller, and consequently if they are neglected, by truncating the matrices to dimensions a x a after each convolution, no great error will be introduced. An example of the effects of truncation is shown in Chapter III. The significance of the error will obviously be dependent on the shape of the point spread function, but this question has not been investigated thoroughly.

If this truncation is performed after each iteration, and if the convolution $psf(-\underline{r}) * psf(\underline{r})$ is stored after the first iteration, then each subsequent operation will require $a^2(a^2 + 2)$ arithmetic operations. If truncation were not done, then the number of operations required to calculate the nth order filter from the (n-1)th would be very approximately $\sim 16n^2a^4$ so that for example to calculate the 6th order filter the computer time might be over 400 times more than it is when truncation is performed. Thus although this calculation of the filters need only be done once to provide filters for use on many images, the computer time when no truncation is done might be totally prohibitive, and certainly would be a serious deterrent to the calculation of the filters.

Once the filters are obtained, the processed images can be calculated either directly in the space domain, or more quickly, in the frequency domain:

$$p^n(\underline{r}) = f(\underline{r}) * q^n(\underline{r}) = \text{F.T.}^{-1}\left[F(\underline{\omega})Q^n(\underline{\omega})\right]$$

Here the calculation was performed in the frequency domain, using FFTs.

(ix) Programs for computing and applying Metz filters

The programs described here use Algorithm II to calculate Metz filters in the space domain from a given point spread function.

The Metz filters are then transformed to the frequency domain using a FFT subroutine and stored on magnetic tape in this form for later use. To apply the filter to an image, the image is transformed to the frequency domain, multiplied by the specified filter retrieved from magnetic tape and then transformed back to the space domain for viewing.

The subroutine IMAGE1 calculates Metz filters from a digitized point spread function and stores them on magnetic tape. The point spread function is recorded and digitized in the same way as any other image, as a 64 x 64 array, for example. As discussed in Section B(viii) when the Metz filters are calculated in the space domain, the arrays resulting from the convolution procedures must be truncated if the calculation is not to put totally unrealistic demands on computer core space and time, and in fact, if elements near the edge of the original point spread function array contain negligible counts, the truncation will introduce no significant error since the elements lost by truncation would make no significant contribution to the elements of interest in the next iteration. However, even with truncation after each convolution to the size of the original a x a array the computational time can be very large. It is approximately proportional to a^4, so that reducing a can have a considerable effect in reducing the number of operations required. In view of this and of the fact that most useful point spread functions do decrease to negligible values within 5 or 10 elements of the peak, the subroutine will truncate the 64 x 64 array to a much smaller one centred on the peak of the point spread distribution. The program calculates the filters in the space domain but transforms them into the spatial frequency domain because they

are then ready for later use, and also because they are then in a convenient form for display and comparison. The subroutine IMAGE2 is then used to apply the filters to images.

CHAPTER III

Application of the Metz Filter

Abstract

The practical problems of calculating Metz filters and applying them to images obtained from a γ-camera-computer system are discussed in detail. The validity of the assumptions made is examined, and the properties of the filters obtained are shown. The problem of choosing the optimum order of filter to apply to a given image is then investigated by considering the application of various orders of the filter to images of a Siemens' star phantom recorded with different levels of noise. Images of the Siemens' star phantom have been used by others to calculate modulation transfer functions and here the frequency responses in the presence of noise are calculated from unprocessed and processed images of this phantom. Levels of frequency response obtained and the magnitudes of the fluctuations in frequency response are used to assess the distortion of the images caused by noise and so how the filter affects image noise level. From this a rough criterion is obtained for selection of the optimum order of filter under the conditions of this experiment.

CHAPTER III

Application of the Metz Filter

A. Assumptions in the derivation of the Metz filter, and their validity for a gamma camera system

(i) Stationarity of a gamma camera system

The validity of the derivation of the Metz filter rests, among other things, on the stationarity of the imaging system for a real object. A gamma camera system with an older-type gamma camera[1] was used for the experimental work described later and it is this system which is discussed here. Similar factors must be considered when using any other system, for example, a rectilinear scanner.

When considering some complex three-dimensional object at rest in front of the gamma camera, the question arises as to whether the response function (collected with high counts so that statistical noise is negligible) would be identical for the same point source placed at any point in the object, and so whether the response is the same for each point in a complex activity distribution. The responses may differ in magnitude or in shape, and further, the processes which cause these differences may interact with one another in a complex way. However, it will be seen that in many circumstances these variations may be small, so that the variation in the magnitude of the response may be compensated for by the "uniformity" correction, and variations in shape as well as the interactions between the various factors, may be neglected.

The components of the system which form the image and which cause the point source response to have a spread of finite width about its peak and the way in which they may vary will be discussed

in brief[2,3]. The system is shown diagrammatically in Figure III A. An image is formed when Y-rays from the object go through the parallel multihole collimator to the crystal where they are absorbed; the resulting photons are detected by the array of photomultiplier tubes, and the circuitry on these tubes is arranged so that their outputs give rise to signals indicating the position of the original scintillation. This positional information is then passed on to be displayed and/or recorded.

Consider the formation of an image from counts emitted by one active point P in a complex object; from the emission of Y-rays to the recording of positional signals, there are numerous sources of variation and error which give rise to three main contributions to the observed response to this point source of activity - the "geometric", "penetration" and "scattering" effects. The magnitude of the response and the nature of these effects may vary according to the position of P, as mentioned above.

The "geometric" contribution to the point spread function is generated only by those γ-rays which are emitted in a direction sufficiently nearly parallel to the collimator axis to travel along one of the holes of the collimator and enter the NaI crystal without being absorbed or scattered anywhere along their route. Clearly if the collimator holes are uniformly spaced, the same number and distribution of γ-rays should reach the crystal from a point source of the same activity placed anywhere in the same plane in the gamma camera field. This distribution will be narrow, contributing only to the observed central peak of the point spread function. However its width may increase for points further from the collimator since γ-rays emitted at small angles to the collimator axis may then reach the crystal at points further from the centre

of the distribution. In practice the objects scanned are usually not very long from front to back and so this effect will be very small.

The other two contributions to the formation of the point spread function are both due to γ-rays which do not take this "geometric" route to the crystal. The "penetration" contribution is caused by γ-rays which enter the collimator at an angle to its axis and penetrate the septa of the collimator, and around the edges of the collimator also by those γ-rays which originate from outside the region of the object which is in the field of the collimator but which penetrate the outer shielding. Obviously for a given collimator the importance of these effects depends mainly on isotope energy, and for low energies it may not be significant at all. Once again it can be seen from purely geometric considerations that the width of the distribution of these γ-rays at the crystal face may increase with the distance between the origin of the γ-rays and the collimator, since γ-rays emitted at an angle to the collimator and having energies sufficient to pass through say, 2 or 3 septa, may then arrive at points further from the centre of the point spread function. This effect too should be stationary across the plane of the collimator except near the edges of the field where stray radiation from outside the geometrical field of view of the collimator may be observed.

The third contribution to the point spread function is made up of those γ-rays which are scattered by the medium between the point source and the collimator. In soft tissue, medium energy γ-rays travel an average of 5 to 7 cm before undergoing Compton scattering[2];

the resulting secondary γ-rays may not reach the crystal, but if they do it will be at a point corresponding to the point of scattering and not the point of emission of the primary γ-ray. Obviously this effect will be less important for higher energy γ-rays which are less likely to interact with the surrounding medium. As well as scattering the γ-rays passing through it a medium may absorb them, and different points in a complex three-dimensional object may have media with varying thicknesses and scattering and absorbing properties between them and the collimator. Therefore this effect may be far from stationary over the object field, and can lead to "incorrect" points in the image and loss of γ-rays emitted in the object.

By whatever route the γ-rays reach the crystal surface, they must then interact within the crystal to give rise to a scintillation which will be detected by the adjacent array of photomultiplier tubes, if they are to be processed and recorded. The variations and statistical uncertainties in the interaction within the crystal, the response of the photomultiplier tubes and associated circuitry and of the data handling and recording devices all contribute further to the width of the point spread function in the sense that in these parts of the system too there is not a unique output for every input. Also, since the response of the ADCs, for example, is not necessarily stationary over the whole image, stationarity may also be affected.

Ideally the incident γ-ray will enter the crystal in a direction parallel to the collimator axis and give up all its energy in a photoelectric interaction thus producing a secondary electron which

will cause scintillation along its pathlength, typically of about .25mm long[2], and so effectively at the same position in the crystal plane as the γ-ray entered the crystal. In practice however, the incident γ-ray may not give up all its energy in a single photoelectric interaction, but instead it may undergo one or more Compton scattering interactions to give rise to secondary γ-rays and Compton electrons; the secondary γ-rays themselves may then give up their energy in photoelectric interactions, or they may escape from the crystal without giving up their energy. If they do escape from the crystal, the only scintillation will be that due to the Compton electron, which will be correctly located, but if the secondary γ-rays undergo photoelectric interaction the resulting centre of luminous activity of the scintillations due to the photoelectron and the much lower energy Compton electron will depend on the distance travelled by the secondary γ-ray before it undergoes photoelectric interaction. In thin crystals the average distance travelled is small ~ 2.5 mm[2] so that the position signals will mostly be almost correct, and this effect will not give rise to much loss of resolution, although when the energy of the original γ-ray is above about 200 keV initial Compton scatter may occur as frequently as photoelectric interaction.

A further contribution to the point spread function which is caused by interactions within the crystal only affects γ-rays incident near the edges of the camera field and is caused by internal reflection of light at the edges of the crystal. The NaI crystal has a high refractive index, and so when scintillations occur near the edges of the crystal the light may be reflected and the photomultiplier tubes will respond again to this reflected light,

and the number of counts recorded in these regions will exceed the true number.

There is also a loss of resolution due to the variation inherent in the use of a photomultiplier array for determining position. The output of a photomultiplier tube depends on the number of electrons produced in response to incident light on the photocathode, and although this number is proportional to the brightness of the light it is also governed by statistical factors. The more light there is the less the relative variation since the loss of resolution is proportion to the inverse of the square root of the brightness of scintillation[2] and consequently this factor is less important for high energy γ-rays.

The response of the photomultipliers to scintillations which occur at intermediate points between the tubes may not be good; although there are deflectors to direct light from these points towards the nearest tubes, and although the proportionate division of light among the tubes should not be affected, counts may be lost here giving areas of diminished activity in the final image.

When a scintillation occurs the total amount of light produced, and so the total response of the photomultiplier tubes will, as mentioned above, depend on the energy of the secondary electron transferred to it from the original γ-ray; but the proportionate division of light among the tubes depends on the position where the scintillation occurred, since the tubes nearest in position to the scintillation will be activated more than the distant ones. The circuitry is designed to use this positional information to produce position signals representing the X and Y coordinates of the position

of the scintillation. If the camera is well-tuned these signals should give an accurate representation of the positions of the counts. These signals are then passed to the data handling and recording system.

However the use of photomultiplier tubes to provide position signals involves a dependence on the total energy present to charge the tubes, although the circuitry can be designed to avoid gross variation with energy. To eliminate errors due to this the sum of the outputs of all the photomultiplier tubes, which is proportional to the energy, is fed through a pulse height analyzer. As a result those position signals which might be incorrect because the energy of the γ-ray producing them is outside the selected range are not included in the image.

The exclusion of these counts has many advantages since in fact most of those γ-rays with higher or lower energies will in any case contribute to errors in the image, as mentioned above. Most background radiation will be excluded, and so will much of that due to scattering in the object and surrounding medium since most scattered γ-rays will have considerably lower energies than the primary ones. Signals due to low energy Compton electrons produced in the NaI crystal will also be rejected.

Those signals which are accepted by the pulse height analyser are then transferred to the data handling and recording system. Within the γ-camera itself the positional information is used to light up points at appropriate positions on an oscilloscope screen, and photographs may be taken from this. When the data is also to be digitized, analyzed and recorded, the signals pass through analogue-to-digital converters and generally into a digital computer

or onto digital magnetic tape. All these stages of processing have their sources of variation; in particular the analogue-to-digital converters may not be completely linear in their response causing rows or columns of raised count rate in parts of the image, although this effect may not be marked with good analogue-to-digital converters.

The overall process of image formation by a gamma camera system is summarized in Table IIIA. It can be considered in two stages. Firstly scintillations are produced in the NaI crystal, at positions subject to random variation about the point of origin of the γ-rays as described by the point spread function. This process (described by stages 1 and 2 in Table IIIA) is almost uniform over the crystal face, but then these scintillations are transmitted to the recording system by a process (described by stages 3 and 4 in Table IIIA) involving constant non-uniform distortion in the photomultiplier array and the analogue-to-digital converters. The non-uniform distortions in the earlier stages of the process and the random variations in the later stages are assumed to be negligible. If and when these assumptions are valid, it seems justifiable to use a standard uniformity correction to correct for the distortions due to non-uniformity, and the Metz filter to correct for the finite spread of the point source response.

These assumptions are most likely to be valid when the object is thin, when scattering throughout the object is low and fairly uniform, and when the isotope energy is not too low (the acceptable range of radioisotope energies is from about 80 to 500 keV provided thicker collimators are used as energy increases), and the final number of counts in the image high.

(ii) Linearity of the gamma camera system

A second relevant property of the system if any sort of deconvolution approach to image processing is to be applied is linearity, or in other words, how the sum of the images recorded when many different objects are recorded separately compares to the image recorded when all the objects are observed together. In the gamma camera system linearity is broken mostly by statistical noise, proportional to the square root of the number of counts[4], and this is obviously relatively more significant when there are few counts. In practice the signal-to-noise ratio is low chiefly in the higher spatial frequencies, where the noise is allowed for in the Metz filter approximation. However if there are very high noise levels, lower orders of the filter have to be used, and these may obscure features of interest as well as removing noise.

(iii) Edge effects

Obviously the image is not recorded outside the field of view of the gamma camera and assumptions must be made about the distribution of activity outside this field. The simplest assumption is that all regions outside this field have no activity; an alternative assumption which is also easy to use in the digital computation of convolutions is that the activity distribution around the region of interest may be represented by reflecting the 64 x 64 image matrix about its edges. In practice both these assumptions may introduce errors if there is activity close to but outside the circular field of the gamma camera which may give rise to counts being recorded within this field, as described by the point spread function. In this case, errors will already be introduced by

using the 64 x 64 matrix when the actual sensitive field of the camera is a circle within this matrix.

These errors will be minimized if the activity is localized in an area well covered by the circular field of the camera.

(iv) Assumptions made in digital processing

As discussed previously, if digital Fourier Transforms are to be performed then the frequency spectra of the point spread function, the Metz filters, and the original and processed images must all tend to zero near the Nyquist frequency.

For the gamma camera system used here, the diameter of the field is 27.5 cm and the field can be divided into an array of 64 x 64 cells or 128 x 128 cells, though in general the 64 x 64 cell array gives adequate detail. The Nyquist frequency will therefore be 1.18 cm^{-1} and one can check by observation of the spatial frequency spectra mentioned above that they do all tend to zero as required, and only when the count density in the image is very low may this assumption be broken.

B. Calculation and Application of the Metz filters

(i) Conditions of operation of the gamma camera system

The complete procedure of recording a point spread function, calculating Metz filters, and using them to process an image is described as an illustration of the methods and principles mentioned above. In this case it was decided to study and process the image of a test object containing hot regions of ^{133}Xe, which emits 80 kev γ-rays. The test object chosen was a Siemens' star phantom placed 8.5 cm from the collimator face in water. The collimator used was a low energy collimator which has relatively thin septa since there is very little septal penetration with such low energy radiation, and if the septa are narrow only very little radiation is lost due to absorption in the septa.

To calculate the Metz filters it is necessary to obtain the point spread function for the system under the same conditions as the object itself would be scanned, and so it is useful to consider which conditions are important in this respect. Firstly the pulse height analyser of the gamma camera is set to include the photopeak part of the spectrum of γ-rays reaching the NaI crystal, and to exclude most of the Compton-scattered γ-rays. For such low energy γ-rays as are emitted by ^{133}Xe this is a difficult compromise to reach since the Compton scatter spectrum considerably overlaps the photopeak. However after observation of the entire energy spectrum, it was decided to set the pulse height analyser to admit γ-rays with energies within 25% of the 80 kev centre of the photopeak.

The analogue-to-digital converters are also set to a fixed level of threshhold and gain so that the circular field of the camera is represented by a fixed shape in the digitized image.

This shape can be circular or otherwise, so long as it is reproducible on future occasions when the same Metz filters may be used to correct other images. For reasons of convenience of computer print-out and display, an ellipse with diameters of 60, 50 cells was chosen for all these studies. The performance of the ADCs does vary from time to time but the threshhold and gain are adjusted so that this fixed shape is maintained.

These conditions of selecting the collimator, the pulse height analyser settings and ADC settings define the non-uniform response for an isotope of a given energy of emission. This characteristic non-uniform response is found by recording the image of a large flat uniform source of the selected radioisotope for sufficiently long to obtain good statistics of the cell-to-cell variation in count density - generally at least 300,000 counts in the image are required. This non-uniform response may change from day to day according to the condition of the photomultiplier tubes and the electronic circuitry, and so this uniformity image must be recorded every time a study is performed.

(ii) The point spread function

Once the gamma camera has been set up appropriately, a point source response may be recorded. Obviously the point source should be as small as is practical, but it may be difficult to obtain a high activity in a very small volume, and so again a compromise must be reached. In this case ^{133}Xe dissolved in saline was placed in a very small source and was scanned at a distance of 8.5 cm in water from the collimator face. The point source was placed near the centre of the camera field to ensure that the tail of the response function would not be lost.

To investigate how small a point source is required to get a good estimate of the response without additional blurring due to the finite width of the source, response functions were recorded from "point" sources of various widths. No difference was detected between the various "point" sources used and because it comes out of solution very readily, it was much easier to obtain ^{133}Xe in a slightly larger container, and so the widest "point" source was used.

Once again it is necessary to record many counts in order to obtain a good assessment not only near the peak of the function where the count rate is relatively high but also near the edges where the count rate will be low, and may in fact be comparable with background levels. Thus in order to obtain a good estimate of the point spread function alone without the background, it is necessary to record a separate image with no source in place, and to subtract this background image from the recorded point source response. The measured point source response must also be corrected for the non-uniformity of the gamma camera.

For ^{133}Xe in water at 8.5 cm the point spread function was found to have circular symmetry and its full width at half maximum was 3.7 cells or 1.59 cm. It differed only slightly from a Gaussian. It was seen to have decreased to 1% of its maximum within 8 cells or 3.44 cm, so that calculations of Metz filters using truncated versions of this function are likely to be fairly accurate.

(iii) Calculations of Metz filters

The Metz filters were calculated in the space domain using the program described in Chapter II. To assess the effects of truncating the point source response, the modulation transfer function

and the Metz filters were calculated using different levels of truncation. It was apparent that truncation from 64 cells to 31 cells led to no observable distortion, but after truncation to 21 cells the modulation transfer function was very slightly altered; as one would expect the MTF calculated from the 21 x 21 cell version had very slightly less of the high frequency components and more of the low frequency ones than the 31 x 31 cell version. There was also a difference, but only a very slight one, in the Metz filters. Since calculations using the 31 x 31 matrix are not impractically long, this version in fact was used to calculate a set of filters for use for image processing, but in fact the 21 x 21 cell version would certainly have given results which were not noticeably different.

The characteristics of the Metz filters can be displayed in various ways as illustrated in Graphs IIIA, B. Since the point source response was circularly symmetric, the Metz filters also have this symmetry.

(iv) Recording and processing an image

The object was recorded in water at 8.5 cm from the collimator. For good statistics many counts are recorded (clearly in clinical situations this may not be possible) so that the image will be as good as possible and also so that the image processing will not give rise to loss of image detail through the necessity to avoid amplifying statistical noise.

The image is first corrected for the non-uniform response of the camera, and then Metz filters of the desired orders are applied. Examples of the results are shown (see Figs. IIIB, C, D, E).

C. Investigation of the performance of the Metz filter under varying signal-to-noise ratio using a Siemens' star phantom and ^{133}Xenon

(i) Object of the experiment

One of the chief problems in using the Metz filter is how to select the most suitable order of the filter to apply to a given image. In general the higher the signal-to-noise ratio the higher the order of Metz filter that can be used without severely amplifying the noise and so degrading the image. To assess the performance of the filters, images of a phantom were recorded under the same conditions but with differing count densities, and so differing signal-to-noise ratios, and these images were then processed with several orders of the Metz filter. The phantom chosen was the Siemens' star phantom, because, under certain conditions, it enables one to calculate quantitative indices of filter performance from the image[5].

(ii) Structure of the phantom

The Siemens' star phantom used for this study was a hollow plastic container; its external thickness was about 1.9 cm and its length about 32.2 cm so that it almost filled the gamma camera field. The hollow space inside the phantom was shaped so that the inside depth varied sinusoidally along any arc of a circle centred at the vertex 0; the maximum depth was about 0.6 cm and the minimum zero. When the phantom is filled with a liquid of constant activity per unit volume, the resulting activity distribution can be described by the formula $a(r,\theta) = A \cos(\omega\theta)$
where A is a constant depending on the activity present, the vertex of the phantom is the origin of the polar coordinates (r,θ), and ω

is the frequency in radians^{-1}. Activity is maximum for $\theta = 0$, $\pi/12, \ldots n\pi/12$ so that $\omega = 24$ radians^{-1}, and the activity distribution along any arc of radius r centred at the vertex is a pure sine wave with wavelength $r\pi/12$ and spatial frequency $12/\pi r$.

In the absence of noise the image corresponding to this object will be formed by the process $F(\underline{\omega}) = M(\underline{\omega})\ \Phi(\underline{\omega})$ but it is clear here that if the modulation transfer function is circularly symmetric, so that $M(\underline{\omega}) \equiv M(|\underline{\omega}|)$, then the image count distribution will be of the same form as the object distribution and so may be described by $c(r,\theta) = C \cos(\omega\theta)$. In the case of ^{133}Xe the modulation transfer function is circularly symmetric. ^{133}Xe emits 80 keV gamma rays, and at this low energy there is no collimator septum penetration and so the chief contribution to the increase in width of the point spread function beyond the geometrical limits is due to scattering in the medium between the source and the collimator. Since this is not a directional phenomenon, it should give rise to a circularly symmetric point spread function which will result in a circularly symmetric modulation transfer function. The point spread function obtained from ^{133}Xe was found to be circularly symmetric to within the limits of experimental error. Thus the image count density distribution when using ^{133}Xe should be of the form $c(r,\theta) = C \sin(\omega\theta)$ where $\theta = 12/\pi r$ and C is constant, and in fact the images obtained do appear to be of this form.

(iii) Experimental conditions and calculations

The phantom was placed 8.5cm from the collimator face in a tank of water. Water has scattering properties similar to soft tissue. The gamma camera and the associated HP 2100 computer have been described in a previous section.

The ability of the system to transfer information from the object to a noiseless image may be assessed by looking at the modulation transfer function i.e. the ratio between modulation of count densities in the image to the modulation of activity in the object at a given frequency.

$M(\underline{\omega}) = F(\underline{\omega})/\Phi(\underline{\omega})$

or for a circularly symmetric point spread function

$M(\omega) = F(\omega)/\Phi(\omega)$ where now $\omega \equiv |\underline{\omega}|$.

Similarly, when considering transfer of information from the object to a processed image, the processed frequency response, $S^n(\omega)$, may be used to describe the process.

$S^n(\underline{\omega}) = \Phi^n(\omega)/\Phi(\omega)$ where $\Phi^n(\underline{\omega})$ is the count distribution, in the spatial frequency domain, of the nth order processed image.

Now $\Phi^n(\underline{\omega}) = Q^n(\underline{\omega})\ F(\underline{\omega})$

$\therefore S^n(\underline{\omega}) = Q^n(\underline{\omega})\ F(\underline{\omega})/\Phi(\underline{\omega}) = Q^n(\underline{\omega})\ M(\underline{\omega})$

Thus $S^n(\underline{\omega})$ may be calculated from $Q^n(\underline{\omega})$ and $M(\underline{\omega})$.

In theory, if they are circularly symmetric, both the modulation transfer function and the processed frequency response may be measured from the Siemens' star phantom, since object and image contain pure sinusoidal distributions of activity and counts respectively.

Modulation of activity distribution in the object at frequency ω is equal to $(a_p - a_t)/(a_p + a_t)$ where a_p, a_t are the activities at the peaks and troughs of the star phantom, respectively, at frequency ω. However since $a_t = 0$ at all troughs of the sine wave, this ratio is equal to 1 for all ω.

Modulation of count distribution in the image at frequency ω is equal to $(c_p - c_t)/(c_p + c_t)$ where c_p, c_t are the count densities at the peaks and troughs of the image, respectively.

Now $M(\omega) = (c_p - c_t)/(c_p + c_t)$ simply, where now $M(\omega)$ is the modulation transfer function for spatial frequency ω in any direction.

The modulation transfer function is defined for the unprocessed image; the processed frequency response is defined exactly analogously but for the processed image, and it can therefore be calculated from processed images of the star phantom in the same way as the modulation transfer function is calculated from the unprocessed image.
Thus $S^n(\omega) = (c_p{}^n - c_t{}^n)/(c_p{}^n + c_t{}^n)$ where $c_p{}^n$, $c_t{}^n$ are the count densities at the peaks and troughs respectively of nth order Metz filtered images, and $S^n(\omega)$ is the processed frequency response for spatial frequency ω in any direction.
Thus $M(\omega)$ and $S^n(\omega)$ can be calculated from the Siemens' star phantom if an image is obtained with sufficient counts for it to be effectively a noiseless image. This would require a very large number of counts because while it may be easy to estimate the count density at the peaks with very little error, many more counts must be recorded to give good estimates of the counts at the troughs of the distribution. However if sufficient counts are recorded the modulation transfer function and processed frequency response functions obtained in this way should be exactly the same as those calculated as the Fourier transform of the point spread function and $Q^n(\omega)M(\omega)$ respectively.

$M(\omega)$ and $S^n(\omega)$ describe the performance of the system in the absence of noise by measuring how well modulations are transferred from the object to the unprocessed and processed images respectively. In order to assess the image quality achieved in practice in unprocessed and processed images in the presence of noise, it is useful to define empirical functions, $M_E(\omega)$ and $S_E{}^n(\omega)$ which are analogous

to $M(\omega)$ and $S^n(\omega)$ and are calculated from the unprocessed and processed images in just the same way, but in the presence of noise.
i.e. $M_E(\omega) = (c_p - c_t)/(c_p + c_t)$ and $S_E^n(\omega) = (c_p^n - c_t^n)/(c_p^n + c_t^n)$ where c_p, c_t, c_p^n, c_t^n are measured in the presence of noise and $M_E(\omega)$, $S_E^n(\omega)$ describe the transfer of modulations from the object to the unprocessed and processed images in the presence of noise. These empirical functions are useful for descriptive purposes, as will be seen in the next section, but they are not uniquely defined; their forms depend on the noise level in the image, and also, since noise is a statistical phenomenon, the exact form of the function will not be identical even for images with the same noise levels.

(iv) Results - information transfer in the presence of noise

In the noiseless image, information transfer is described by the modulation transfer function, and in the noiseless processed image, by the processed frequency response function. The forms of these functions are discussed in Chapter II A(vii). For low frequencies the modulation transfer function is 1.0, i.e. transfer is perfect, but at higher frequencies it gradually decreases to zero. The processed frequency response curves remain near 1.0 to higher and higher frequencies as the order of the Metz filter increases, but they then decrease to zero more rapidly than the modulation transfer function. This is because Metz filters aim to improve the image at the low frequency end of the spectrum, and to eliminate completely the higher frequency components where noise predominates and degrades the image. The empirical frequency response curves obtained in this experiment were considered in order

to assess how well this aim is realized in the presence of increasing levels of noise.

The appropriate modulation transfer function and processed frequency responses were obtained prior to this experiment. This was done by recording an image with a very large number of counts of a point source of ^{133}Xe placed in water 8.5cm from the collimator face, correcting this for the non-uniformity of the camera, and calculating $M(\omega)$ = F.T.(psf) and $S^n(\omega) = Q^n(\omega)\ M(\omega)$. These curves are referred to in this section as the "theoretical" curves to distinguish them from the empirical curves measured from the star phantom in the presence of noise. These are shown in Graphs III C, D, E, F together with curves representing the empirical frequency responses in the presence of noise, calculated from unprocessed and processed images of the Siemens' star phantom. It can be seen that the empirical curves obtained at all levels of noise are similar in their general shape to the corresponding theoretical frequency curves. However when the curves are examined in detail some differences are apparent.

The curves are overall somewhat lower than the corresponding theoretical ones. This is because the sample size in the digitized images is approximately 6mm, and although this is small, it is too large to isolate troughs and peaks exactly, so that the counts at a peak will always be underestimated and the counts at a trough overestimated, thus lowering the modulation measured at all frequencies.

As well as this general lowering of the curves, there is a further obvious difference of the empirical frequency response curves from the corresponding theoretical ones in that the empirical curves are not a series of smooth curves but show considerable apparently random variation about such curves. These variations increase for lower image count densities, describing the deterioration

in image quality as noise increases at low count densities. Although the signal-to-noise ratio is relatively high at low spatial frequencies, random noise is present throughout the frequency spectrum. It may therefore increase or lower the amplitudes of components of any spatial frequencies, thus giving rise to the observed variations in the empirical frequency response curves. When there are variations in the frequency response as shown by these curves, distortions may be introduced since, owing to the presence of noise, some low frequency components which according to the modulation transfer function the system is able to transfer well may be supressed, and some high frequency components which the system is unable to transfer well so that their amplitudes are not accurately known may be raised substantially by the addition of noise. These variations may also indicate that components at frequences close to each other in the spectrum may be modulated very differently from one another, and these sharp edges in the frequency spectrum may lead to production of artifacts in the final image giving it a confusing and mottled appearance.

Similar effects are seen in the frequency response curves for all the unprocessed and processed images, but the variability of the curves differs for the unprocessed frequency response curves and for each order of Metz filter. All the curves become increasingly variable at low count densities, but at any given count density, the higher the order of Metz filter, the less smooth the curve. The processed frequency response curves for Metz filters up to about tenth order all appear smoother than the corresponding unprocessed curves. The increased variation for higher order Metz filters is to be expected since higher order Metz filters will amplify components of all frequencies more.

The variations in the curves due to noise obscure any other effects and in order to investigate this further and to make the observations regarding the general level and the fluctuations in frequency response more quantitative, attempts were made to fit the curves to some analytic functions. A function for fitting the curves was calculated by assuming that the point spread function was approximately Gaussian and then deriving an analytic form to which the theoretical and so also the empirical frequency response should approximate.

The formula used was

$$S^n(z) = p_1 - (1 - p_2\, e^{-p_3/z^2})^{n+1}$$

where p_1, p_2, p_3 are the parameters to be fitted and for reasons of convenience the variable is not spatial frequency ω, but $z = 12/\pi\omega$, so that z is the radius (in cells) of the arc on the image of the Siemens' star phantom which corresponds to the activity distribution with spatial frequency ω. Derivation of this formula is given in Appendix III A. The curve fitting was carried out using a nonlinear least squares fitting program from the BMD programs[6] and the empirical frequency response curves appeared to fit functions of this form well (see Graph III G).

With the aid of these analytic curves, the performance of the filters in the presence of noise was investigated firstly by plotting and inspecting these analytic curves and secondly by calculating a quantitative index to describe the level of random noise. Analytic curves for the same orders of Metz filter at different noise levels are shown in the graphs. These curves show that with increasing levels of noise there is a tendency for lower frequencies to be amplified less and higher frequencies more than when there is very little noise.

Random noise gives rise to the random variations in the empirical processed frequency response curves and so to distortions and artifacts in the image. The magnitude of the effects of the noise on the image was assessed by calculating the sum of squares of the deviations of each empirical curve about the corresponding fitted analytic curve. The behaviour of this sum of squares for unprocessed and processed empirical frequency response curves with varying image count density is shown in Graph III H. The sum of squares increases with decreasing count densities, and at any given count density the higher the order of Metz filter, the greater its value is, although it is still not as great as for the corresponding unprocessed image. Since it reflects the observed extent of variation of the curves in this way, this sum of squares has been used as a quantitative index to describe empirically the level of image noise.

(v) Discussion

The object of this experiment was to examine the performance of the system consisting of the gamma camera interfaced to the computer with or without the Metz filtering process, and to see under what levels of noise a processed image is better than the unprocessed one, or the converse, and if processed images are better, which order filter is optimum. It is clear that Metz filtering results in some information, particularly at lower frequencies, being more effectively transferred from object to image, but at high noise levels the amplification caused by the filter may enhance the effects of noise. This gives rise to increased variation in the frequency spectrum corresponding to the presence of more artifacts in the image. However the unprocessed image itself may have much noise and therefore some artifacts, and some of this noise may be lost as a result of suppression of high frequencies

by the Metz filter. In considering whether or not to process images, it is therefore useful to consider when the processed image is likely to contain more artifacts than the unprocessed, and at high levels of noise whether the use of Metz filters does still improve the overall level of information transfer.

These two factors may be considered by examining the analytic fitted curves and the behaviour of the quantitative index. Inspection of the curves themselves reveals that (i) for all levels of image noise the frequency response at low frequencies is greater than that at high frequencies i.e. the signal-to-noise ratio is always greater at the low end of the frequency spectrum, (ii) at very high levels of noise, the frequency response is, however, lowered; this effect becomes more marked for higher orders of Metz filter because there is then greater amplification of these frequencies, (iii) at high frequencies there is a tendency for the empirical frequency response to be slightly higher when the noise level is greater - this increase can of course only be due to noise and not to a real increase in information transferred from object to image. Thus on the basis of the forms of these analytic fitted curves one would expect that Metz filtering is always beneficial even from the point of view of image noise, since amplification of low frequencies relative to higher ones should always improve the overall signal-to-noise ratio in the image. However, the improvement achieved by filtering would be more significant for less noisy images.

It is also necessary to consider if and in what way these conclusions are modified when the variations of the observed frequency response about these fitted curves are examined. This is described by the performance index mentioned in the previous section (sum of squares of the deviations of the observed points

from the corresponding fitted empirical frequency response curve); the behaviour of this index is shown in Graph III H. The deterioration in image quality of higher orders of Metz filter is shown in the increase in this index. For a given order of Metz filter the index also increases as noise level becomes greater. However, this increase is not steady; it is only gradual at lower noise levels and then increases more rapidly. The transition between the slow increase and the faster one occurs at lower noise levels for lower orders of Metz filter e.g. for order 10, at a noise level indicated by about 200 K image counts, and for order 3, at a noise level indicated by about 20 K image counts.

Now it is evident from the fitted curves and from observations of the processed images, that at high count levels, indicated by 400 K image counts for example, higher order Metz filters give better images. Therefore until image counts and so overall-signal-to-noise ratio decreases to a level where the observed noise, as measured by the performance index, increases significantly for a given order of Metz filter, then it is better to use that order than a lower one. It should be noted though that if very high order Metz filtering were used, the performance index would rise above that for the unprocessed image. This did not occur here since only filters up to order 10 were applied, but this would provide another higher limit to the order of Metz filter which would be of use.

When attempting to apply these rules for determining the optimum order of Metz filtering for processing, the problem arises as to how to compare the count densities of images for this purpose. To judge the images by their total numbers of counts is obviously not reasonable since an image containing small hot structures in a

cold background may be clearly defined with fewer counts than an image with larger hot areas and only small cold spots. Maximum counts per unit area within the region of interest seems a reasonable measurement to try, and applications of the above criteria, using this measurement, are discussed in Chapters IV and V.

APPENDIX IIIA

The derivation of the model used for the empirical frequency response curves is given here.

Assume that the point spread function is approximately a Gaussian with mean μ, variance σ

$$psf(x) = \frac{1}{\sqrt{2\pi}\,\sigma} \exp\left[- \frac{1}{2\sigma^2} (x-\mu)^2 \right]$$

$$\therefore M(\omega) = F.T.\ \{psf(x)\} = \int_{-\infty}^{\infty} psf(x) e^{-2\pi i\omega x}\, dx$$

$$= \frac{1}{\sqrt{2\pi}\,\sigma} \int_{-\infty}^{\infty} \exp\left[- \frac{1}{2\sigma^2} (x-\mu)^2 - 2\pi i\omega x \right] dx$$

$$= \frac{1}{\sqrt{2\pi}\,\sigma} e^{-2\pi i\omega\mu} \int_{-\infty}^{\infty} \exp\left[- \frac{1}{2\sigma^2} (x' + 2\pi i\omega\sigma^2)^2 - 2\sigma^2\omega^2\pi^2 \right] dx'$$

where $x' = x-\mu$

$$\therefore M(\omega) = e^{-2\pi i\omega\mu}\, e^{-2\pi^2\sigma^2\omega^2}$$

and $|M(\omega)| = e^{-2\pi^2\sigma^2\omega^2}$

$$\therefore S^n(\omega) = Q^n(\omega)M(\omega) = 1 - \left[1 - |M(\omega)|^2 \right]^{n+1}$$

becomes $S^n(\omega) = 1 - \left[1 - e^{-4\pi^2\sigma^2\omega^2} \right]^{n+1}$

However since we notice general lowering of the curve, in the model the initial constant 1.0 is replaced by the parameter p_1. Also since the actual frequency response is a modified Gaussian, the parameters p_2 and p_3 are introduced:

$$S^n(\omega) = p_1 - \left[1 - p_2 \, e^{-p_3/z^2} \right]^{n+1}$$

where $z = 12/\pi\omega$

Table IIIA

Contributions to the Point Spread Function in a Gamma Camera System

Factors determining position in an image at which γ-rays emitted at a source point in the object are detected

	Relative magnitude	Variation over object field (i) across camera field (ii) with increasing distance from collimator	Variation with increasing isotope energy
1. Path from source to crystal surface (a) Geometric contribution - narrow distribution corresponding to peak of psf	Chief contribution	(i) - (ii) width up slightly	-
(b) Penetration contribution - wider distribution	Small contribution	(i) edge effects only (ii) width up slightly	Magnitude and width up slightly
(c) Scattering contribution - wider distribution	Small contribution - also counts lost	(i) & (ii) depend on source and medium around it	Magnitude down
2. Interactions within crystal (a) Single P.E. interaction - narrow distribution corresponding to peak of psf.	These contributions may be partly eliminated by use of pulse height analyser	-	Relative magnitudes of these contributions depend on isotope energy.
(b) Compton scattering + 2^{o} e^{-} going out of crystal - narrow distribution.		-	
(c) Compton scattering + 2^{o} e^{-} undergoing P.E. interaction - wider distribution.		-	
(d) Internal reflection of light from edges of crystal.		Edge effect only	

Table IIIA Continued

3. Use of photomultiplier (pm) array (a) Responses of pm tubes - statistical variation in pm tube output		-	Less important for high energies
(b) Light incident between pm tubes and deflected to nearest tubes - counts may be lost		Effect only between pm tubes	
4. Processing positional information in electronic analogue circuitry, ADCs etc. Non linearities may arise, also statistical variation		Effects may be local or general	

Fig. III A Diagrammatic representation of the gamma camera system

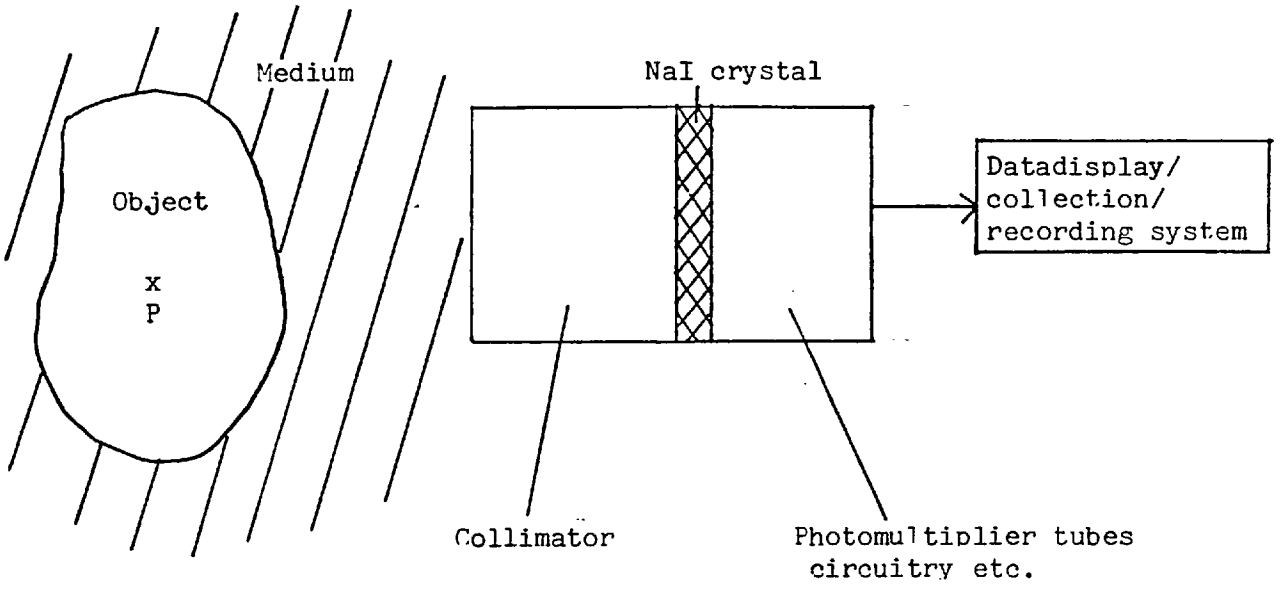

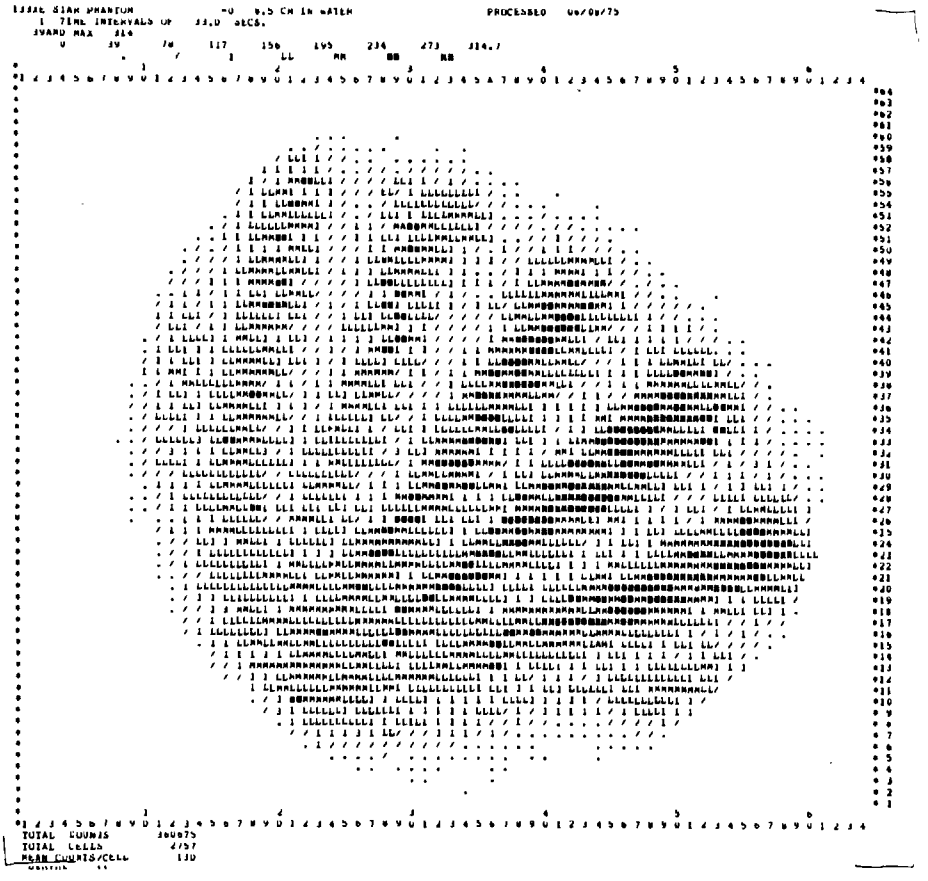

Fig. III B Siemens' star phantom - ^{133}Xe in water at 8.5 cm - 360.7 K counts.

Unprocessed

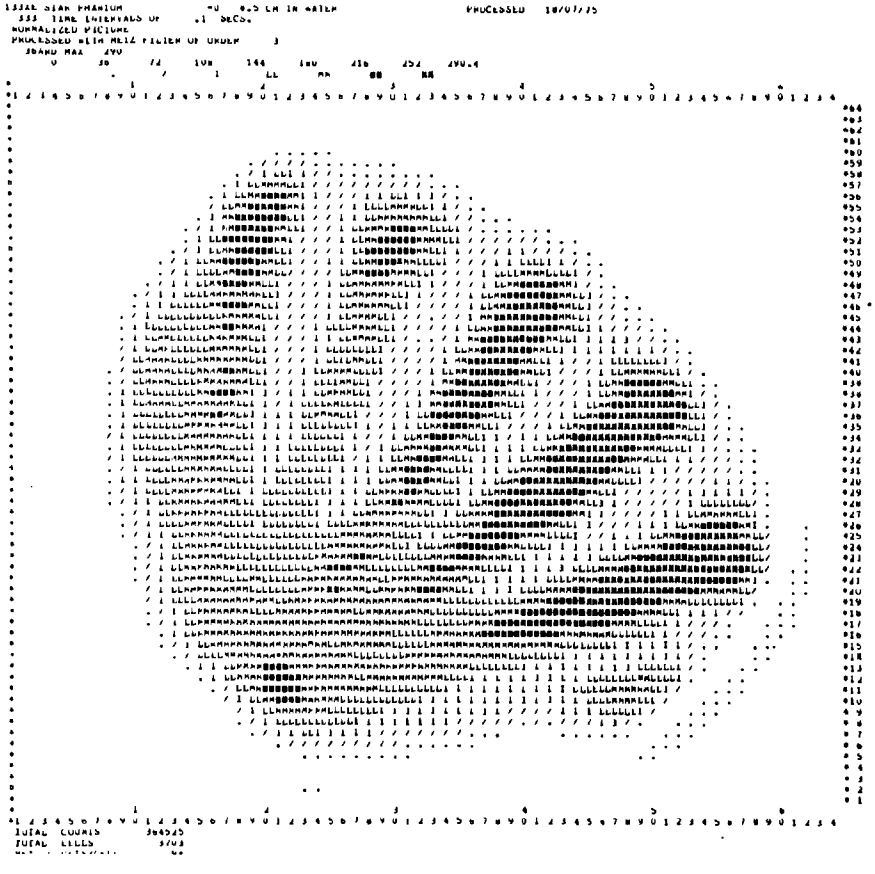

Fig. III C Siemens' star phantom - ^{133}Xe in water at 8.5 cm - 360.7 K counts.

Processed with 3rd order Metz filter.

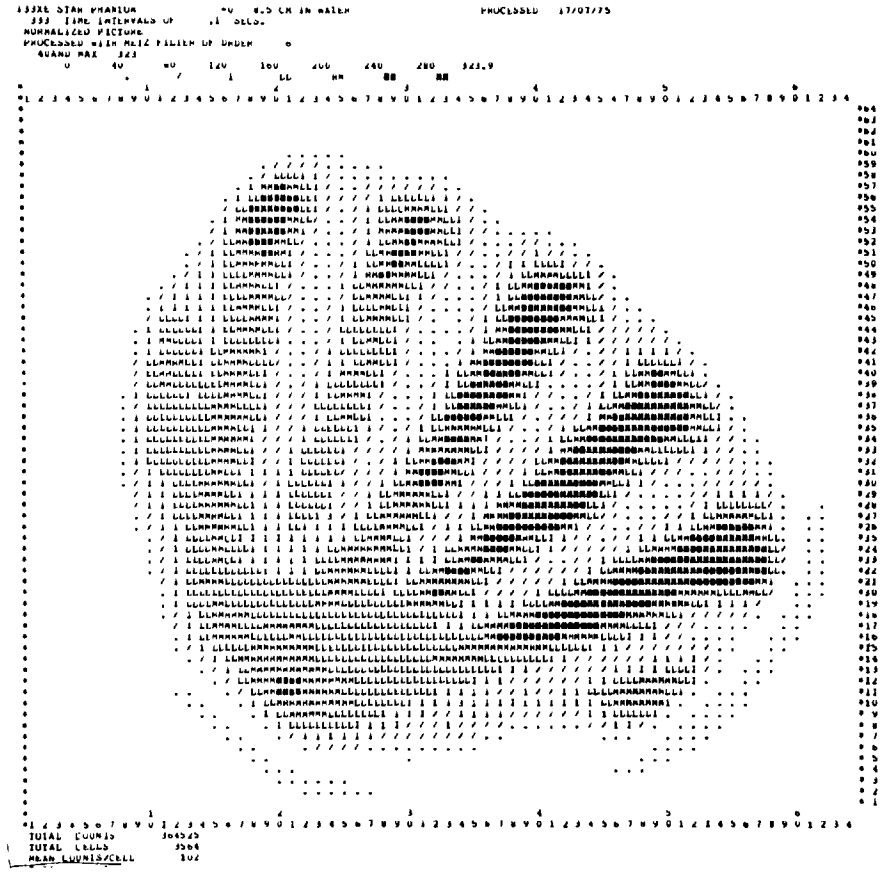

Fig. III D Siemens' star phantom - ^{133}Xe in water at 8.5 cm - 360.7 K counts.

Processed with 6th order Metz filter.

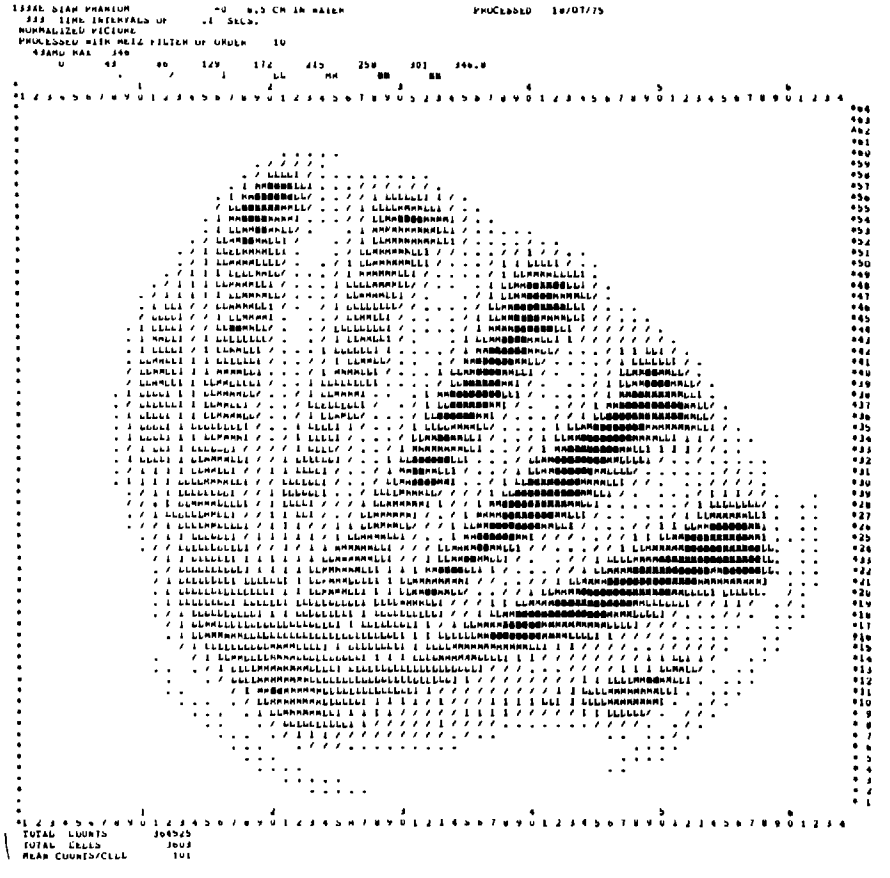

Fig. III E Siemens' star phantom - ^{133}Xe in water at 8.5 cm - 360.7 K counts.

Processed with 10th order Metz filter.

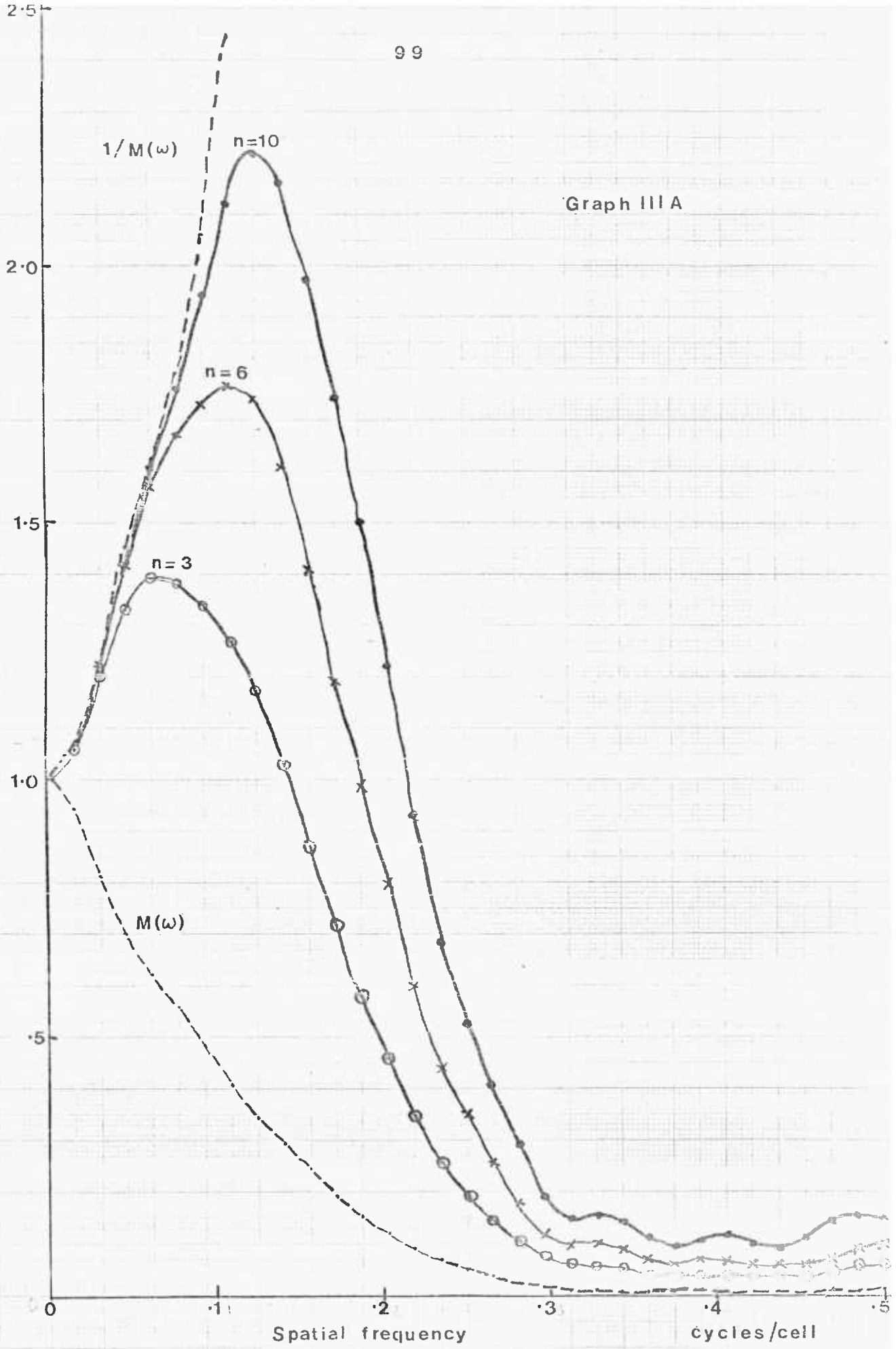

Processor frequency response – Metz filters

^{133}Xe in water at 8.5 cm

Graph III B

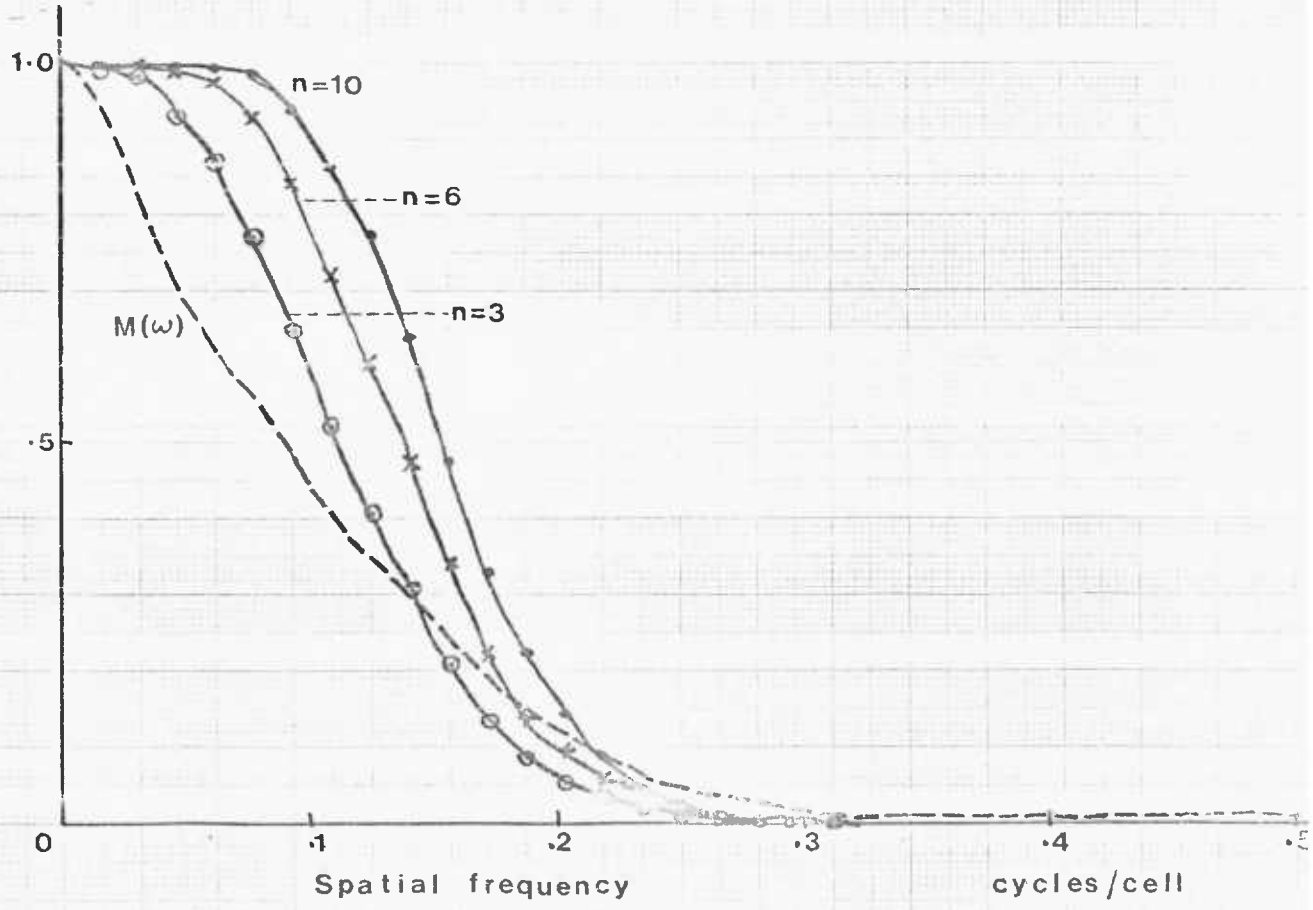

Processed frequency response – Metz filters

^{133}Xe in water at 8.5 cm

Graph III C - Theoretical and empirical frequency responses - unprocessed

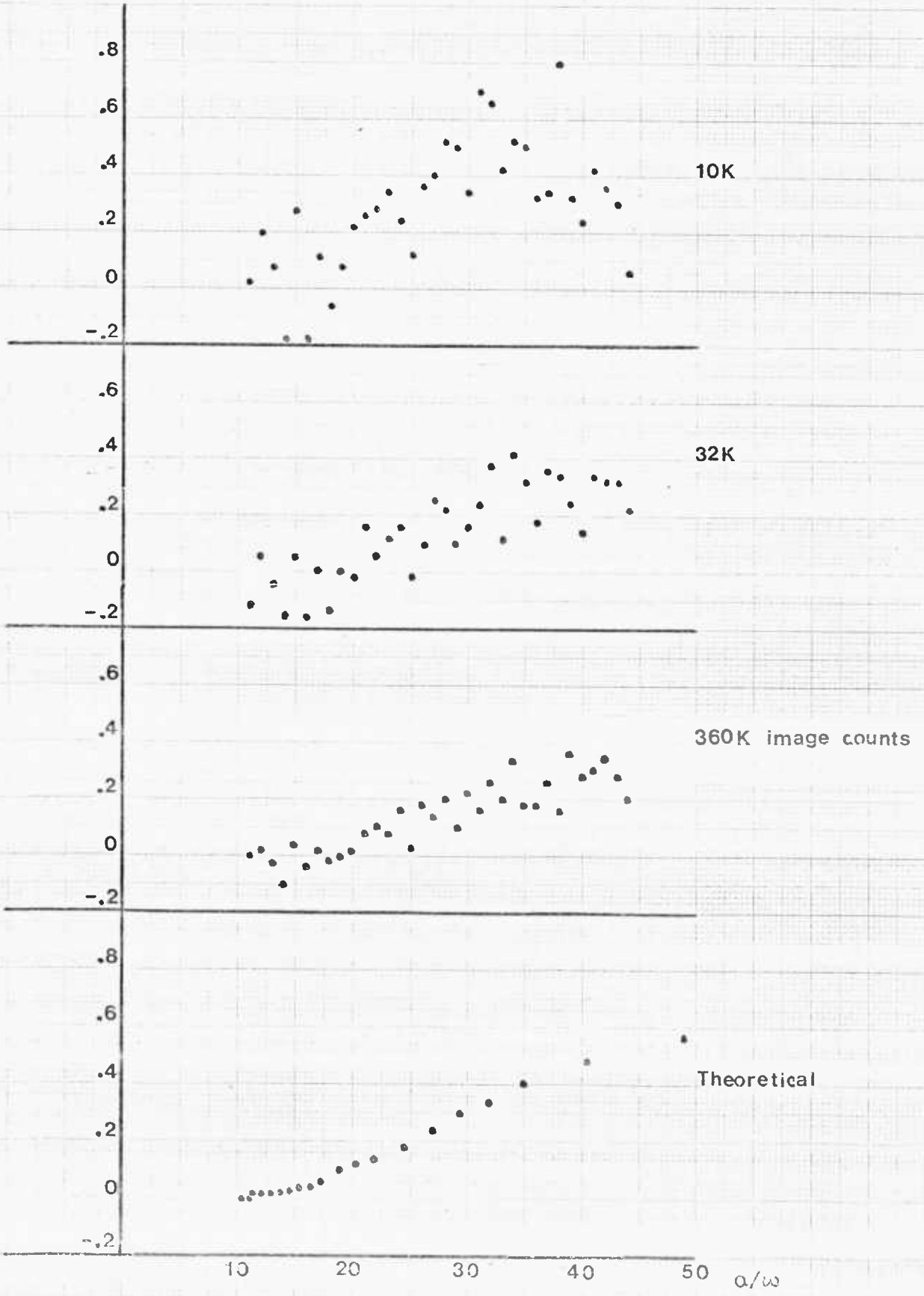

Graph IIID - Theoretical and empirical processed frequency responses -
3rd order
Metz filter

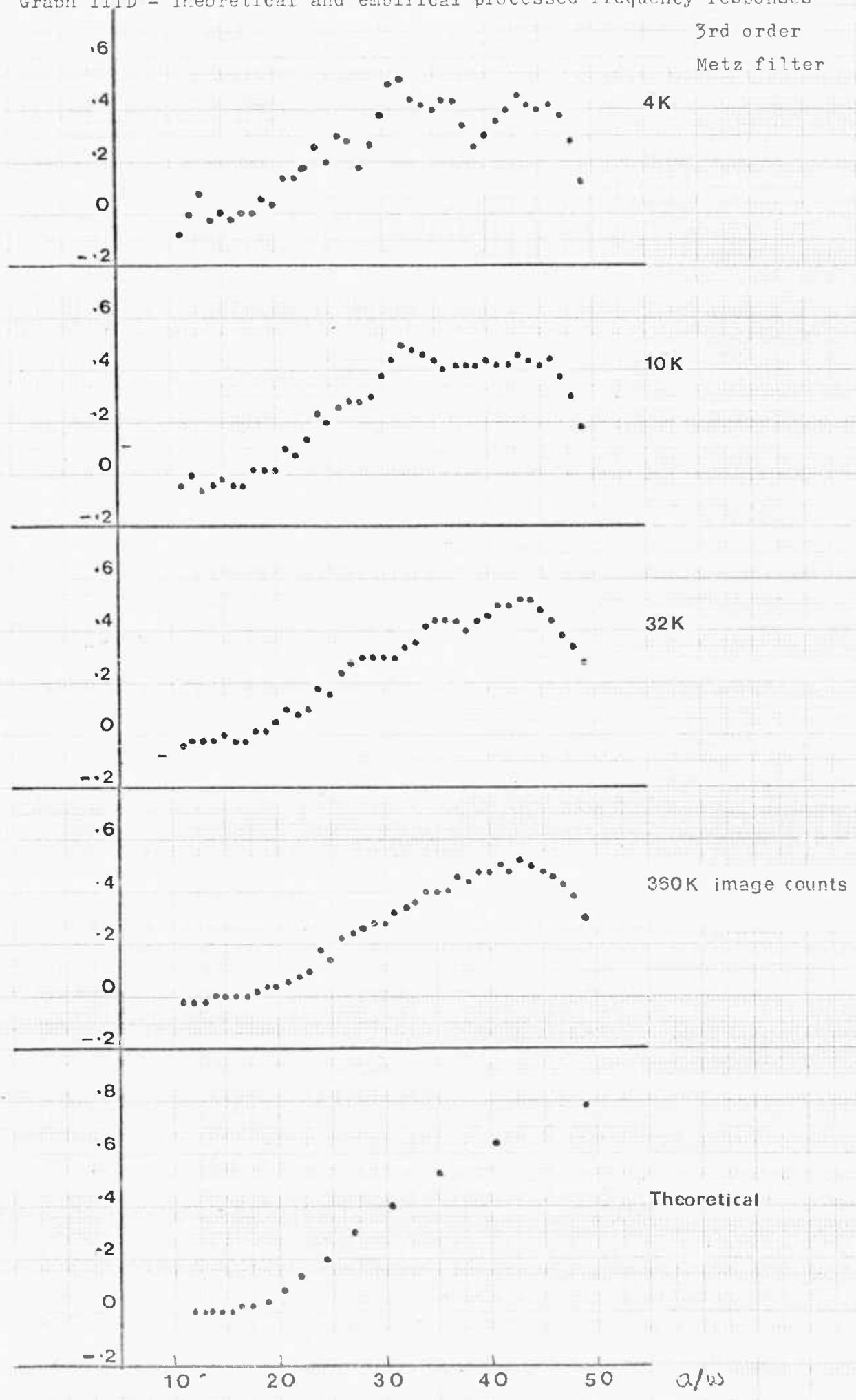

Graph III E - Theoretical and empirical processed frequency responses

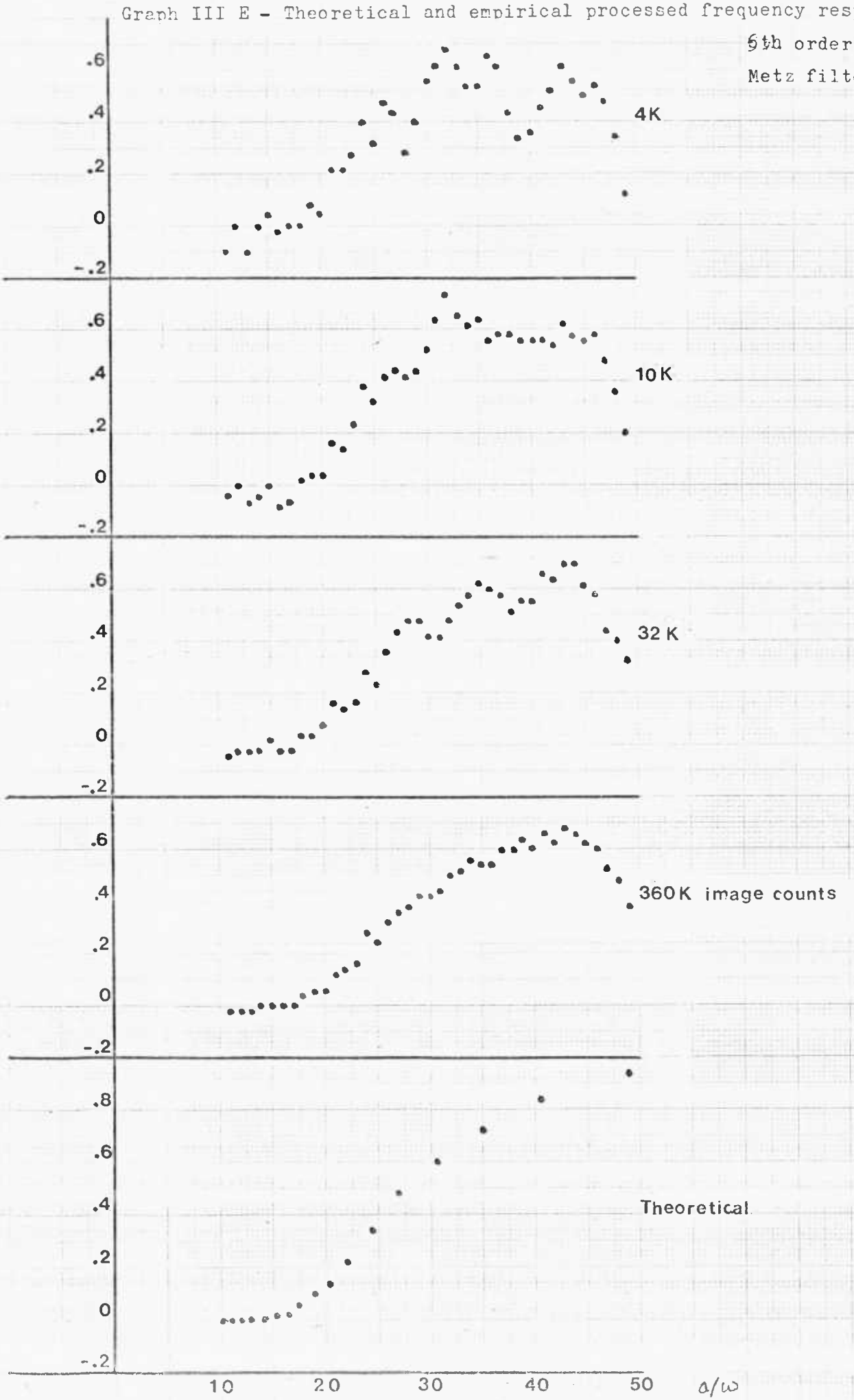

Graph III F – Theoretical and empirical processed frequency responses – 10th order Metz filter

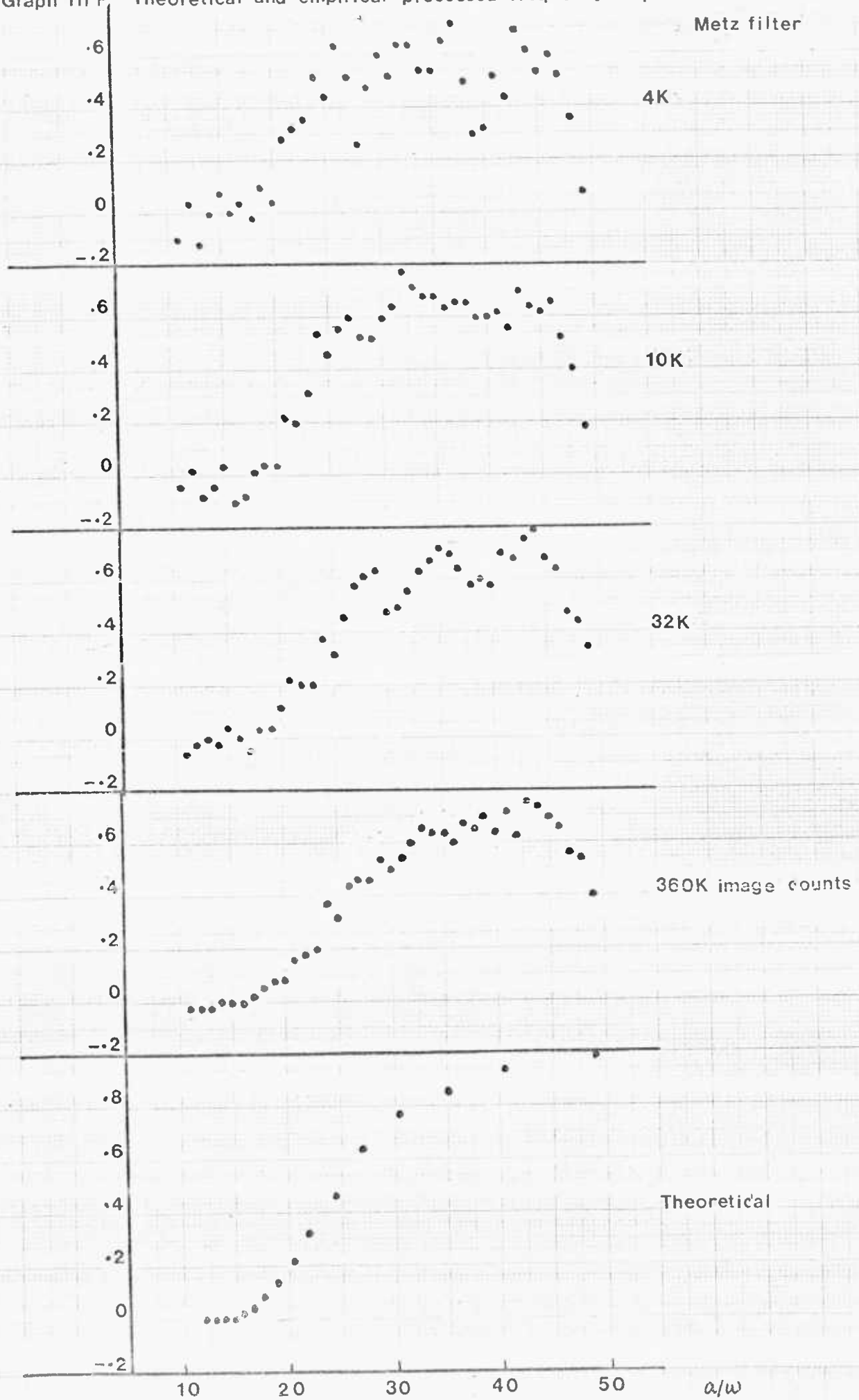

Graph IIIG

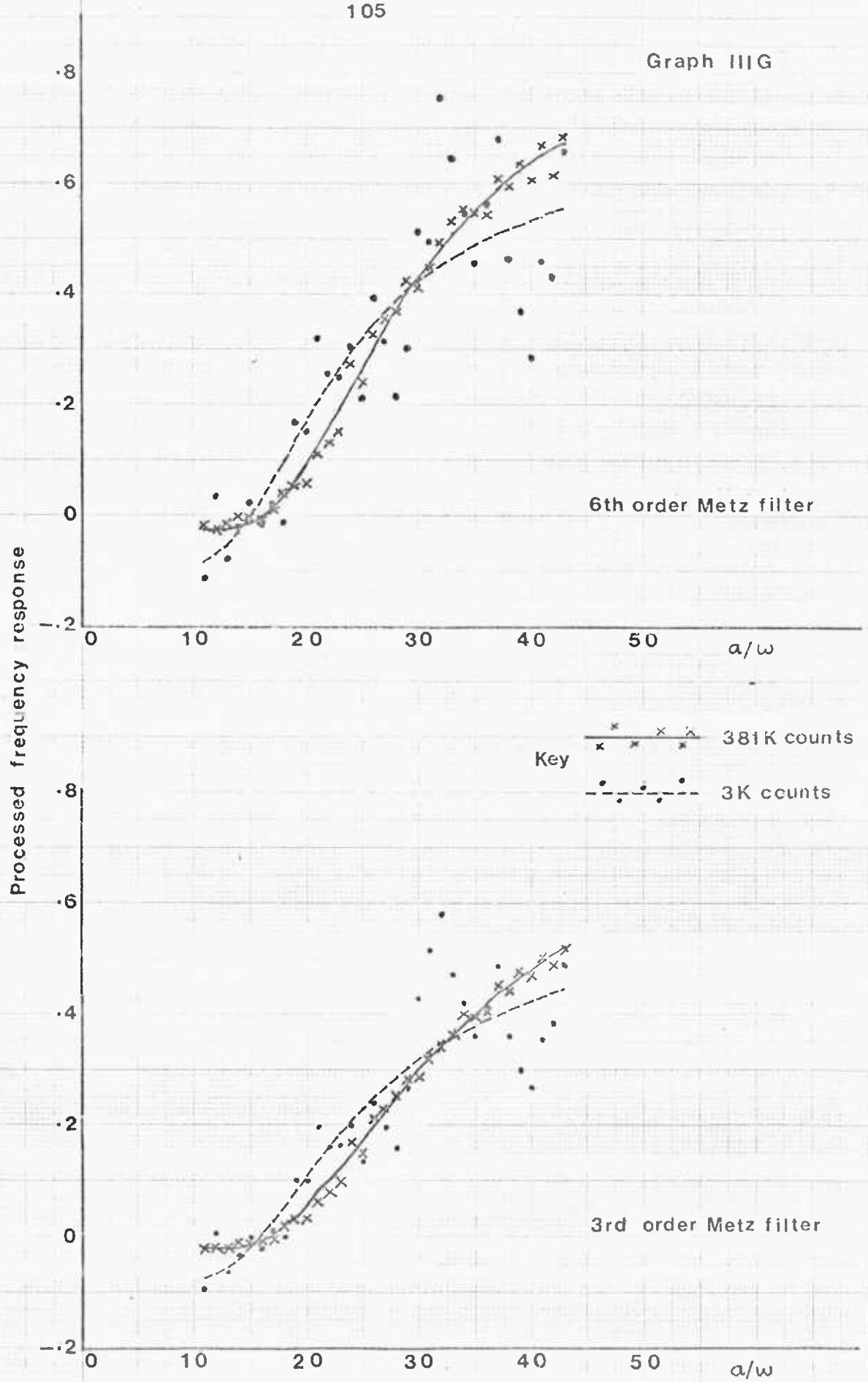

Examples of empirical frequency response with corresponding fitted curves for different image count levels

Graph III H

Variation of performance index with image counts for different orders of Metz filter

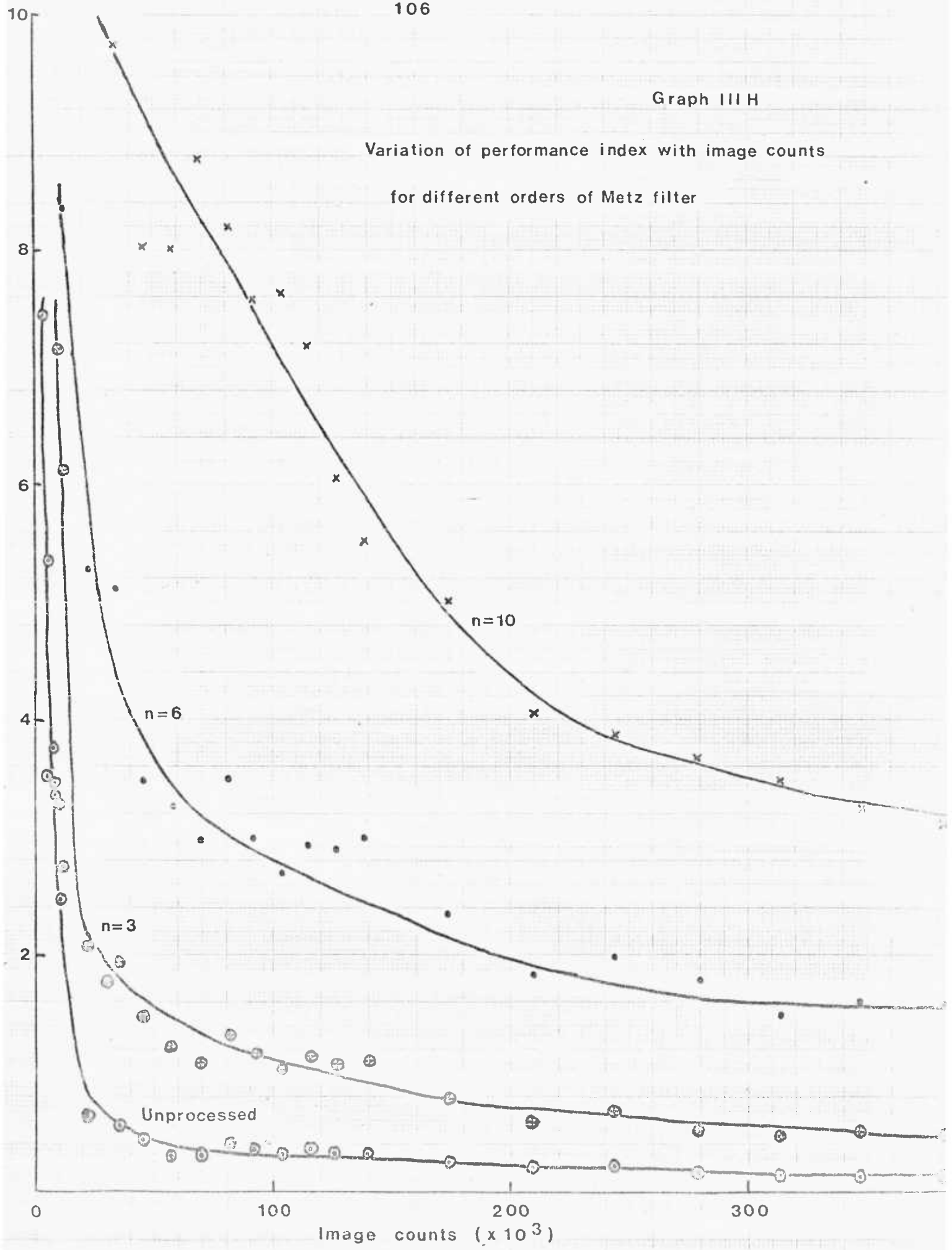

CHAPTER IV

Application of the Metz Filter to Quantitative Assessment of Bone Scans Using ^{99m}Tc EHDP

Abstract

A quantitative study is discussed in which ^{99m}Tc EHDP is used to assess the change occurring as a result of treatment to bone metastases in cases of cancer of the breast. The calculation of appropriate Metz filters and their application to the images obtained in this study are described. Conditions here are sufficiently similar to those in the experiment described in Chapter III for the approximate criterion derived there to be used in selection of the optimum order of Metz filter. Application of the criterion indicates a higher order of filter than that chosen by visual inspection of images in the examples given. Closer examination of the situation reveals that this is not due to inadequacy of the criterion in allowing for the interaction of Metz filters with noise, but it is a result of edge effects which are very important here because of the presence of areas of high count density (in the example shown, the bladder) near the edges of the image, and which prevent the use of high order filters. Thus choice of the optimum order of filter in cases such as this, must also take edge effects into account.

Inspection of images processed with suitable orders of Metz filter shows that not only are they visually clearer than the corresponding unprocessed images but also the quantitative information calculated from them reflected the known clinical condition of the metastases more closely. In the example shown, improvement of the metastases after treatment was suggested by clinical evidence;

unprocessed images indicated slight improvement, not statistically significant, while on the filtered images the improvement was significant.

CHAPTER IV

Application of the Metz Filter to Quantitative Assessment of Bone Scans using ^{99m}Tc EHDP

A. Introduction: Choice of method and materials

(i) Object of the studies

The clinical studies described in this chapter were used to monitor changes in bone metastases during therapy. Metz filters were applied to the radioisotope scan images in order to see if this would facilitate the investigations. The intention was to examine the application and performance of the Metz filters, with particular reference to the conclusions reached in Chapter III.

Bone metastases may occur in patients with advanced carcinoma of the breast, and these metastases may be treated by radiotherapy and/or various forms of chemotherapy. However the success or otherwise of a particular regime of treatment cannot be reliably predicted for an individual patient, and so it is important to have a sensitive method of monitoring the response to treatment. Without this, treatment which in itself may be very distressing to the patient, may be continued when it is subsequently found to be having no effect in slowing down the progress of the disease, and when alternative forms of therapy might be considered.

Bone metastases show up on X-rays, if the metastases are severe enough to alter the density of the bone significantly. However, since radioisotope scans show up differences between diseased and normal areas in their uptake of the radioactively labelled compound, metastases have been shown to be detected on these scans before

they give rise to significant changes in bone density. Several studies have been carried out where bone metastases were demonstrated by radioisotope scans while there was still no X-ray evidence for them, but the presence of these actively growing bone metastases was demonstrated later by X-rays and in some cases also at post-mortem[1,2]. The bone metastases show up as hot areas on the scans since increased uptake appears to be associated with imperfections in bone structure.

Thus radioisotope scans are now thought to be more informative than X-rays in the initial detection of skeletal metastases. The advantages of radioisotope scans are also relevant to the problems of monitoring the response of lesions to therapy, since metastases remain visible on X-rays even after they have become inactive as a result of therapy, while only active lesions show up on radioisotope scans[1]. Comparison of radioisotope scans taken before and after therapy should therefore give a good indication of the success or otherwise of the therapy. There are some problems however in the interpretation of the scans since in the case of radiotherapy treatment, uptake of the labelled compound may be suppressed throughout the irradiated area, giving rise to areas of high counts at the boundaries of this area[2]. There are also reports of areas of anomalously high counts seen in normal parts of the irradiated area as an effect of radiotherapy[2]. When chemotherapy is used, it has been argued that measurable change in uptake may only occur some months after the course of therapy is begun; however the results of this study indicate that this is not so, and that scans taken a few weeks after the start of therapy may be very informative.

(ii) The need for quantitative studies

As described in Section A(i) above, the main object of these studies is not to detect the presence of metastases (although on one or two scans previously unknown metastases were observed and obviously note was then taken of them), but to follow up changes in known metastases. The changes which may occur during the few weeks between the initial scan and the later one are generally slight and it is more useful to have a quantitative assessment of the state of the metastases than only a subjective consideration of the appearance of the scans. Clearly the quantitative assessment must be in terms of their sizes and their increased count densities relative to that of normal bone.

(iii) Aims of Metz filtering in quantitative bone scanning

The quantitative studies involve comparison of recorded counts between regions of differing count densities. The regions to be compared may have to be chosen very close to one another if there are numerous metastases and only small normal areas between them. Also the differences in count densities between the regions to be compared may only be slight if the lesions are not severe. In such situations blurring, as described by the finite width of the point spread function, may obviously occur and may degrade the image and reduce the difference in count density between healthy and diseased regions. When this occurs, the ratio between count densities in metastases and normal regions is incorrect, and the corresponding image recorded after treatment may have a different count distribution so that blurring and errors will be different for this image. Consequently any comparison between ratios of count densities calculated from the images taken before and after treatment

will involve these unknown errors. Since the differences between the ratios before and after treatment would be expected to be small anyway it seems very useful to apply Metz filters in an attempt to correct for this degradation.

(iv) Use of ^{99m}Tc-EHDP

A variety of radioactively labelled compounds have been used to scan for skeletal lesions such as bone metastases e.g. ^{18}F, ^{85}Sr, ^{87m}Sr, and several compounds labelled with ^{99m}Tc including polyphosphates and ethylene hydroxydiphosphonate (EHDP)[3]. A labelled compound to be used for this purpose must be fairly readily available and not prohibitively expensive, and it must satisfy various requirements as regards its physical properties and its physiological behaviour. Clearly the radioisotope must emit radiation of an energy suitable for the scanning device to be used, and also it must be possible to obtain good images of the skeleton without injecting so much radioactivity that the radiation dose to the patients becomes unacceptable.

As yet no single bone scanning agent has been proved superior to all others and in this case ^{99m}Tc EHDP was used; this emits γ-rays at 140 kev. This energy is most suitable for the γ-camera since it is not so high that efficiency of detection is reduced as a result of γ-rays passing through the detector without interacting, or that image degradation due to septal penetration in the collimator is considerable. On the other hand this energy is not so low that much emitted radiation would be lost by absorption in soft tissue on its way out of the patient's body or scattered so that if it reaches the detector it may degrade the image. An energy of 140 kev

is also suitable from the point of view of the radiation dose to the patient; obviously the activity administered may be kept low if detection is efficient, and radiation dose tends to be less for radioisotopes of lower energies.

^{99m}Tc is also convenient for clinical studies because of its half-life of 6 hours. Radioisotopes with very short half-lives, of the order of minutes say, tend to be difficult and expensive to obtain, and very large doses may have to be administered unless uptake is so swift that scans can be performed very soon after injection of the isotope. On the other hand, if the half-life is very long, this may increase the radiation dose to the patient unless the radioisotope is rapidly removed from the body by physiological processes.

To obtain clear images of the skeleton it is important that the labelled compound should be selectively taken up by bone so that radioactivity in soft tissue will not obscure the images and so that sufficient counts may be obtained from the bone to give good counting statistics in the image. If the proportion of the injected activity taken up by the bone is high, the radiation dose may be kept low since little of the activity administered will be "wasted" by adding to the dose in the patient's body without contributing to the quality of the image. Another factor affecting the radiation dose to the patient is the biological half-life of the labelled compound, since the longer the radioisotope remains in the body, the greater the dose; however when the half-life of the radioisotope itself is short, this is not so important.

^{99m}Tc EHDP satisfies these requirements quite well, having the advantage over other ^{99m}Tc compounds that it is taken up less by the soft tissues, especially the liver[3].

(v) Patient material

The patients studied all had primary carcinoma of the breast, with bone metastases diagnosed as a result of complaints of pain by the patient and evidence of X-rays and/or previous radioisotope bone scans. Each patient was scanned shortly before treatment to the bone metastases was begun, and then again after 3 - 6 weeks so that the effects of the treatment given during this period could be assessed.

(vi) Radiation dose

The dose of ^{99m}Tc EHDP administered was approximately 10 mCi. This dose gave a high count rate, of the order of 10^3 counts per second for the γ-camera at the time of scanning. Thus only a short time was required to build up an image with good counting statistics. It was not feasible however to reduce the dose, since many of the patients had bone metastases to be studied in various parts of the skeleton and so the entire series of scans required might take a long time although the count rate was high. The absorbed radiation dose after injection of 10 mCi of ^{99m}Tc EHDP is estimated to be 110 mrad to the whole body and 450 mrad to bone[3].

B. Method

(i) Scanning conditions

For scanning, digitizing and recording the data, a gamma camera and the Hewlett Packard HP2100 computer to which it was linked via ADCs were used. This system and the way in which it must be set up have been described in Chapter IIIB. For these studies a collimator suitable for ^{99m}Tc and its energy of 140 kev was selected for the gamma camera, and the pulse height analyser was set to admit γ-rays with energies within 25% of 140 kev. The voltage on the camera

was peaked and the ADC settings were adjusted to give a digitized image of the standard shape and size.

(ii) Initialization procedures

With the system set up as described, the image of a uniform source containing ^{99m}Tc was recorded onto magnetic tape so that it could be used for the 'uniformity correction'; this was done before every scanning session.

The image of a point source of ^{99m}Tc positioned at 10 cm from the collimator surface in air was recorded so that it could be used for calculating Metz filters. It was only necessary to do this once for the whole series of studies. Preliminary tests showed that Metz filters of orders 3 - 6 were the most suitable for use on the scans obtained in these studies and these filters were calculated from the point source response using the subroutine IMAGE1, and stored on magnetic tape for future use.

(iii) Scanning procedure

In each case the patient was given an intravenousinjection of approximately 10 mCi of ^{99m}Tc EHDP, and the scans were then made about 4 hours later, when it has been shown that the ratio of amounts of this labelled compound in the bone to that in the blood is at its maximum. The patient lay on a couch, and the gamma camera was positioned above the region of the patient to be studied, so that the distance from the collimator face to the organ of interest was approximately 10 cm. Since there was generally high activity in the bladder, if the regions to be studied were such that the bladder would be in or near the field of view of the camera, lead shielding

was placed over the bladder to prevent the activity in the bladder from "overshadowing" the rest of the image.

As mentioned above in Section A(iv), the count rate was high, so that the time required to build up an image of about 500,000 counts was only 1 - 2 minutes. The patient was instructed not to move during this time, and if it was observed that the patient did move, the scan was repeated. Photographs were taken from the gamma camera oscilloscope screen, and the scan was repeated if the photographs were blurred or indicated otherwise that the scan was inadequate. During each scan the digitized coordinates of the counts detected were recorded by the computer and stored on magnetic tape. Anatomical markers were recorded after each scan as reference points, so that the positions and extents of metastases could be checked on the two series of scans taken before and after treatment.

(iv) Processing the images

Using the HP 2100 computer, digital images were formed from the counts recorded during the scans and these were recorded on magnetic tape. The magnetic tape was then transferred to the CDC 7600 computer. The images were corrected for the non-uniform response of the gamma camera and Metz filters of orders 3 - 6 were applied to them using the subroutine IMAGE2 described in Chapter II. These Metz filtered images, together with the corresponding unprocessed images were then recorded on magnetic tape and transferred back to the HP 2100 computer for assessments and calculations to be carried out.

(v) Display and calculations

Each scan image was displayed on the computer oscilloscope screen and inspected visually in order to assess the effects of Metz filtering and to see the exact locations of metastases. The metastases and suitable areas of normal bone for comparison were outlined on the images using a light pen. In the case of the second set of scans for a patient (after treatment), the recorded anatomical markers were referred to, in order to ensure that the same regions were chosen on the two sets of scans.

For each region of interest the following ratio was calculated:

$$\frac{\text{counts in metastasis}}{\text{counts in normal bone region}}$$

$$\frac{\text{area of metastasis}}{\text{area of normal bone region}}$$

where "area" means the projected area of the region on the image. This process was carried out on the unprocessed image of each scan and also on the corresponding Metz filtered images.

C. Results

(i) Qualitative results - scans

Examples of the images obtained are shown in Figs. IVA - E. These images are examples of those appearing on the line printer output from the CDC 7600 computer, where alphanumeric symbols of varving densities are used to represent the different count densities in the image. As described in Section IV B(iv) the images were also examined on the oscilloscope display screen of the HP 2100 computer. The conclusions drawn from these images appeared to be unaffected by the mode of presentation (i.e. line printer output or computer oscilloscope display) provided that the observer was familiar with images shown in that way. For purposes of comparisons between images,

all images were displayed and examined under the same conditions - on the computer oscilloscope display.

In all cases the metastases which had been previously diagnosed could be seen on the scans, and in some cases the presence of additional metastases was diagnosed from these scans. The examples shown are scans from a patient with two metastases in the left femur, and these are typical of the scans obtained in these studies. The images also show the shadow of the lead shielding over the bladder. The metastases were again present as areas of raised count density on the scans taken after therapy, and their sizes and positions appeared the same as on the earlier scans.

(ii) Qualitative results - effects of Metz filtering

It was clear that the images were improved by Metz filtering; regions of metastases and normal bone could be seen more distinctly and the shapes of the bones were shown in detail and could be seen to correspond to their known anatomical forms. The optimum order of Metz filter was found by trial and error to be about 6; lower orders gave poorer resolution, and when higher orders were used artifacts gradually began to appear. This choice was confirmed by an observer who was unaware which of a series of images had been filtered and which orders of filter had been used, and who immediately selected 6th order Metz filtered images of several scans as being the ones on which he could see most detail and would find it easiest to delineate normal and diseased regions. In agreement with the conclusions of the experiment described in Chapter III, that "any order of Metz filter is better than none", this observer (and others) discarded the unprocessed images first as being the least informative ones.

(iii) Results - quantitative data

An example of the quantitative information obtained from these studies is shown in Table IVA. This data was taken from the images shown in Figs. IVA - C. The metastasis denoted "1" in the table of results is the lower one, and "2" is the one nearer to the pelvis. The choice of a normal region suitable for use for comparison (see Section IV D) was limited in this case. since the patient also had bone metastases in her right femur. As a result the region chosen was the small region of normal bone between the two metastases on the left femur.

The table of results shows that the ratio of count densities in the metastases to that in the normal region decreased after therapy for both metastases. indicating some degree of remission even immediately after 4 weeks of therapy. The patient was suffering from less pain in this region at the time of the second scan, but this is often experienced after therapy whether or not any healing or remission is induced in the lesion. However in this particular case, further follow-up scans were taken a few months later and the metastases in the left femur showed further improvement, so it would appear that the decrease in relative count densities observed after 4 weeks was a true early indication of remission.

(iv) Results - effects of Metz filtering on quantitative information

The quantitative results were calculated from the filtered images in exactly the same way as from the unprocessed images, and an example of these results is shown in the table. As expected, correction of blurring by Metz filtering leads to higher count density ratios between metastases and normal regions on the filtered scans taken both before and after therapy. The measurements on the filtered

images indicate improvement in both metastases after therapy, but here again since the errors in the measurements were not estimated, it is impossible to know how significant the improvements are.

D. Discussion

(i) Selection of regions of metastases

The initial delineation of regions of metastases must involve arbitrary decisions as to where the metastasis ends and normal tissue begins. This procedure could have been carried out by computer, using a program to select the boundaries of the regions by some algorithm. In that case obviously the choice of regions would be fixed for any one image, and would depend on the arbitrary choice of algorithm. However, in this study the regions were chosen by hand on the images displayed on the computer oscilloscope screen, rather than by using a computer method which would be equally arbitrary but more complicated.

For the purpose of this study it is essential to be able to identify the same regions for the metastases on the second, post-treatment scans. As mentioned above, no gross changes in bone structure are likely to occur within a few weeks, and this facilitates the matter. Also anatomical markers were recorded in each case to check that the same regions are found on the post-treatment scans.

(ii) Selection of normal regions for comparison

In order to assess the severity of the metastases through their increased uptake of ^{99m}Tc EHDP, it is necessary to select regions of normal bone which are comparable to them in structure. This is

obviously important, apart from anything else because the recorded count density will depend on the thickness of the bone in the direction perpendicular to the collimator face.

Some authors[4] use a symmetrically placed area on the opposite side of the body where possible, or for examining spinal lesions, an adjacent normal area judged to be of equal thickness of bone. In cases where the patient has many skeletal metastases, so that the symmetrically situated area on the opposite side of the body may not be normal, it may also be necessary to choose a normal region adjacent to the metastasis. This procedure may be preferable on other grounds too, since there is a tendency for uptake to be increased on the dominant side of the body, especially near joints[3]. Further the problem raised by the suggestion that radiotherapy depresses uptake in both normal and diseased regions may be avoided if the normal regions for comparison are chosen close to the metastases so that if radiotherapy was used they will have experienced similar irradiation.

(iii) Choice of a quantitative index for the studies

The need for a quantitative index to describe the state of the metastases is mentioned in Section IV A(ii); generally no gross changes in the metastases would be expected to occur within a few weeks and hence no obvious changes in the appearance of the scans. In order to examine any small changes which may occur, the sizes and count densities of the metastases were considered.

The size of the area of raised count density on the image is the projected area of the metastasis in the plane parallel to the camera face. The increase in count density above that of the surrounding

normal tissue indicates the extent of the metastasis in the plane perpendicular to the camera and the degree of imperfection in bone structure caused by the metastasis. As mentioned above (Section IV A (i)). no great changes in the size of metastases would be expected to occur during a few weeks, and in fact no obvious changes were seen in the sizes of the metastases. It was decided then to examine the changes in count density, since early effects of therapy might have initiated healing in the metastases, leading to a less raised uptake.

However the absolute count rates and count densities in various parts of the bone will depend on the exact dose given and time elapsed between administration of the isotope and scanning and so could not be used. But the ratios between the count densities in different regions for the same patient should be independent of these factors and so should give a useful indication of the difference in function between metastases and normal bone. These ratios were therefore:

$$\frac{\text{counts in metastasis}}{\text{projected area of metastasis}} \Big/ \frac{\text{counts in normal bone region}}{\text{projected area of normal bone region}}$$

(iv) Applicability of Metz filters

In general, the conditions of this study are very favourable for the use of Metz filters. High image count densities can be obtained here (see Section A (vi)), so that the signal-to-noise ratio is good. Under such circumstances Metz filters should produce substantial resolution enhancement without amplification of noise.

The overall region of interest in the scan is generally fairly small and the patient can be positioned so that this region is near the centre of the gamma camera field. However edge effects may still

be troublesome in the use of Metz filters (see Section D (v)) because there may be areas of high activity, outside the region of interest, which give rise to high count densities near the edges of the gamma camera field.

Another of the problems is associated with the fact that the scan images are a two-dimensional representation of a three-dimensional distribution of radioactivity. The Metz filter is essentially a method for correcting the blurring introduced as described, by the point spread function for the system, and the calculation of suitable Metz filters involves measuring the system point spread function under the same conditions as those for the clinical scans to which the filters are to be applied. However although the point spread function alters somewhat with the distance from the collimator face, and the object to be scanned is three-dimensional, it is necessary to use a single point spread function for calculating the Metz filters to be used on these scans. In these studies the problem is not so great since most of the bones studied, although they are three-dimensional, are not thick structures, and the distance from their nearest to their furthest point from the collimator is only a few centimetres, so that the change in the point spread function will only be small. This will certainly be true for bones such as the spine or femur, but not for bones with more complex three-dimensional structure such as the pelvis. So for example for the study of a femur shown below, the use of a point spread function recorded at 10 cm from the collimator face in air is adequate for calculation of the Metz filters.

(v) Optimum order of Metz filter

As stated in Section C (ii), observation showed that the best

order of Metz filter for these scans was 6; when lower orders were used the images were less clear, and when higher orders were tried artifacts were seen. However, one could also approach the problem of selecting the optimum order of Metz filter by referring to the study of the performance of Metz filters in the presence of noise (see Chapter III). The point spread function of ^{99m}Tc at 10 cm in air is broadly similar to that recorded for ^{133}Xe as described in Chapter III and one would therefore expect the results obtained for ^{133}Xe to hold approximately here too.

Here the mean count density in the region of interest is approximately 250 $cell^{-1}$, and so referring to the graph (IIIH), one would expect a Metz filter of order 10 or still higher to give optimum resolution enhancement without excessive amplification of noise. However in these studies such a high order of Metz filter did not usually produce the optimum image. This is because the limiting factor which gives rise to artifacts in the image here is not the presence of noise but edge effects which are important when there is a region of very high count density near to the edge of the image, and similar features were present in most of the studies, thus limiting the order of Metz filter which could be applied.

(vi) Errors

Estimation of errors in the quantitative measurements made from the scan images is very difficult and no attempt has been made here to do this. Poisson errors in the count rate, errors in the detection, digitization and recording devices all contribute to the overall error. These errors could be estimated if the same measurements were repeated. This has been done by other workers[4] who found good

correlation between two sets of measurements made on each of a series of patients. However this estimation does not include errors due to arbitrary decisions as to where the boundaries of the metastases and normal regions are. Such errors will obviously be more important the smaller the regions considered.

E. Conclusions

This method appears to be a useful method for monitoring changes in bone metastases, and Metz filtering seems to assist in this. However more studies, including estimations of errors and detailed follow-up of patients, would be necessary in order to evaluate the accuracy of the results obtained and the benefits of Metz filtering. Also, in order to achieve still better resolution with Metz filters care must be taken to avoid pitfalls such as including areas of high count density which lead to edge effects ruining images when high orders of Metz filter are used. If this were done it would be possible to test properly what the optimum order of Metz filter would be, and to see if this was in agreement with data from an experiment analagous to that in Chapter III for ^{99m}Tc.

Table IV A

Mrs. W. Left femur — Before therapy		
Normal region		
	unprocessed	Metz 6
area	14	12
total counts	2352	1824
count density	168.00	152.00
Metastasis 1		
area	13	22
total counts	3354	5824
count density	258.00	264.73
count ratio, met.1/normal	1.54	1.74
Metastasis 2		
area	26	26
total counts	6676	7213
count density	256.77	277.42
count ratio, met.2/normal	1.53	1.83

Mrs. W. Left femur — After therapy		
Normal region		
area	13	12
total counts	1537	1241
count density	118.23	103.42
Metastasis 1		
area	18	19
total counts	2794	3166
count density	155.22	166.63
count ratio, met.1/normal	1.31	1.61

Metastasis 2		
area	28	28
total counts	4697	4800
count density	167.75	171.43
count ratio, met.2/normal	1.42	1.66

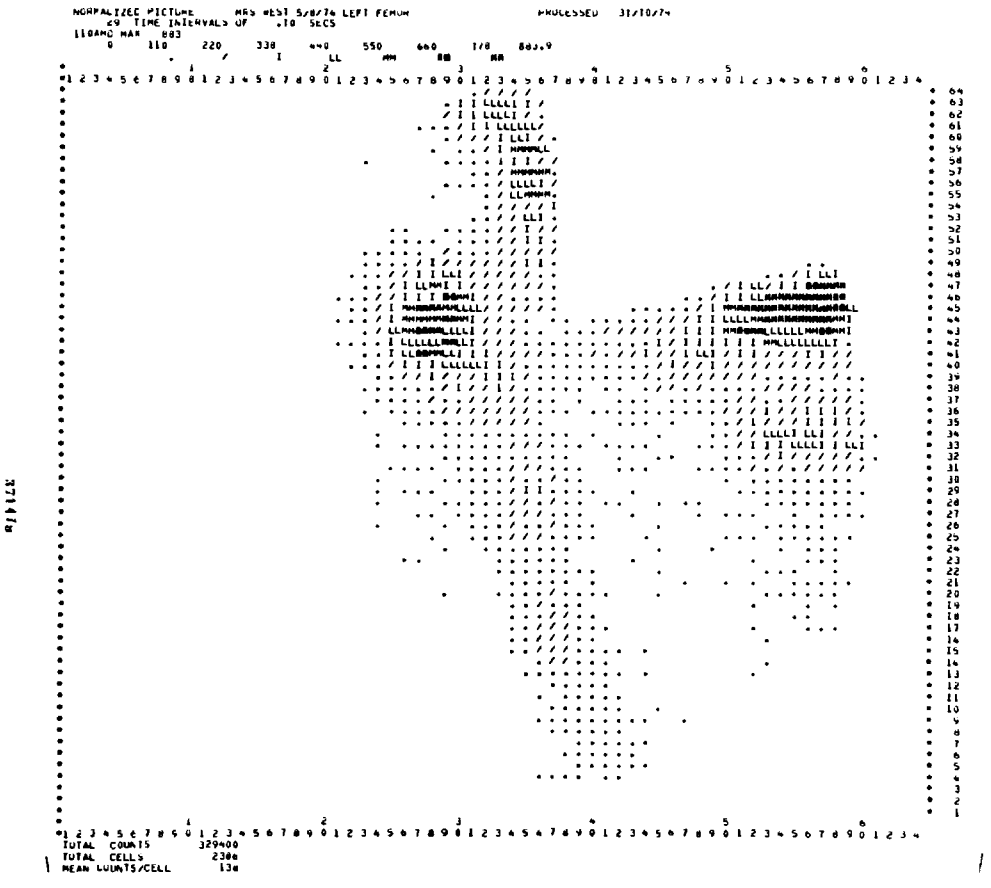

Fig. IV A Mrs. W. Left femur Before therapy. Unprocessed image.

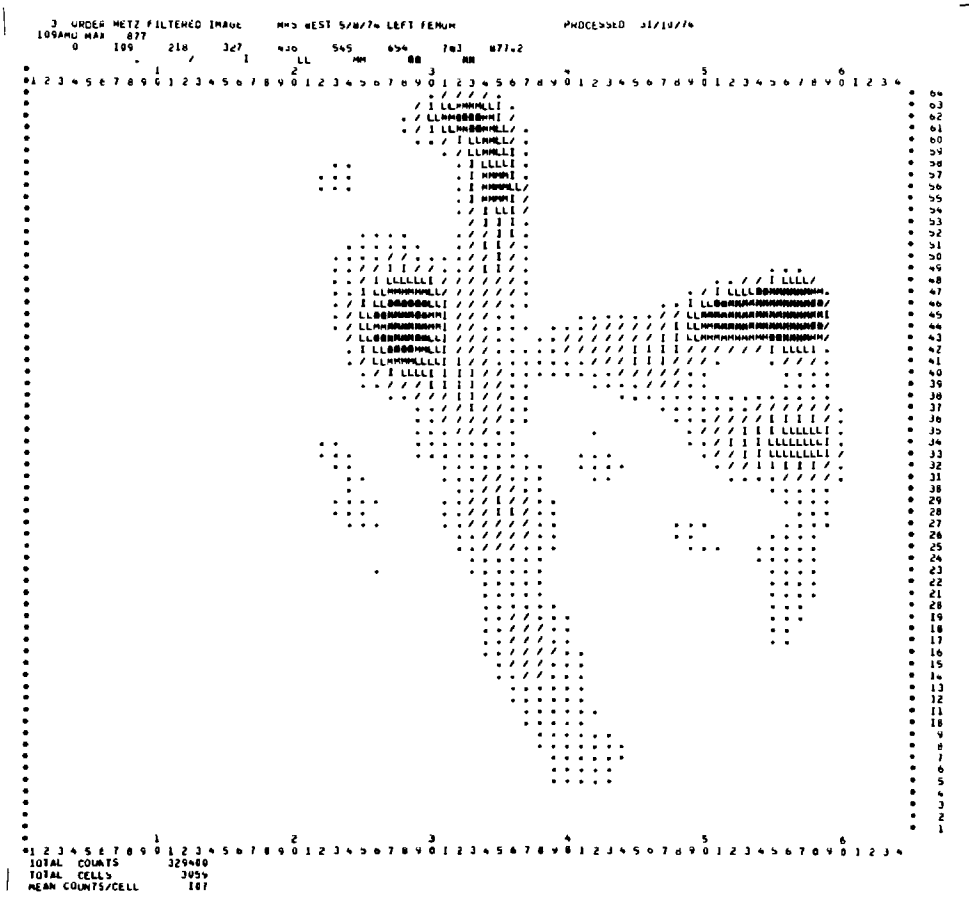

Fig. IV B Mrs. W. Left femur. Before therapy. Processed with 3rd order Metz filter.

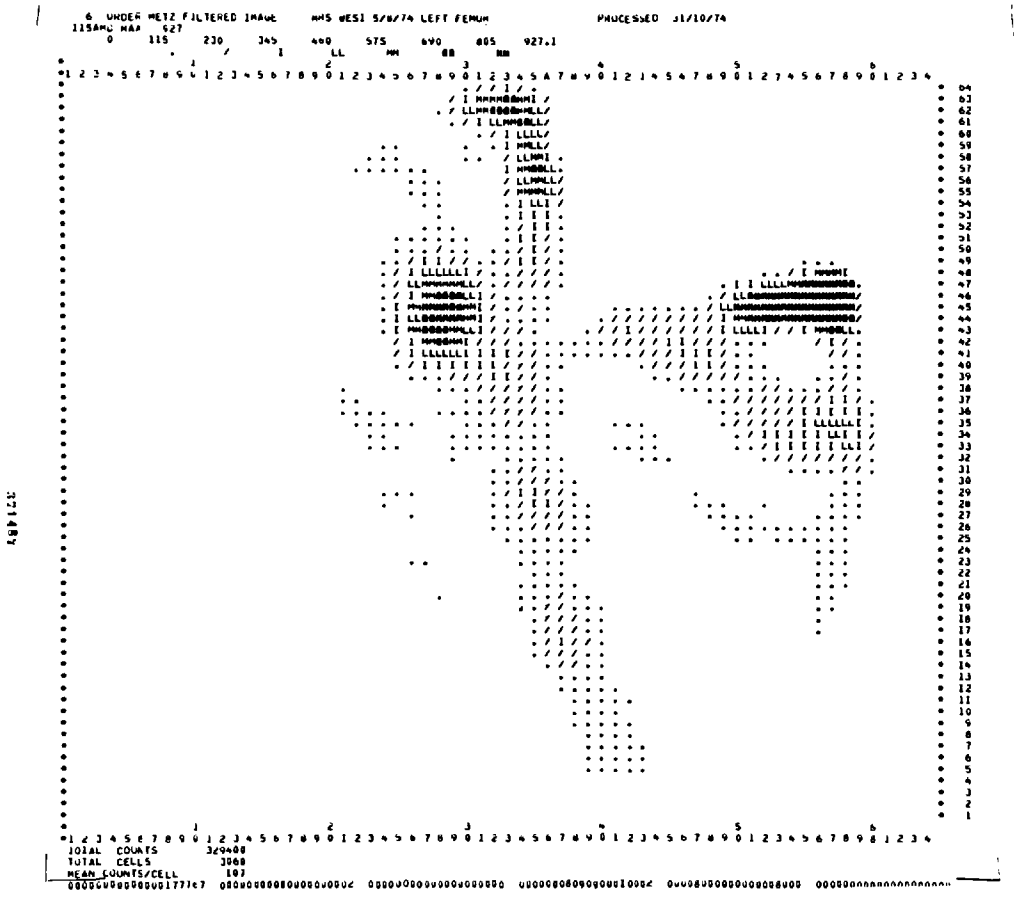

Fig. IV C Mrs. W. Left femur. Before therapy. Processed with 6th order Metz filter.

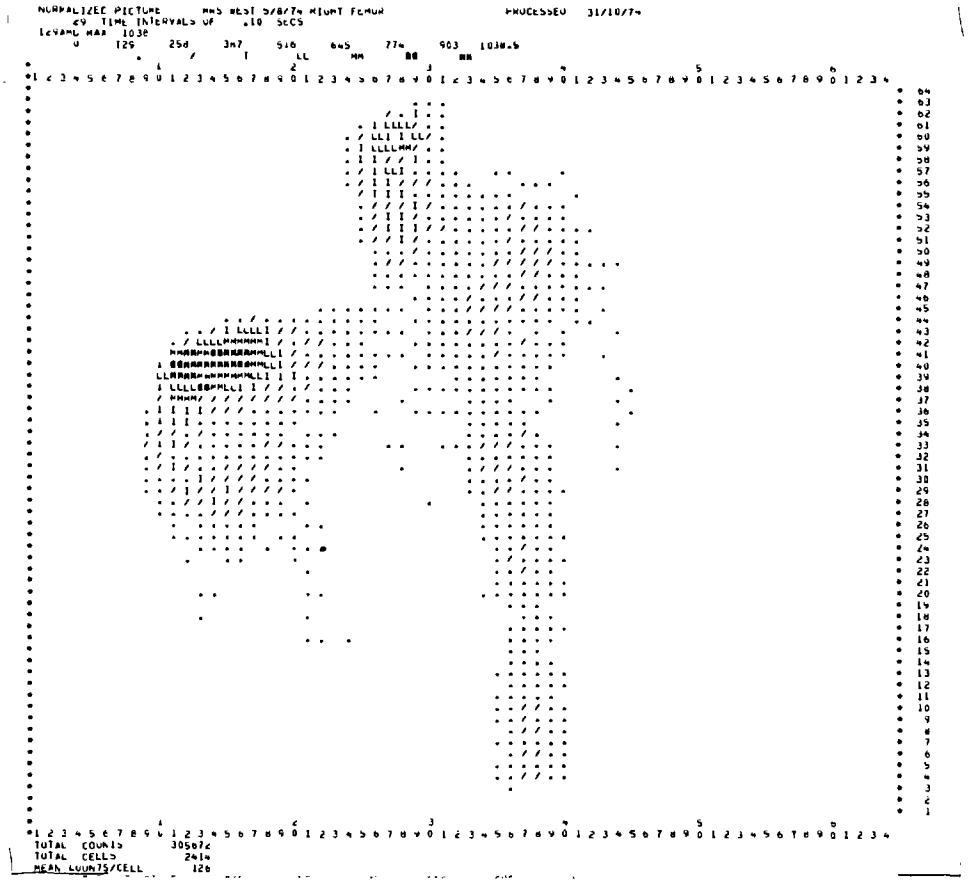

Fig. IV D Mrs. W. Right femur. Before therapy. Unprocessed image.

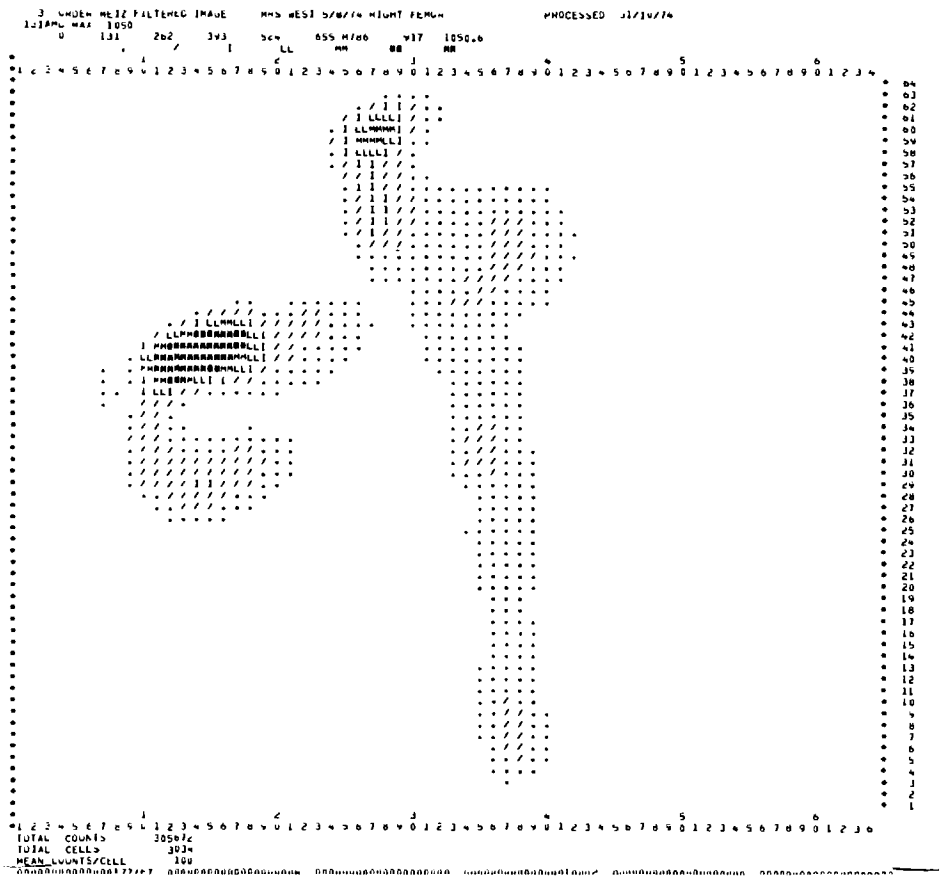

Fig. IV E Mrs. W. Right femur. Before therapy. Processed with 3rd order Metz filter.

Fig. IV F Mrs. W. Right femur. Before therapy. Processed with 6th order Metz filter.

CHAPTER V

Application of the Metz Filter to Regional Lung Function Studies Using ^{13}N in Infants and Children

Abstract

The problems involved in carrying out a complex dynamic study on non-cooperative patients using a short-lived radioisotope are considered. The gamma camera is used to follow the passage of ^{13}N through the patient's lungs after the radioisotope is administered by inhalation, and by intravenous infusion. ^{13}N has a point spread function which is relatively wide and not spherically symmetric and the image blurring caused by this is corrected by Metz filtering. Information on the function of the lungs is obtained by visual inspection of composite images consisting of all counts from ^{13}N in the lungs at any time during the study. Also graphs showing the counts recorded in selected regions of the lungs in successive short intervals of time during the study are plotted. and indices of lung function are then calculated from these graphs. Metz filters are applied to the composite images and also to each of the series of images consisting of counts recorded in the successive short time intervals.

The results of these studies can be compared with information from other tests on the patients, though confirmation of the exact positions and severity of localized disease is only rarely possible. The results of Metz filtering of a clinical dynamic study have not been reported elsewhere and clearly the problems of assessing its affects require much further work. It was not possible to prove that Metz filtering improved the accuracy of the results here, though in several of the cases described. other evidence suggested that the

increased contrast between diseased and healthy areas shown after filtering was a more accurate representation of the condition of the lungs.

CHAPTER V

Application of the Metz filter to Regional Lung Function Studies using ^{13}Nitrogen in Infants and Children

A. Choice of materials and method

(i) Purpose of the studies

In a healthy subject the supply of inhaled air and the flow of blood are distributed in a similar way to all parts of the lungs and the rates of ventilation and perfusion are matched[8]. Respiratory problems may be caused by local or generalized defects in perfusion or ventilation or both. The use of the gamma camera to detect the distribution of radioactivity during and after introduction of a radioisotope into the inhaled gas or into the blood supply to the lungs enables the passage of gas or blood through the different parts of the lungs to be studied and so regions of diseased lung may be located. These studies were carried out on babies and young children who were undergoing investigation for a variety of respiratory diseases. These studies are described in detail from a clinical point of view elsewhere[1,2], and an account of the mathematical analysis of techniques used is also referred to[9].

(ii) The need for quantification

The object of these studies was the investigation of the flow of blood and air through the lungs by following changes in radioactivity within the lungs. Of necessity this involves quantitative measurement as well as visual examination of scan images. Also quantitative indices

are useful for comparisons between patients and for cross-checks with other methods of assessing lung function.

(iii) The use of ^{13}Nitrogen

The choice of a suitable radioisotope for these studies depends on several factors. It must emit radiation of an energy suitable for detection by the gamma camera. Furthermore, the gas must be relatively insoluble in blood and fat and biologically inert so that it is not metabolized by the body but immediately washed out from the lungs after inhalation, and after infusion in the blood supply it will then come out of solution as soon as it is brought into contact with the air in the lungs. If these conditions are met, then the lungs alone should appear in the gamma camera image, and it is possible to interpret inflow and outflow curves in physiological terms.

^{133}Xenon has been used for regional lung function studies[3,4,5], but it has several disadvantages. It emits γ-rays at 80 kev which is somewhat low for the gamma camera and scattering and absorption occur in the media between the organs of interest and the collimator. As a result, penetration is poor so that there is an enhanced view of the near side of the object, and also scattered radiation which does reach the camera gives rise to blurring in the image. The effects of this are however not so important in these studies on infants, since the object, in this case the child's lungs, is fairly thin and there is not much tissue between the lungs and the gamma camera.

More important for this study, although xenon is fairly insoluble in water, a small amount of it will remain in solution, and furthermore it is quite soluble in fat so that any xenon which does dissolve in the blood may then be carried around the body and remain in the fatty tissues, thus confusing the image. Nitrogen on the other hand is much

less soluble in water or fat so that this problem is very much less significant. Suitable radioisotopes of nitrogen are not readily available. ^{13}Nitrogen, which has a half-life of only ten minutes, can be produced in a cyclotron[6]. ^{13}Nitrogen is a pure positron emitter, thus effectively giving γ-radiation of energy 511 kev which is acceptable for the gamma camera although it is high enough to give considerable collimator septal penetration resulting in degradation of the image.

(iv) Metz filtering

As with the studies in Chapter IV, Metz filters were applied here to the radioisotope scan images in order to see whether this would assist the investigation by improving both the scan images and the accuracy of the quantitative information derived from them.

As described in Section V A(iii), when ^{13}N is used degradation of the image results chiefly from penetration of the septa of the collimator by the 511 kev annihilation radiation; at this high energy there is not much scattering. It is therefore the septal penetration which mainly determines the shape of the point spread function.

Examination of the recorded point spread function confirms this, and shows that when septal penetration is important, the point spread function is not necessarily circularly symmetric, but shows a symmetry determined by the arrangement of holes in the collimator, since the point spread function will have a longer tail along those directions in which the number and thickness of septa is least. In this case the point spread function was elongated along five equally spaced lines, corresponding to the hexagonal arrangement of collimator holes, and this five-pointed star could be seen when photographs were taken. However even along the five axes where counts were maximum,

the count rate was small compared to that at the centre, and the deviations from circular symmetry and from a Gaussian cross-section were small. The full width at half maximum of the point spread function is greater than that for ^{133}Xenon or ^{99m} Technetium. and so the modulation transfer function is narrower. The blurring is therefore more serious in the unprocessed image and the influence of noise will be greater since the signal itself is not so well transferred. The shape of the modulation transfer function, and of the filters calculated is not as regular and smooth as in the cases of ^{133}Xenon and ^{99m}Technetium.

Considerable degradation may result from this wider point spread function with its lack of circular symmetry. This affects not only the composite "static" images which are viewed, but also the washout curves, which are obtained from series of images. and indices calculated from the curves. Thus if the Metz filters are effective they should enable one to obtain better "static" scan images and more accurate quantitative information about the "dynamic" part of the study.

(v) Patient Material

The patients studied were aged between 2 weeks and 10 years old. These infants and children suffered from a variety of respiratory problems, and the investigations were performed in order to aid or confirm diagnosis of the nature and extent of the disease.

(vi) Radiation Dose

The amount of activity required to give an adequate count rate for data analysis while minimizing the dose to tissues was calculated

to be 0.3 mCi/kg body weight, up to a maximum of 2 mCi for each study. The dose received by the lungs was calculated to be less than 200 mrads.

B. Method

(i) Scanning conditions

The gamma camera was set up for these studies with a 11.5 cm thick collimator, to minimize septal penetration by the 511 kev γ-rays, and connected via analogue-to-digital-converters to the Hewlett Packard 2100 computer. The pulse height analyser of the gamma camera was set to admit γ-rays with energies within 25% of 510 kev. The voltage on the camera was peaked and the ADC settings were adjusted to give a digitized image of the standard shape and size.

The computer was set up to generate time markers at 0.1 second intervals so that the arrival and disappearance of radioactivity from the camera field could be followed very precisely. An 'event marker' was also provided so that 'events' such as the exact time of commencing and ending the injection of ^{13}Nitrogen could be marked on the recording.

(ii) Initialization Procedures

With the system set up as described above, a recording of the count distribution from a uniform plane source was made before the start of each session so that subsequent records could be corrected for the non-uniform response of the gamma camera. The plane source contained ^{85}Strontium since this has a half-life of several weeks and

is therefore more readily obtainable than ^{13}Nitrogen, but it emits γ-rays at approximately 511 kev and therefore the non-uniform response of the camera is effectively the same for ^{85}Strontium as for ^{13}Nitrogen.

The image of a point source of ^{13}N positioned at 8 cm from the collimator surface in water was recorded so that it could be used for calculating Metz filters. It was only necessary to do this once for the whole series of studies. Preliminary tests showed that Metz filters of orders higher than 10 were unlikely to be useful in these studies, and filters of orders 1 to 10 were calculated from the point source response using the subroutine IMAGE1. and stored on magnetic tape for future use.

(iii) Scanning procedure

The patient was placed supine over the gamma camera; the smaller patients lay on a supporting platform located immediately over the collimator face. and the older children lay on a light trolley, so that in either case the distance from the patient's lungs to the collimator face was only a few centimetres. The patients were all lightly sedated so that they would lie still and breathe normally.

Two studies were carried out on each patient. For each study 0.3mCi of ^{13}N per kg body weight (up to a maximum of 2mCi) was administered. ^{13}N dissolved in sterile saline was injected intravenously as a bolus, and the activity distribution in the lungs was recorded during the injection and then continuing until the count-rate had dropped to background levels. ^{13}N as a gas was then injected. also as a bolus, at the end of an expiration. into the gas to be

inhaled in the nasopharynx via a nasal catheter, and once again the passage of activity into and out of the lungs was followed. For both infusion and inhalation studies recording was stopped after 5 minutes if the count rate had not dropped to background levels by then. Expired radioactive gas was removed by means of a pump and wide-bore tube placed close to the patient's face, so that it did not increase the general background radiation and confuse the gamma camera image, and is not inhaled by the patient or investigators.

All the counts recorded were stored on magnetic tape in raw data mode, i.e. as a list of the coordinates of points at which counts were detected, stored in the order in which they were received. Anatomical markers were also recorded after each study to aid location of the lungs on the scan images.

(iv) Inspection of the gamma camera images

Initially a composite digital image showing the distribution of all the counts recorded during the study was formed by the HP 2100 computer and viewed on the computer oscilloscope. The lungs were delineated on this image using a light pen, and each lung was divided for the purposes of analysis into an upper and a lower region. The anatomical markers were used as a reference in doing this. This is particularly important in cases where the shape of the lungs was unusual, for example, as a result of skeletal abnormalities such as scoliosis.

The specified areas of the image were recorded on magnetic tape together with the images themselves so that the function of the lungs in these areas could be examined.

(v) Processing the gamma camera images

All further processing was performed on the University of London CDC 7600 computer. A Fortran program package "GAMMA" was used to input the gamma camera data from magnetic tape and process it[7]. A subroutine was written to run with this package, to direct input of raw list mode data and timing information, process images and perform the calculations which are described in Section B(vi).

The raw data is first collected into 'frames', each consisting of a 64 x 64 array specifying the count distribution recorded over the gamma camera field during some time interval. In practice frames were usually formed over time intervals of 6 seconds, since finer time intervals often gave too few counts for accurate estimation of counts in particular regions.

These frames were first corrected for the non-uniformity of the gamma camera. A Metz filter of a specified order could then be applied to each of the series of frames. In this study all the images in a series for use in a calculation as described in Section B(vii), were processed with the same order of Metz filter. However several orders of Metz filter were applied to the entire series so that their effects could be compared with one another, and also with the corresponding unprocessed images.

(vi) Calculation of counts v. time curves

Counts v. time curves for selected parts of the image may be simply obtained from the series of processed or unprocessed images described above. Such curves were obtained for the four selected regions of the lungs (c.f. Section B(v)) and for a background region. The drop in count rate with time shown by these curves is due to the radioactive

decay of ^{13}N as well as to washout of ^{13}N from the lungs. Corrections are therefore made for this radioactive decay so that the decreasing count rate may then be interpreted as washout of ^{13}N from the lungs. Correction was also made for the tissue and natural background count level by subtracting the counts v. time curve obtained for a region of the image away from the lungs from those obtained for the lungs.

The corrected activity v. time curves were then plotted out. Inspection of these may reveal the presence of gross abnormalities in lung function, and also allows approximate comparison to be made between regions. However inspection alone does not always permit defects of ventilation to be separated from perfusion problems in infusion studies, and quantitative indices are useful for comparisons between patients, and with other methods of assessing lung function.

(vii) Calculation of quantitative indices

The object of this study was to calculate quantitative indices of lung function from the counts v. time curves describing the passage of ^{13}N through the lungs following its administration as a bolus by inhalation and by infusion. A brief description of the theory from which such indices and their significance may be deduced is given in Appendix V A.

The following indices have been used in this study. The peak heights of bolus infusion and inhalation curves give the total perfusion and total ventilation of the region. respectively, in terms of the amount of ^{13}N administered. The ratios of peak heights for perfusion or ventilation, respectively, for different parts of the lungs. therefore give the ratios of their total perfusions or ventilations. Here the peak counts for each of the four chosen regions have been calculated as a proportion of the peak counts for the whole of both

lungs. If the four regions are of equal sizes, this proportion should be approximately $\frac{1}{4}$ for each region, if there is no localized lung disease. It is often not possible or desirable to choose all the regions of equal size, and in that case, an index which will give an approximate guide to the regional differences in perfusion or ventilation is

$$\frac{\text{peak counts for region}}{\text{peak counts for whole lungs}} \Big/ \frac{\text{projected area of region}}{\text{projected area of whole lungs}}$$

This will give a value around 1 for all regions if ^{13}N is uniformly distributed; however it is clearly only an approximate measure of lung perfusion or ventilation, since the sizes of the regions should really be judged here by their volumes, which are unknown, and not by their projected areas as measured from a two-dimensional image.

The ratio of peak counts for inhalation to peak counts for infusion is proportional to the ventilation:perfusion ratio. The constant of proportionality is the same for all regions in a study, and so this index shows the variation of the ventilation:perfusion ratio from one region to another.

The ratio of the height to the area under the clearance curve for a bolus inhalation study gives the ventilation per unit volume of the region of lung considered. The corresponding "height/area" ratio for the bolus inhalation study does not have a straightforward physiological significance since it involves both ventilation and perfusion in a complex manner, but it is still useful to calculate this ratio, since it will be low if ventilation is poor as compared to perfusion.

C. Results

(i) "Static" images

Examples of the images obtained are shown in Figs. VA - P. These "static" scan images are cumulative count distributions, each collected over an entire study. Generally the lungs were shown clearly and could easily be delineated so that changes in count rate within identified regions of the lungs could then be followed throughout the studies.

However difficulties did sometimes arise in determining the extent and shape of the lungs. There were cases where parts of the lung showed up very poorly above the background count level. because these regions of lung had very little activity in them throughout the study and/or because the background was very high, as it might be for example in infusion studies if a patient has a cardiac shunt resulting in some ^{13}N circulating around the body before reaching the lungs. In such cases the true extent of the lungs could generally be seen by examining the image in conjunction with the recorded anatomical markers. These markers were also particularly useful for indicating the shape and position of the lungs in cases where the abnormal appearance of the lungs on the image may result from skeletal abnormalities such as scoliosis, rather than from localized defects in lung function.

As well as indicating the position of the lungs, the static image may show up defective regions of lung since localized disease often gives rise to local change in count density in the cumulative image. e.g. case 3 inhalation study (Fig. V A). Here the total activity in the lower part of the left lung is low, implying that inhalation is poor there.

However some local defects do not show up in the static image since the total number of counts depends on the total amount of ^{13}N entering the lung and how long it remains there. For the same reason, even when defects do show up, their significance is not always apparent. For example, case 5 infusion study (Fig. V M) shows high counts in the right upper region. Inspection of the counts v. time curves reveals that there is initially only slightly more activity in this region than one might expect. and that the high count density in the composite image is due mainly to the very slow washout.

(ii) "Static" scan images - Metz filtering

Examples of images processed with various orders of Metz filter are shown in Figs. V A - P. The images are visibly improved in that contrast between lungs and background is enhanced, and the boundary between the two lungs, which is sometimes indistinct. became clearer. Also in infusion studies where the edge of one lung may be in close proximity to the vein through which the ^{13}N was infused, the edge of the lung was resolved more clearly. Fine detail within the lungs is also more plainly visible, which may be useful when selecting small regions in order to assess localized functional defects.

The choice of the most suitable order of filter depends on the image count density, as can be seen from these examples. In case 5 inhalation study (Figs. V I - L), where there are few counts, Metz filter of order 3 gives a slight improvement on the unprocessed image, but artifacts can be seen when filters of orders 6 and 10 are applied. In case 3 inhalation study (Figs. V A - D), the number of counts is

higher and the Metz filter of order 6 gives rise to clear improvement, but when the 10th order filter is used artifacts and the characteristic mottling appear. When there are still more counts in the image as in case 5 infusion study (Figs. V M - P), even Metz filter of order 10 can be used, and in this case the resulting image is much clearer than the unprocessed one, and there is no mottling.

Thus it can be seen that for images with greater count densities, higher orders of Metz filter can be used with increasing benefit to the images, and without introducing the visible distortion and spurious noise which are seen if images with low count densities are processed with such high order filters. However it is not often possible to confirm conclusively that the processed images represent the "true" state of the lungs more accurately. Some information regarding the shape and size of the lungs and the presence of diseased regions may be known from x-rays or from other clinical tests, but obvicusly if all the information to be found was available by other non-traumatic techniques, the ^{13}N studies would be unnecessary. However in some of the cases studied, surgery was subsequently indicated to be necessary, and then verification of the shape and position of the lungs and the extent of disease was available; or in one or two cases where the patient died later, evidence was available from post-mortem.

(iii) Results of "dynamic" studies

The results are presented in the form of activity v. time curves for the regions of lung selected, and the quantitative indices described above - the peak counts and the "height/area" ratio. Diseased regions may be recognised by their contrast with the normal ones which have higher initial activity and slower washout. In cases where

there is generalized disease of both lungs, curves and indices can be assessed with reference to an estimated normal range.

Examples of the results obtained with and without Metz filtering are described in Section C(iv) below.

(iv) Results of ^{13}N lung studies and the effects of Metz filtering

Case 1 - this patient was 2 months old and showed clinical evidence of a hypoplastic left lung, while the right lung was thought to be normal. The gamma camera images supported this, showing a left lung much smaller than the right one which appeared to be of normal size and shape. In both infusion and inhalation studies, the initial amounts of ^{13}N, as estimated by the peak counts, were much greater in the right than in the left lung. The values of the peak counts in the two lungs when normalized for the area of the lung indicated that the difference in peak counts could not be accounted for only by the smaller size of the left lung, and so that the left lung was functioning poorly. Also in both studies, height/area ratios were lower for the left lung than for the right. In the infusion study the height/area ratios are low for both lungs but the value obtained for the right lung falls just within the normal range, while for the left lung it is lower. The height/area ratios for the inhalation study, which give the ventilation per unit volume, are high for both lungs, but again a little lower for the left than the right. Thus the study shows an almost normal right lung, but with slightly slow washout after infusion, and a small left lung with lowered perfusion and ventilation.

As can be seen from Table VA, in this case use of Metz filters emphasized the differences between the right and left lungs thus

confirming the clinical evidence that the right lung is completely normal.

Case 2 - this patient, aged 5½ years, had been diagnosed as having McLeod's syndrome, a condition in which one lung, in this case the left one, functions poorly, while the other is normal. The gamma camera study confirmed this diagnosis, as can be seen from Table VB and grom the graphs in Figure V Q. As with the previous case, Metz filtering emphasized the contrast between the normal right lung and the poorly functioning left lung. The graphs in Figure V Q give a comparison of the counts v. time curves for the infusion study with and without Metz filtering and show how the counts are re-distributed when the filter is applied, emphasizing the contrast between the healthy and diseased regions.

Case 3 - this patient, aged 6½ years old, also had McLeod's syndrome, once again the left lung was affected, and the right one normal. The "static" images for this case are shown in Figures V A - M. Table VC shows that here use of Metz filters again increased contrast in the infusion study but only slightly, and no improvement was obtained in the "dynamic" part of the inhalation study.

The lack of increased contrast obtained here in the "dynamic" part of the study by Metz filtering is probably due to the larger size of the patient who was 6½ years old and her lungs were considerably larger and further separated than those of the 5½ year old child described above as case 2. Consequently the effect of the activity in one lung on the counts recorded at the other would be less, and so would any corrective effect of the Metz filter be.

Case 4 - this patient, aged 9 8/12 years, was suspected of having sequestrations in the lower parts of both lungs. The affected

regions in such a condition are supplied with blood from the aorta instead of from the pulmonary artery, and consequently in a ^{13}N infusion study, these regions would receive no ^{13}N. In practice since it is not possible to isolate the sequestred regions in such a study the 'lower regions' chosen here would include a small amount of normal lung too and so would receive some radioisotope in the infusion study. Further although these regions have no basic inhalation defect, it is quite common for the lungs to adapt so that inhalation to the sequestred areas is decreased since it is useless for exchange of oxygen and carbon dioxide between air and blood. This is shown by the ^{13}N study to be true in this case.

Table V D indicates that Metz filtering increases the contrast between the upper and lower regions of both lungs, with the exception of the peak counts in the left lung in the inhalation study where there is little change - it is not apparent why this might be.

It should be noted that while this patient was older and larger than case 3 where the effects of Metz filtering were small owing to the regions to be compared being relatively distant from one another, with this patient although the lungs were also large, the behaviour of regions which are immediately adjacent to one another but functioning differently is being considered.

D. Discussion - Problems and Errors

(i) Selection of lung areas

Errors and problems arise at all stages in the procedure. Firstly in choosing lung regions the object was to choose four regions which in total include the whole of both lungs and nothing that is not lung, to avoid errors in assessment of lung function. To assist with

this, anatomical reference markers are recorded to indicate the boundaries of the patient's lungs. However, errors can easily occur for example if only a small number of counts were recorded, the lungs may be poorly defined because of poor statistics. If there is a region of lung that is scarcely if at all ventilated or perfused, it will not show up on either study and the true shape and extent of the lungs can only be guessed at. A problem which arises quite frequently in the infusion studies is the appearance on the composite image of the vein through which the ^{13}N is infused, and sometimes a small amount of the radioisotope lingers in or around this vein throughout the study; as a result it may be difficult to distinguish clearly where the lung boundary is, particularly when the ^{13}N is infused through a vein in the arm in which case the upper edge of the lung on that side may be unclear. In very young babies the radioisotope is generally infused through a scalp vein and in that case ^{13}N does not seem to linger or to confuse the image. Also in infusion studies, ^{13}N passes through the heart before entering the lungs and it is difficult to draw the outline of the lungs to avoid the heart. This may be still more confusing in patients with cardiac shunts such that some of the blood containing ^{13}N may recirculate round the heart several times before passing through to the lungs, or in some cases a proportion of the radioisotope may be carried around the body and back to the heart several times before entering the lungs thus increasing the general background as well as the image of the heart. In all cases the image may be blurred as a result of movement of the lungs in the course of respiration and as a consequence of any other movements the patient may make during the

study. Metz filtering of the images was found to improve visualization and this could also facilitate the selection of lung areas. However in these studies the areas were not chosen from the Metz filtered images, since this would have introduced another complication and would have made assessment of the effects of Metz filtering the dynamic studies more difficult.

(ii) Activity v. time curves

The activity v. time curves also have errors. The calculated curves show the numbers of counts recorded in successive 6 second time intervals; thus these curves do not show exactly the variations in count rate with time but average over the finer peaks and troughs, which is mostly useful since much of the small scale variation is due to statistical variation or to respiration, neither of which are of interest. However this procedure may also average over features of the curve that are relevant to this study, such as the peak itself, and 6 seconds is an arbitrary length of time which has been kept fixed mostly for simplicity of programming and of comparing results. Rate of respiration may vary considerably in babies and and children, depending on the age and condition of the infant, and statistical variations in the numbers of counts recorded in a fixed time interval depend on the count rate. For optimum accuracy the choice of time intervals should be made after consideration of these two factors, and during the earlier part of the study where the count rate is near its peak, finer time intervals could be used than later on in the washout.

(iii) Quantitative indices

When assessing the accuracy of the indices which can be calculated

two questions must be considered, firstly how accurately are the peak count rate and the area under a clearance curve described by use of 6 second time intervals, and secondly under the circumstances under which the studies are carried out on patients, how valid are the assumptions made when attributing physiological significance to the peak heights, ratios of peak heights and height/area ratios.

Considering first the errors due to arbitrary choice of 6 second time intervals. Statistical errors undoubtedly occur in measuring the peak height and the area under the curve; however statistical errors in calculating peak heights are usually small since the number of counts at the peak is high, unless the region concerned has very low supply of ^{13}N in blood or air, or unless very little of the radioisotope is administered. On the other hand as a result of the use of 6 second time intervals, the peak count rate will be averaged down and therefore the measured peak will always be an underestimate of the true peak count rate, and the faster the ^{13}N enters and leaves the lungs i.e. the sharper the peak, the greater the underestimate will be. The area under the clearance curve is the total of all counts recorded during washout, and therefore use of discrete time intervals should have no effect on this calculation.

The meaningful interpretation of the peak counts for inhalation and infusion studies, the height/area for inhalation studies, and the ratios of peak counts for inhalation to those for infusion, requires that the radioisotope is administered at a constant rate for a short period of time. The administration of the ^{13}N is controlled by hand, and it is therefore not at a completely constant rate, and in the case of an infusion study, even if it entered the bloodstream at a constant rate, it might not enter the lungs in this constant manner. However

these perturbations are probably not of great significance. In the inhalation study, the ^{13}N can be administered very swiftly, but in the infusion study this is not so since the ^{13}N is usually dissolved in 3 - 4 mls of saline, and this cannot usually be infused in less than a few seconds because infants' veins are small. It is shown in Appendix V B that for a slightly longer infusion, the peak counts obtained in the infusion study depend on the ventilation as well as the perfusion of that part of the lung, as indeed one would expect when the time for infusion is long enough for the amount of ^{13}N which is expired during the infusion to be significant. In this situation the perfusion will be underestimated by considering it to be represented by peak height in an infusion study where the infusion is not so short. Further since how short an infusion time is 'short' depends on the ventilated regions may be accurately given by the peak height, whereas the perfusion will be underestimated in well-ventilated regions, and as a result when ventilation-perfusion ratios are calculated from the peak heights errors may be made and ventilation-perfusion imbalance may be falsely predicted.

(iv) Effects of Metz filtering on "dynamic" studies

Here the results of Metz filtering are discussed with reference to the effects which this processing would be expected to produce. The shape of the washout curves may be altered by the fact that counts are transferred from one region to another by Metz filters and clearly the way in which counts are transferred in a given image depends on the spatial distribution of counts. Whether counts are moved from one part of an image to another depends on the distance between these

regions in the image and on the directional relationship between them since the point spread function does not have circular symmetry.

Generally in any frame counts will tend to be moved from regions of lower count density towards regions of higher count density. Therefore as long as the counts in the lungs are higher than those in the background, counts will be collected in from the background to the lungs so that at least the initial part of the washout curves will be raised. Similarly counts may be transferred from regions of lung with relatively low counts at a given time to adjacent regions with higher counts. This will result in the peak of the curve being increased in a region of high initial counts close to another region with low initial counts, and the peak in this second region will be lowered. Later in the washout curve, regions with higher counts as a result of slow washout rates will have increased counts, indicating even slower washout. Thus Metz filtering may be expected to reveal more plainly the differences in function in adjacent regions which may otherwise be obscured by blurring in the images. An example of this is the infusion study for case 2 (see Section C(iv)), where contrast between the right and left lung regions shows up more clearly in the curves after filtering.

Metz filtering may also be expected to correct for other errors. In an infusion study the region adjacent to the infusion line may have incorrectly high readings at the start of the study owing to the activity in the infusion line, and so after Metz filtering the peak for this region may be lowered. Also in the infusion studies, counts resulting from activity in the heart in the initial part of the study, and also later if there is a shunt, may be distributed to adjacent regions, and there may therefore be fewer counts in these

areas after processing. All these effects may occur, and they interact in such a way that the results of processing a particular study cannot be predicted in advance, but the observed changes in the curves may be interpreted bearing in mind the interplay of these factors.

These changes in the shape of the counts v. time curves as a result of Metz filtering will also affect the quantitative indices of lung function discussed in Section B(vii). Peak count rates may be increased as a result of counts being collected in from the background. However this should not alter the ratios between peak counts for different regions, since the extent of spread to the background is approximately proportional to the count density in the region. Metz filtering should also lead to better resolution between adjacent regions of high and low count densities, and therefore contrast in peak counts between adjacent areas with differing function may be increased after processing. As mentioned above, in infusion studies, the peak height of the curve for regions close to the infusion line or to the heart may be corrected by Metz filtering. When considering the index, 'height/(area under washout curve)', this obviously may also be altered, but the way in which it may change is complex since the 'height/area' depends on the proportion of the activity initially entering the lung which remains there later, whereas the effects of the Metz filter will depend on the activity at a given time relative to the activity in adjacent regions at that time. However in some cases one can predict what might happen. For example, consider an infusion study where two adjacent regions are equally well perfused, but one is less well ventilated than the other. In such a case, later in the study there will be greater activity in

the poorly ventilated region than in the well ventilated one, and owing to blurring, some of the counts from the activity in the poorly ventilated region may be attributed to the other region, making it appear less well ventilated than it is, and making the poorly ventilated region seem less poor than it really is. In this case the Metz filter might reduce the area under the clearance curve for the well ventilated region and increase that for the poorly ventilated one, thus increasing contrast between the 'height/area' ratios for the two regions. Thus it appears that Metz filtering should enable one to resolve differences between areas more clearly in terms of quantitative measurements obtained from the images as well as through improving visualization.

(v) Optimum order of Metz filter for processing "static" images

As with the ^{99m}Tc bone studies described in Chapter IV, here too the choice of Metz filters would be expected to be roughly in agreement with the rules obtained in Chapter III, since once again the point spread function is similar. In the examples referred to in Section V C(ii) this can be seen to be so. For example the optimum orders of Metz filter were observed to be as follows:

Table V E

Case	Approx. count density in region of interest	Opt. filter
5 Inhal.	15 $cell^{-1}$	3
3 Inhal.	35 $cell^{-1}$	6
5 Infus.	80 $cell^{-1}$	10

These orders are in agreement with what one would expect from Graph III H.

(vi) Choice of order of Metz filters for "dynamic" studies

The choice of the order of Metz filter is governed by image count density. In the case of these dynamic studies the Metz filter is applied to a series of images each consisting of all counts collected in a particular time interval of 6 seconds. The number of counts in any one of these images will depend on how much radioisotope was administered, and also at what stage in the study this image was accumulated, since clearly near the peak there will be higher count rates.

Ideally one would like to assess each frame to decide which order of Metz filter would be best for processing it, but without exact and reliable criteria for making this decision, this would be very difficult. It would also probably not be worthwhile since for the purposes of the study, the 6 second frames, processed or otherwise, are not viewed or assessed individually, but only in terms of the curves and indices derived from them.

The only frame of which individual use is made is the frame in which the peak counts are observed, and possibly an improvement in accuracy could be achieved if special attention were given to selecting the optimum order of Metz filter for this frame. However, here for simplicity all frames were simply filtered with the same order of Metz filter.

In some but not all of the examples the 6th order Metz filter seems to have a greater effect than 3rd order, but sufficient data was not available to determine which filter was better for this purpose.

E. Conclusions

The problems of carrying out a study of considerable complexity on patients who are too young to be cooperative, and using a radio-isotope which is short-lived and difficult to obtain, are apparent. These difficulties lead one to question the justification for applying a sophisticated image processing method in such a situation. However it has been seen that Metz filtering gives an improvement in visualization of the scan images, resolving features which may be indistinct on account of the small size of the patient. The results of processing the "dynamic" part of the study also give one reason to believe that at least in some cases, Metz filtering can be useful for distinguishing more accurately between regions which are close together but differ in their function.

In order to follow up these conclusions it will be necessary to carry out studies on more patients and assess the accuracy of the results by considering them together with other clinical evidence. The accuracy of the quantitative indices could be improved by choosing shorter time intervals near the peak of the curve, and further investigations could then also be made to assess which order of Metz filter is best, and the benefits of applying different orders of Metz filter to the frames in the washout curves.

APPENDIX VA

The theory presented below is described briefly in order that the approximations and errors involved in the assessment of lung function in terms of simple indices may be understood. This is taken from reference 9.

The lung cannot be described as a single unit, since, especially in disease, it behaves as a very inhomogeneous structure; however, it may be considered as a large number of small homogeneous units, not necessarily corresponding to any physiological structures, arranged in parallel. Since these studies attempt to measure net transfer of gas over many respirations, the periodicity of respiration is neglected in this analysis. In the course of these ^{13}N studies, the radioisotope is moved by bulk flow of gas as a result of pressure gradients between the mouth or nose and the alveolar-capillary membrane, and by diffusion across this membrane between blood in the capillaries and gas in the lungs. The bulk flow of gas is the rate-limiting process, and so diffusion is considered here to be instantaneous. The gas in transit is assumed to be a homogeneous sample of that in the compartment from which it came, and to mix instantaneously with the gas in the compartment it enters.

Consider one homogeneous lung unit of volume V_1 with flow of gas between this unit and the outside air at a rate λ, and supplied with blood at a rate θ. Consider the outside air to be a reservoir of volume V_o.

At time t, let the number of tracer molecules in the lung unit be N(t),
let the number of tracer molecules in the external reservoir be $N_o(t)$,

let the concentration of tracer molecules in the blood be f(t).

In the time interval t to t+Δt,

number of tracer molecules entering lung unit from external reservoir

$$= \frac{\lambda N_o(t)\Delta t}{V_o}$$

number of tracer molecules leaving lung unit for external reservoir

$$= \frac{\lambda N(t)\Delta t}{V}$$

number of tracer molecules entering lung unit from blood = $\Theta f(t)\Delta t$, assuming that all ^{13}N passing through the lung capillaries in the blood passes through to the air in the lungs. Since nitrogen is so insoluble, it may also be assumed that no ^{13}N passes from the air in the lungs into the blood.

Thus the net change in the number of ^{13}N molecules in the lungs is

$$\Delta N(t) = \left[\lambda N_o(t)/V_o - \lambda N(t)/V + \Theta f(t) \right] \Delta t \qquad \text{I}$$

$$\text{ie. } \frac{dN(t)}{dt} = \frac{\lambda N_o(t)}{V_o} - \frac{\lambda N(t)}{V} + \Theta f(t)$$

$$\therefore N(t) = e^{-\lambda t/V} \left\{ \int_o^t \left[\Theta f(t) + \lambda N_o(t)/V_o \right] e^{\lambda t/V} dt + N(0) \right\} \qquad \text{II}$$

where N(0) = no. tracer molecules in the lung unit at time t = 0.

This expression may be considerably simplified in the cases where the

radioisotope is administered by infusion alone or by inhalation alone.

Infusion study

Here $N(0) = 0$, and $N_o(t) = 0$ for all t if all expired gases are removed throughout the study.

II now becomes:

$$N(t) = e^{\frac{-\lambda t}{V}} \{ \int_o^t \Theta f(t) e^{\lambda t/V} dt \} \qquad \text{III}$$

If the infusion is given in the form of a constant concentration of ^{13}N, say h_1 > from time $t = 0$ to $t = \tau_1$, and then no further ^{13}N is given, this integral may be simply evaluated:

$$\text{For } t < \tau_1,\ N(t) = \frac{h_1 \Theta V}{\lambda} \left[1 - e^{-\lambda t/V} \right] \qquad \text{IV}$$

$$\text{For } t > \tau_1,\ N(t) = \frac{h_1 \Theta V}{\lambda} e^{-\lambda t/V} \left[e^{\lambda t_1/V} - 1 \right] \qquad \text{V}$$

describing the wash-in and wash-out phases of the study, respectively. For a short bolus infusion, the infusion time may be so short that the proportion of the gas in the lung unit removed by ventilation during the infusion time is very small, an approximation may be made which further simplifies the expressions.

$$\text{For } \frac{\lambda \tau_1}{V} << 1,\ e^{\lambda \tau_1/V} \sim 1 + \frac{\lambda \tau_1}{V}$$

$$\therefore \text{ for } t < \tau_1,\ N(t) \simeq h_1 \Theta t \qquad \text{VI}$$

for $t > \tau_1$, $N(t) \simeq h_1 \theta \tau_1 e^{-\lambda t/V}$ or $N(t) \simeq h_1 \theta \tau_1 e^{-\lambda t'/V}$ VII

Thus in this case the peak counts in the lung unit, $h_1 \theta \tau_1$, depend only on the blood supply and the amount of ^{13}N infused, and the rate of elimination of ^{13}N depends only on λ/V i.e. ventilation per unit volume.

Inhalation study

Here $N(0) = 0$, and $f(t) = 0$ for all t

II becomes $N(t) = e^{-\lambda t/V} \{ \int_o^t \frac{\lambda N_o(t)}{V_o} e^{\lambda t/V} dt \}$ VIII

If the ^{13}N is inhaled at a constant concentration h_2 from time $t = 0$ to $t = \tau_2$, i.e. $\frac{N_o(t)}{V_o} = h_2$, and thereafter $\frac{N_o(t)}{V_o}$ is negligible, this integral may be evaluated:

For $t < \tau_2$, $N(t) \simeq h_2 V \left[e^{\lambda \tau_2/V} - 1 \right]$ IX

For $t > \tau_2$, $N(t) \simeq e^{-\lambda t/V} h_2 V \left[e^{\lambda \tau_2/V} - 1 \right]$ X

For a short bolus inhalation i.e. τ_2 so small that $\frac{\lambda \tau_2}{V} << 1$,
$e^{\lambda \tau_2/V} \sim 1 + \frac{\lambda \tau_2}{V}$

$\therefore$ for $t < \tau_2$, $N(t) \simeq h_2 \lambda t$ XI

for $t > \tau_2$, $N(t) \simeq h_2 \lambda \tau_2 e^{\frac{-\lambda t}{V}}$ or $N(t) \simeq h_2 \lambda \tau_2 e^{-\lambda t''/V}$ XII

where $t'' = t - \tau_2$.

Thus here the peak counts, $h_2 \lambda\tau_2$, depend on the total ventilation of the lung unit and the amount of ^{13}N inhaled, and once again the rate of elimination of ^{13}N depends only on λ/V, ventilation per unit volume.

Now if the whole lung is considered as a large number, m, of lung units in parallel, each with rate of flow of gas λ_i, rate of supply of blood Θ_i, volume V_i, expressions for the activity time curves can be calculated:

Bolus Infusion: for $t < \tau_1$, $N(t) = h_1 t \sum_{i=1}^{m} \Theta_i$ XIII

$t > \tau_1$, $N(t') = h_1\tau_1 \sum_{i=1}^{m} \Theta_i e^{-\lambda_i t'/V_i}$ XIV

Bolus Inhalation: for $t < \tau_2$, $N(t) = h_2 t \sum_{i=1}^{m} \lambda_i$ XV

$t > \tau_2$, $N(t'') = h_2\tau_2 \sum_{i=1}^{m} \lambda_i e^{-\lambda_i t''/V_i}$ XVI

Indices commonly used for these studies are peak heights of curves and the ratio of the peak height to the area under the washout curve. The area under the clearance curve is given by $\int_{\tau}^{\infty} N(t)dt$. For a bolus infusion study, from XIII and XIV,

Peak counts, $N_{pk} = h_1\tau_1 \sum_{i=1}^{m} \Theta_i$ XVII

Height/area, $H/A = h_1\tau_1 \sum_{i=1}^{m} \Theta_i \Big/ \int_{o}^{\infty} h_1\tau_1 \sum_{i=1}^{m} \Theta_i e^{-\lambda_i t'/V_i}\, dt'$

$= \sum_{i=1}^{m} \Theta_i \Big/ \sum_{i=1}^{m} V_i\Theta_i/\lambda_i$ XVIII

For a bolus inhalation study, from XV and XVI,

$$\text{Peak counts, } N_{pk} = h_2\tau_2 \sum_{i=1}^{m} \lambda_i \qquad \text{XIX}$$

$$H/A = h_2\tau_2 \sum_{i=1}^{m} \lambda_i \Big/ \int_0^{\infty} h_2\tau_2 \sum_{i=1}^{m} \lambda_i e^{-\lambda_i t''} / V_i \, dt''$$

$$= \sum_{i=1}^{m} \lambda_i \Big/ \sum_{i=1}^{m} V_i \qquad \text{XX}$$

Since h_1 and h_2 cannot be measured, and will be different for each study performed, equation XX is the only one of these four equations to give an absolute measure of lung function. Thus the ratio of the height to the area under the clearance curve for a bolus inhalation study gives the ventilation per unit volume of the region of lung considered. The "height/area" ratio for the bolus infusion study does not have a straightforward physiological significance, since it involves both ventilation and perfusion in a complex manner, but clearly, if ventilation is poor as compared to perfusion, this ratio will be low.

The peak heights of bolus infusion and inhalation studies give total perfusion and total ventilation of the region, respectively, in terms of the amount of ^{13}N administered. Since this is constant for all regions in one study, the ratios of peak heights for different parts of the lung will give the ratios of their total perfusions or total ventilations.

The ratio of peak counts for inhalation to peak counts for infusion is given by

$$N_{pk\ inhal}/N_{pk\ infus} = \frac{h_2\tau_2}{h_1\tau_1} \quad \frac{\sum_{i=1}^{m} \lambda_i}{\sum_{i=1}^{m} \Theta_i}$$

$$= \frac{h_2\tau_2}{h_1\tau_1} \quad \frac{\text{Total ventilation for region}}{\text{Total perfusion for region}}$$

where $h_2\tau_2/h_1\tau_1$ is constant for all regions. Thus this index will show the variation of ventilation:perfusion ratio from region to region.

The ratios of successive moments of the clearance curves have been calculated in similar studies, but these also do not have simple physiological interpretations, and they have other disadvantages since they weight heavily the tail end of the clearance curve which has low counts and is consequently not accurately known.

There are other methods for obtaining more information from the curves, but they are much more complex and require lengthy computations. These methods are only applicable when the data is fairly accurate, that is when the count rates obtained are high, which is not always so. Consequently only the curves themselves and the simple indices described above have been used in this thesis.

APPENDIX VB

The magnitude of the error which may be introduced in the calculations by the assumption of a 'short' infusion time is examined here. In the discussion of the indices, the requirement for a short infusion time is that

$$e^{\lambda\tau_1/V} \sim 1 + \frac{\lambda\tau_1}{V}$$

i.e. $(\frac{\lambda\tau_1}{V})^2$ and higher orders are not significant.

The errors involved in this approximation are shown in the table below for various values of $\frac{\lambda\tau_1}{V}$

Table VF

$\lambda\tau_1/V$	$e^{\lambda\tau_1/V}$	$1 + \lambda\tau_1/V$	% Error	$1 + \frac{\lambda\tau_1}{V} + \frac{1}{2}(\frac{\lambda\tau_1}{V})^2$	% Error
0.05	1.051	1.050	0.1%		
0.10	1.105	1.100	0.4%		
0.15	1.162	1.150	1.0%		
0.20	1.221	1.200	1.7%	1.220	0.1%
0.30	1.350	1.300	3.7%	1.345	0.4%
0.40	1.492	1.400	6.2%	1.480	0.8%

From other measurements [2], it has been found that ventilation per unit volume for healthy lung in children may be more than 4 mℓs/min/mℓ. If infusion time $\tau_1 \sim 1$ sec, then $\frac{\lambda\tau_1}{V} \sim 0.07$, in which case the bolus approximation would be justified; however, if $\tau_1 \sim 6$ secs, then $\frac{\lambda\tau_1}{V} \sim 0.40$, in which case the approximation would introduce considerable error, and a

higher order approximation must be attempted.

Here the substitution $e^{\lambda\tau_1/V} \sim 1 + \frac{\lambda\tau_1}{V} + \frac{1}{2}\left(\frac{\lambda\tau_1}{V}\right)^2$ is used. Substituting in equation IV (Appendix VA),

For $t < \tau_1$, $N(t) = h_1\Theta t\left[\, 1 - \frac{1}{2}\frac{\lambda t}{V}\,\right]$

and the peak counts will be

$$N_{pk} = h_1\tau_1 \sum_{i=1}^{m}\Theta_i\left[\, 1 - \frac{1}{2}\frac{\lambda_i\tau_1}{V_i}\,\right] \qquad \text{XXI}$$

from equation XVII (Appendix VA). Thus the peak counts for such an infusion study depend on ventilation, and the observed peak counts are less than the peak counts for a true bolus by an amount which depends on the ventilation of that region.

Table VA Case 1

L = Left lung R = Right lung

Infusion	Peak counts L : R	Ratio	Peak counts Normalized for area L	R	Peak Total	Height/Area ratios L	R
Unprocessed	1152 : 2570	0.45:1	0.81	1.12	3722	1.35	2.03
Metz 3	1079 : 2780	0.39:1	0.73	1.17	3859	1.30	2.11
Metz 6	1164 : 3211	0.36:1	0.69	1.19	4375	1.70	2.39

Inhalation	Peak counts L : R	Ratio	Peak counts Normalized for area L	R	Peak Total	Height/Area ratios L	R
Unprocessed	1977 : 4241	0.47:1	0.83	1.12	6218	5.13	5.38
Metz 3	1833 : 4660	0.39:1	0.72	1.18	6493	5.24	5.53
Metz 6	2175 : 5568	0.39:1	0.72	1.18	7743	5.34	5.67

Table VB Case 2

Infusion	Peak counts L : R	Ratio	Peak counts Normalized for area L	R	Peak Total	Height/Area ratios L	R
Unprocessed	377 : 1986	0.19:1	0.34	1.67	2303	1.98	3.87
Metz 3	273 : 2144	0.13:1	0.23	1.72	2410	2.06	3.99
Metz 6	251 : 2332	0.11:1	0.20	1.78	2543	2.17	4.30

Inhalation	Peak counts L : R	Ratio	Normalized for area L	R	Peak Total	Height/Area ratios L	R
Unprocessed	1584 : 3998	0.40:1	0.59	1.39	5582	3.90	5.89
Metz 3	1491 : 4180	0.36:1	0.54	1.43	5671	3.79	5.88
Metz 6	1573 : 4690	0.34:1	0.52	1.45	6263	4.01	6.15

Table VC Case 3

Infusion	Peak counts L : R	Ratio	Peak counts Normalized for area L	R	Peak Total	Height/Area ratios L	R
Unprocessed	845 : 2372	0.36:1	0.48	1.62	3217	0.53	2.50
Metz 3	837 : 2518	0.33:1	0.46	1.65	3355	0.58	3.08
Metz 6	903 : 2787	0.32:1	0.45	1.66	3691	0.55	3.22

Inhalation	Peak counts L : R	Ratio	Peak counts Normalized for area L	R	Peak Total	Height/Area ratios L	R
Unprocessed	2087 : 5027	0.42:1	0.54	1.56	7114	2.74	4.01
Metz 3	2178 : 5278	0.41:1	0.53	1.56	7456	2.30	4.07
Metz 6	2501 : 5844	0.43:1	0.55	1.54	8346	3.08	4.17

Table VD Case 4

l ≡ lower region u ≡ upper region

Left lung

Infusion	Peak counts l : u	Ratio	Peak counts Normalized for area l	u	Height/Area Ratios l	u
Unprocessed	268 : 1931	0.14:1	0.36	0.96	2.18	2.72
Metz 3	282 : 1817	0.16:1	0.38	0.89	2.20	2.75
Metz 6	204 : 1953	0.10:1	0.26	0.91	2.17	2.89

Inhalation	Peak counts l : u	Ratio	Peak counts Normalized for area l	u	Height/Area Ratios l	u
Unprocessed	343 : 2143	0.16:1	0.44	1.00	1.83	2.52
Metz 3	395 : 2021	0.20:1	0.50	0.94	1.95	2.56
Metz 6	335 : 2133	0.16:1	0.41	0.97	1.96	2.71

Right lung

Infusion	Peak counts l : u	Ratio	Peak counts Normalized for area l	u	Height/Area Ratios l	u
Unprocessed	425 : 2616	0.16:1	0.65	1.43	2.58	3.11
Metz 3	393 : 2803	0.14:1	0.59	1.52	2.71	3.17
Metz 6	341 : 3060	0.11:1	0.49	1.58	2.84	3.30

Inhalation	Peak counts l u	Ratio	Peak counts Normalized for area l	u	Height/Area Ratios
Unprocessed	362 : 2716	0.13:1	0.52	1.40	2.25	2.60
Metz 3	323 : 2856	0.11:1	0.46	1.47	2.26	2.67
Metz 6	232 : 3031	0.08:1	0.32	1.52	2.12	2.90

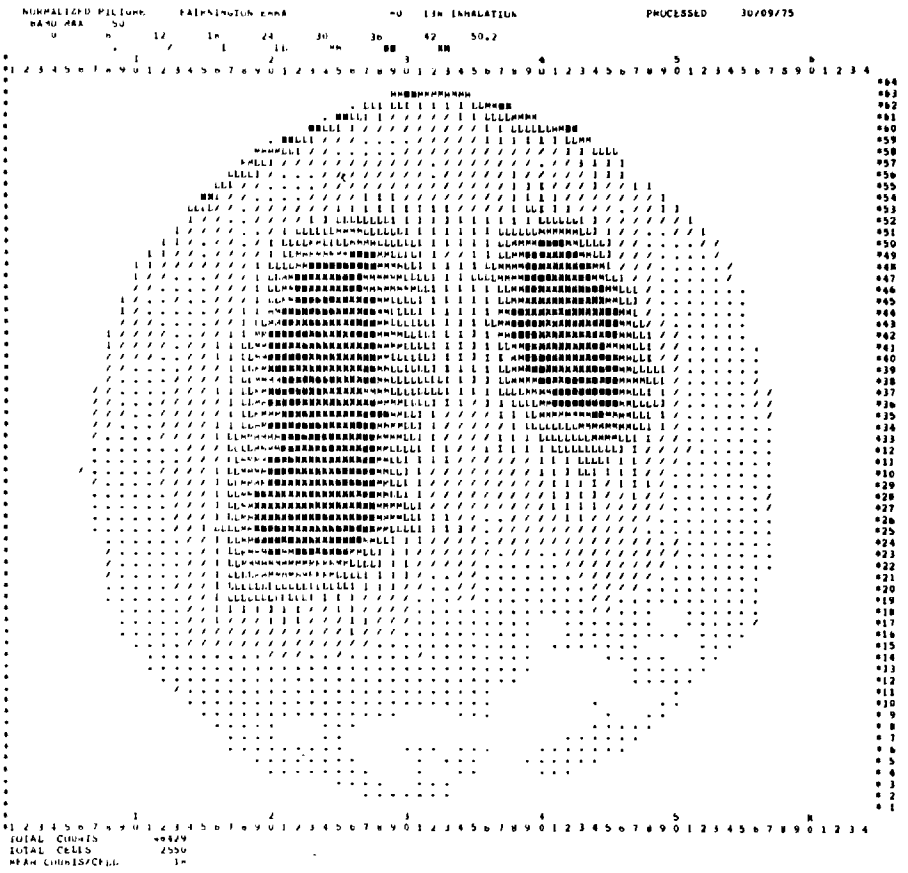

Fig. V A Case 3. Inhalation study. Unprocessed image.

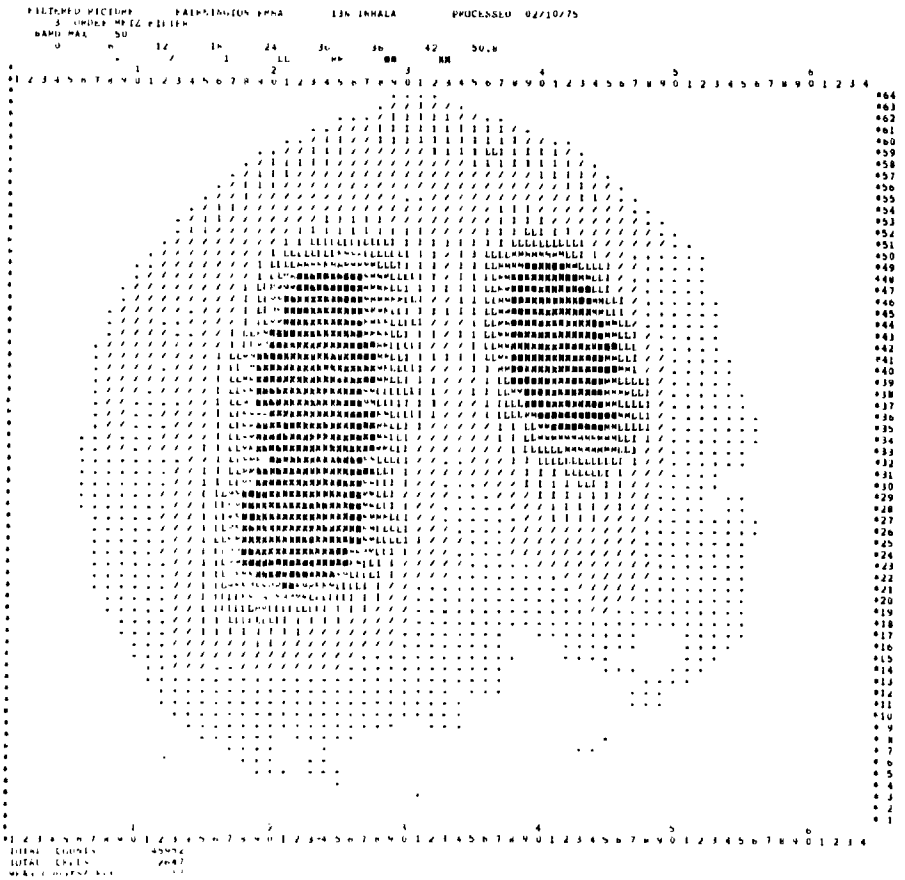

Fig. V B Case 3. Inhalation study. Processed with 3rd order Metz filter.

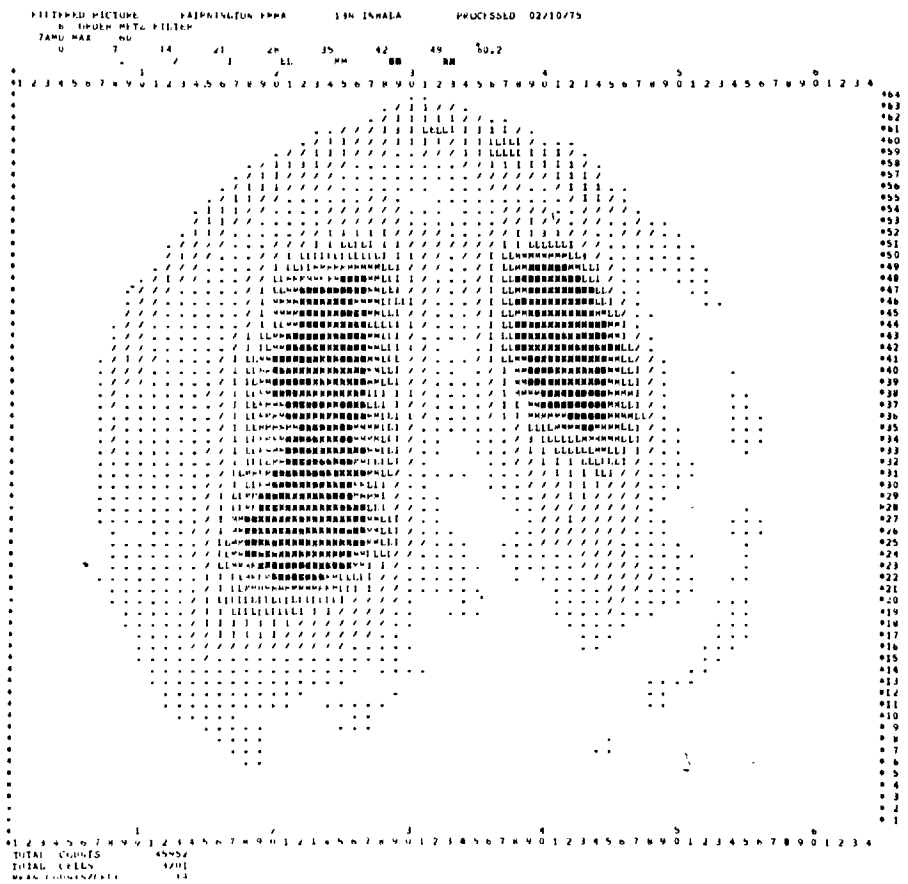

Fig. V C Case 3. Inhalation study. Processed with 6th order Metz filter.

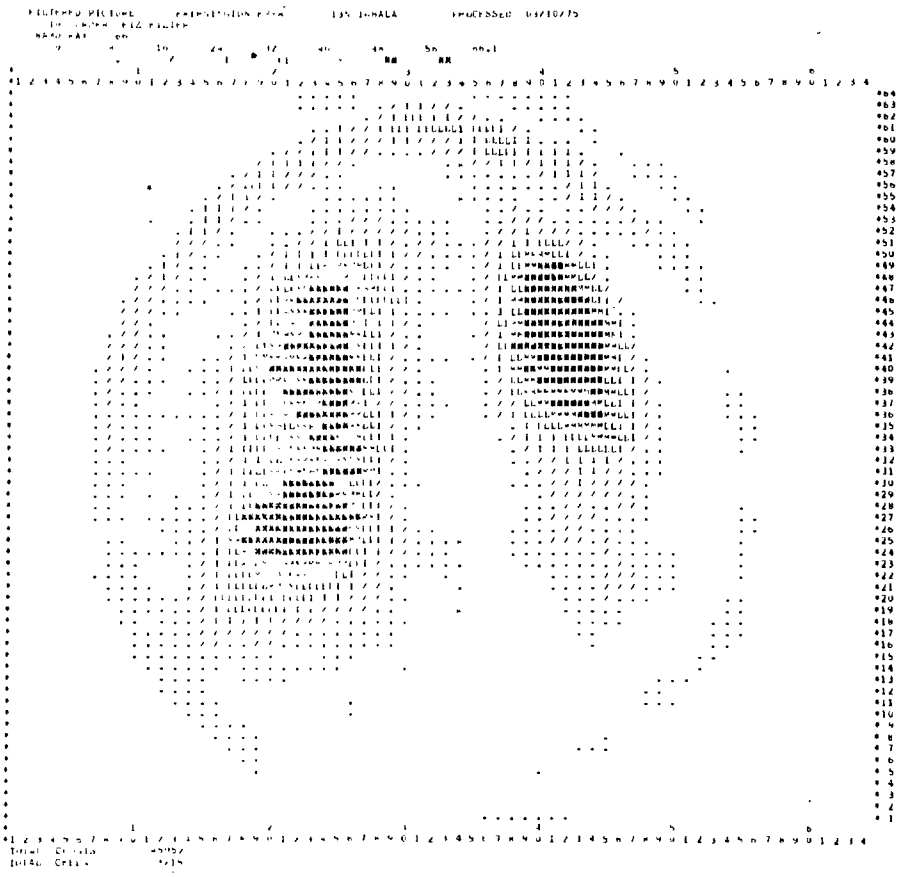

Fig. V D Case 3. Inhalation study. Processed with 10th order Metz filter.

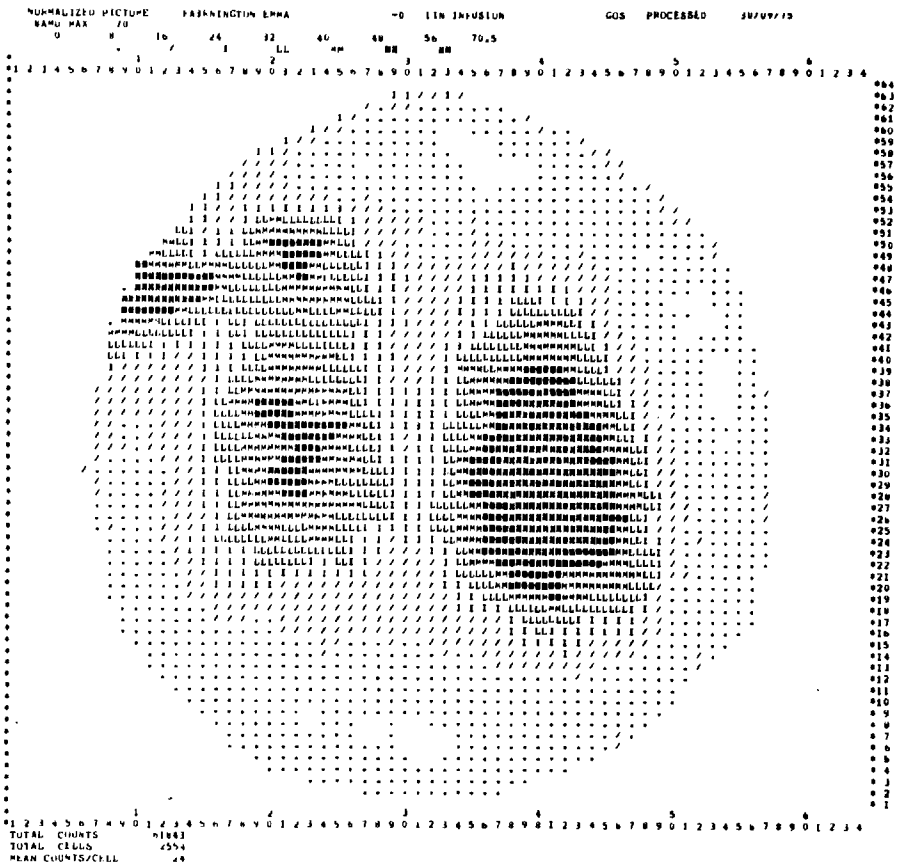

Fig. V E Case 3. Infusion study. Unprocessed image.

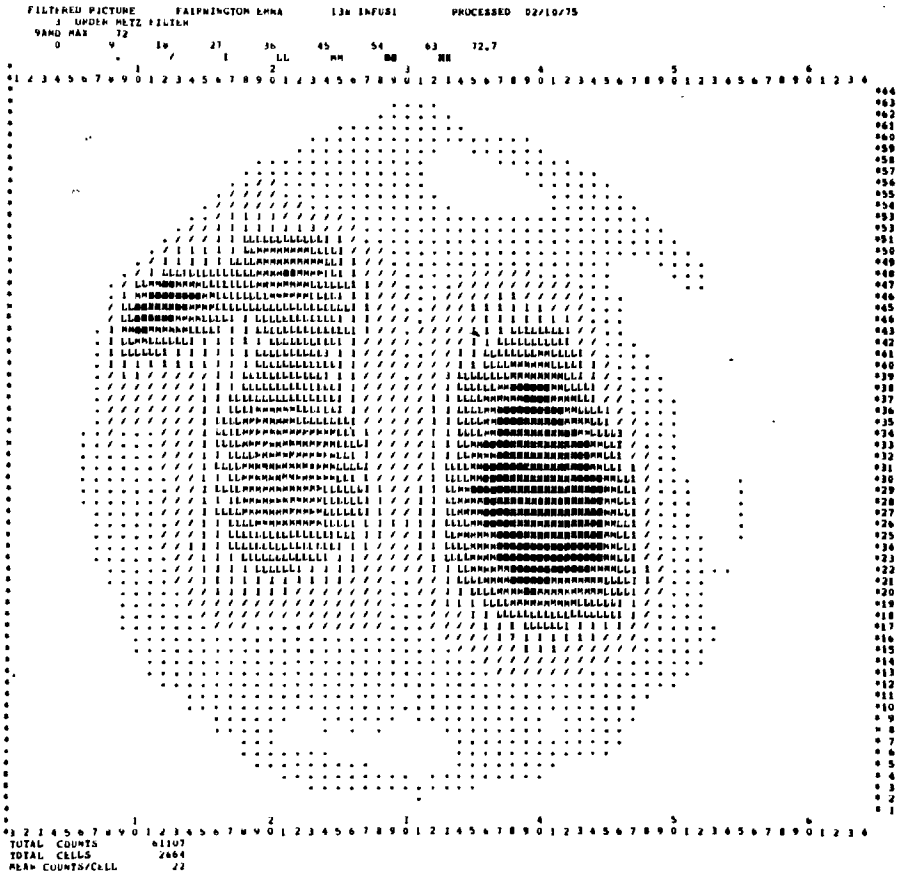

Fig. V F Case 3. Infusion study. Processed with 3rd order Metz filter.

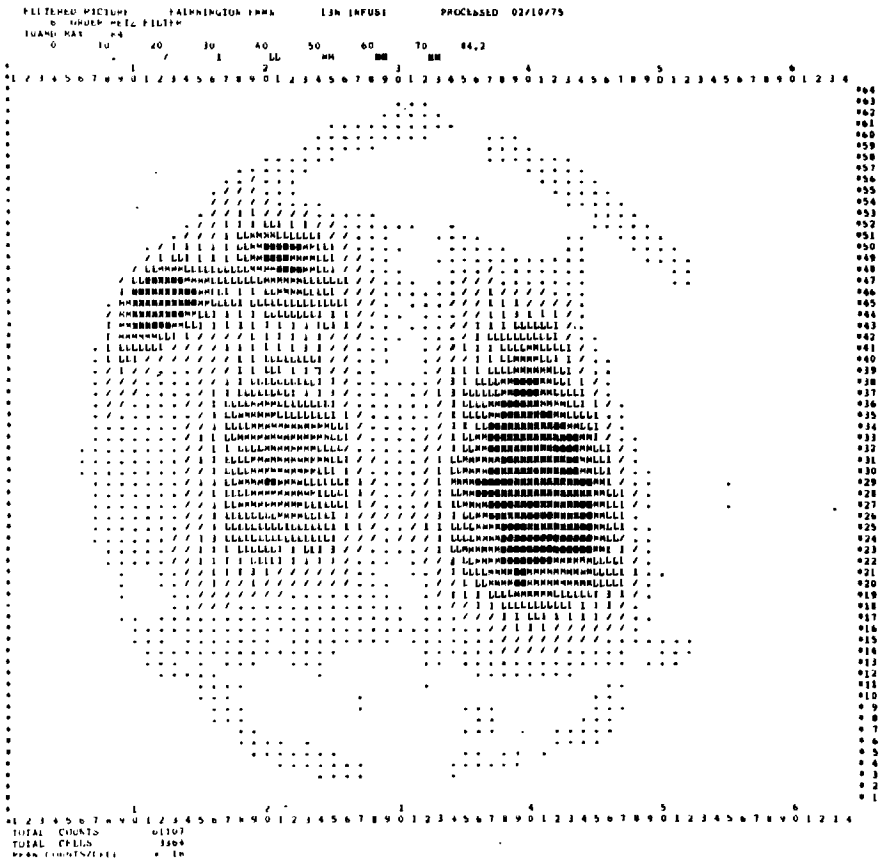

Fig. V G Case 3. Infusion study. Processed with 6th order Metz filter.

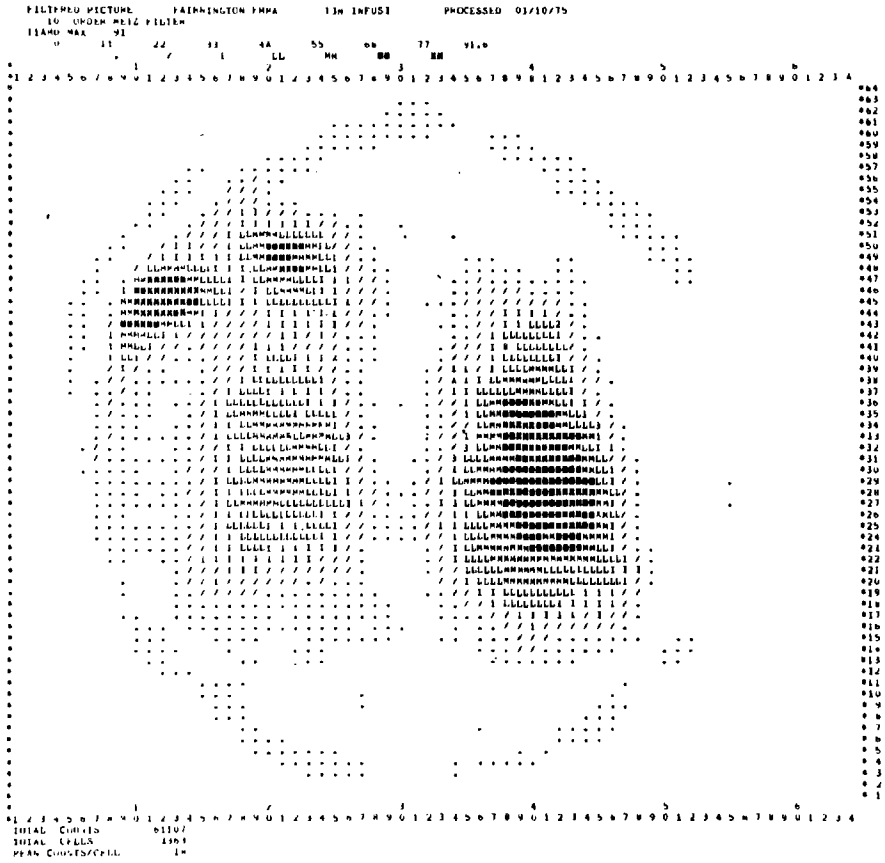

Fig. V H Case 3. Infusion studv. Processed with 10th order Metz filter.

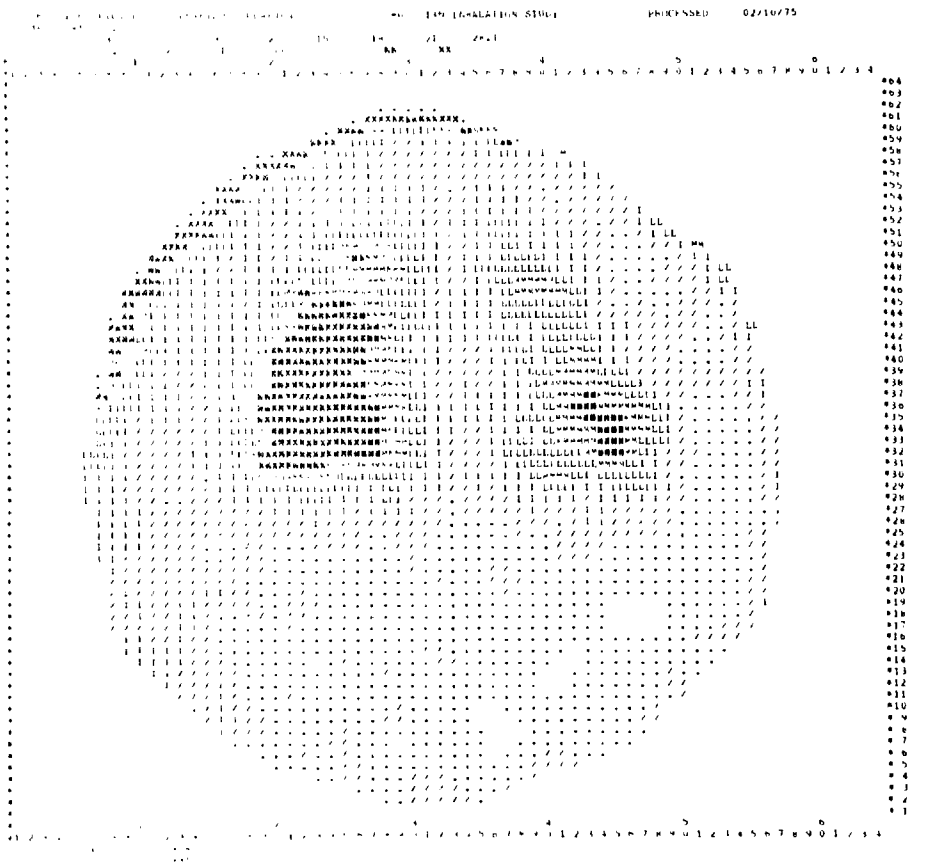

Fig. V I Case 5. Inhalation study. Unprocessed image.

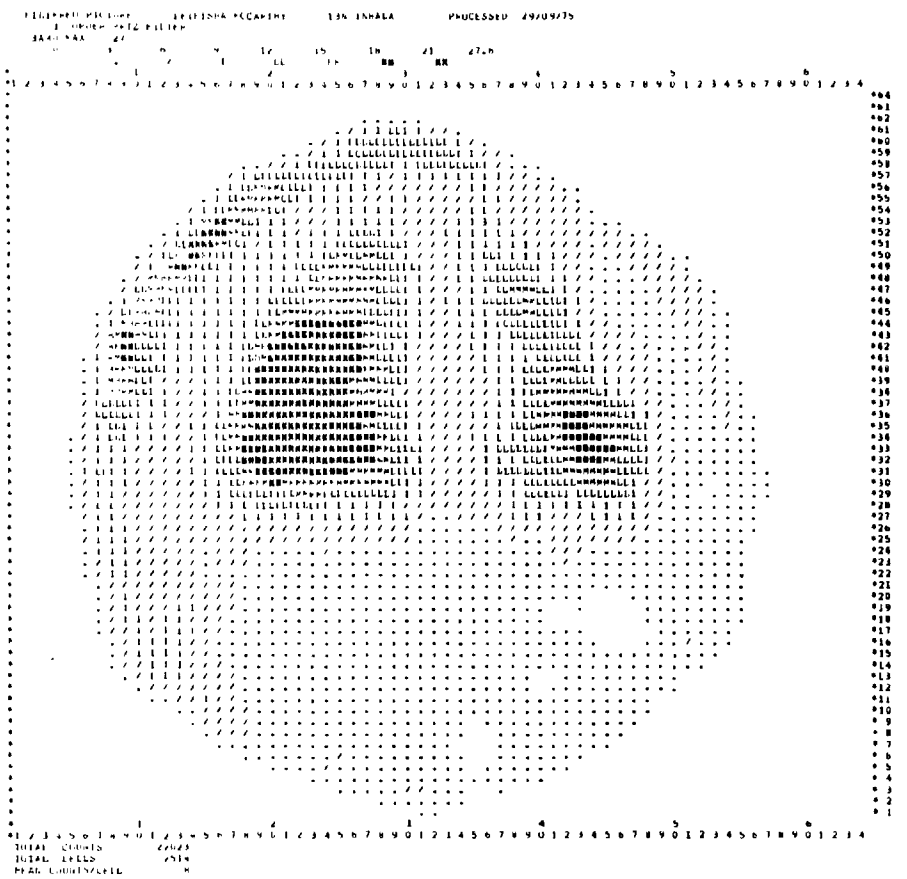

Fig. V J Case 5. Inhalation study. Processed with 3rd order Metz filter.

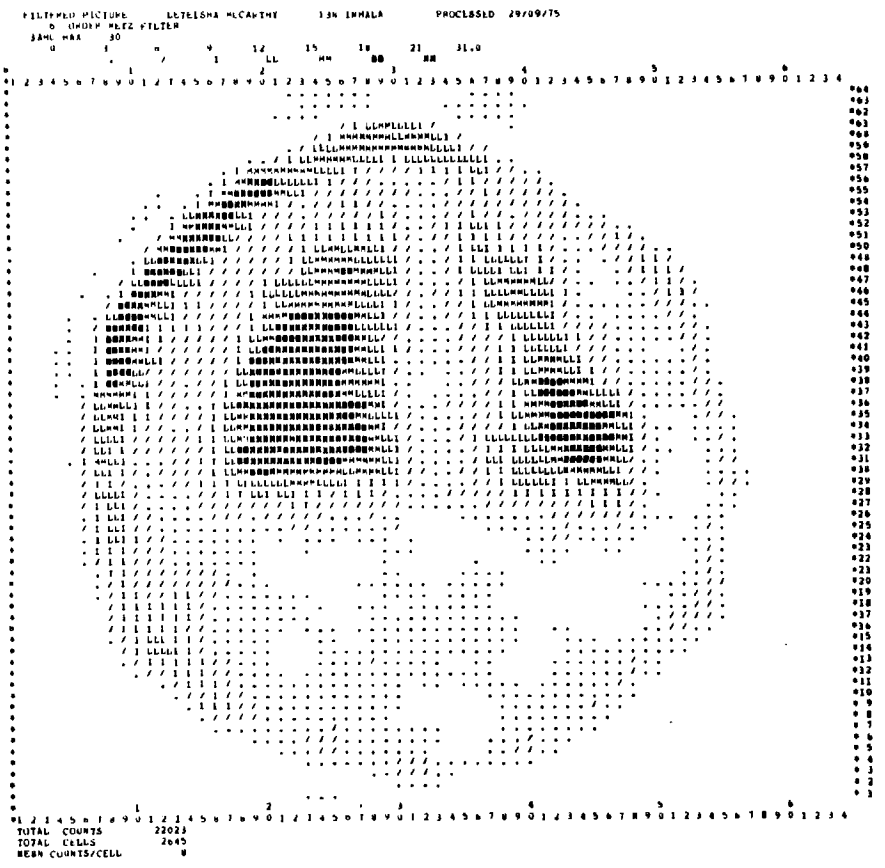

Fig. V K Case 5. Inhalation study. Processed with 6th order Metz filter.

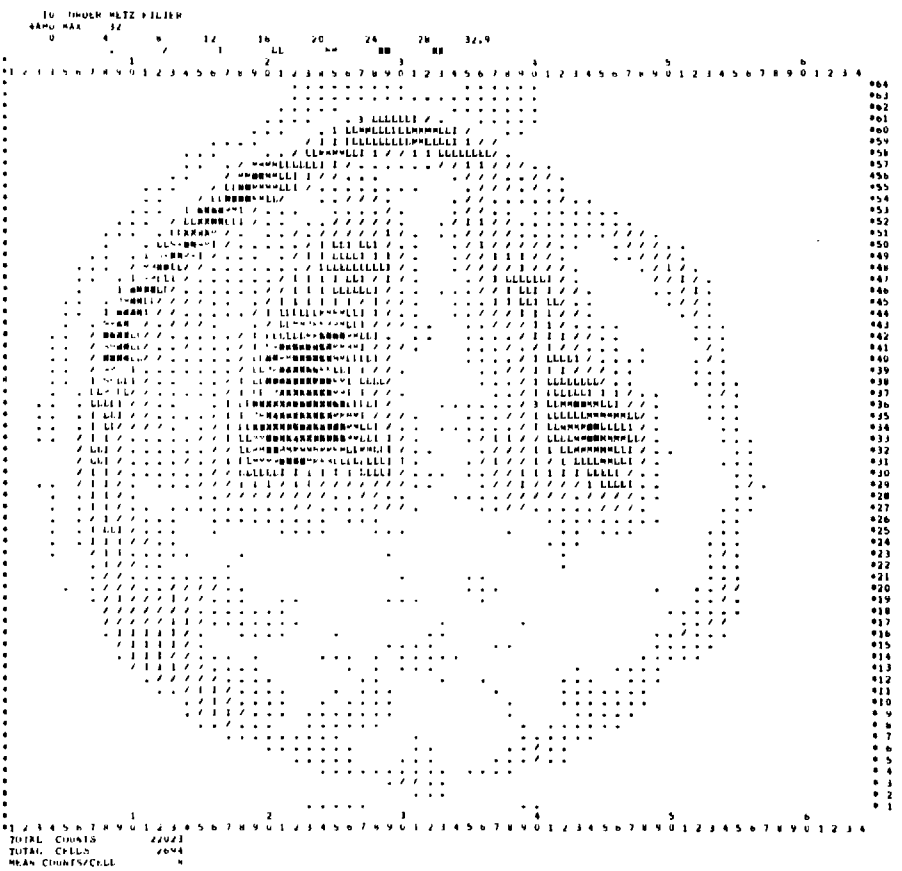

Fig. V L Case 5. Inhalation study. Processed with 10th order Metz filter.

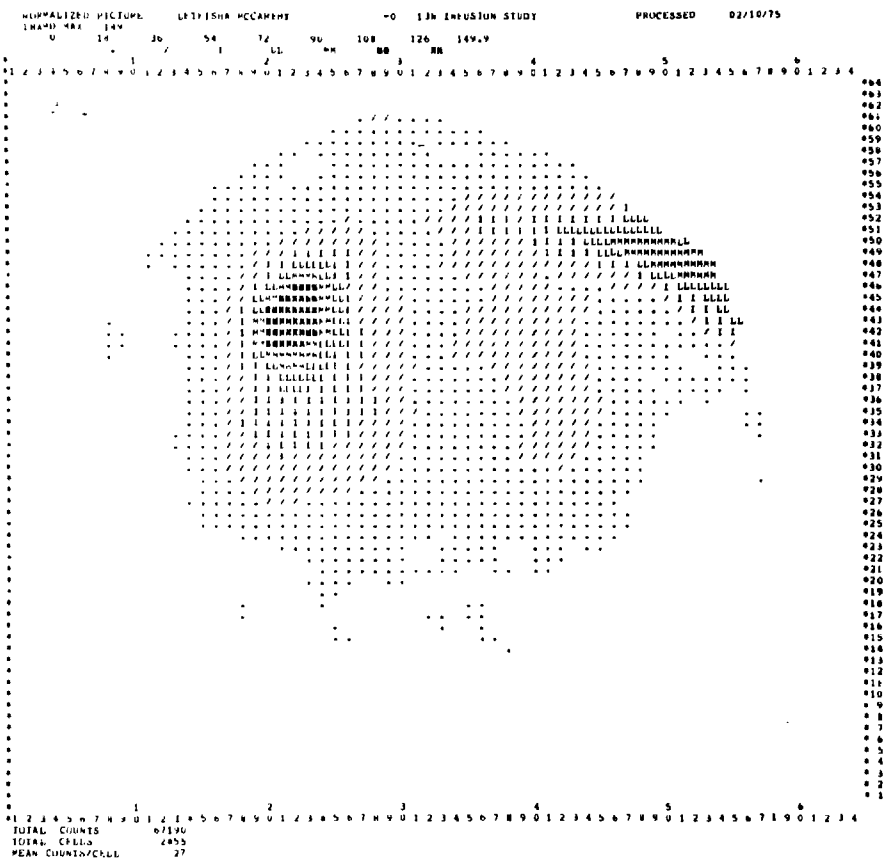

Fig. V M Case 5. Infusion study. Unprocessed image.

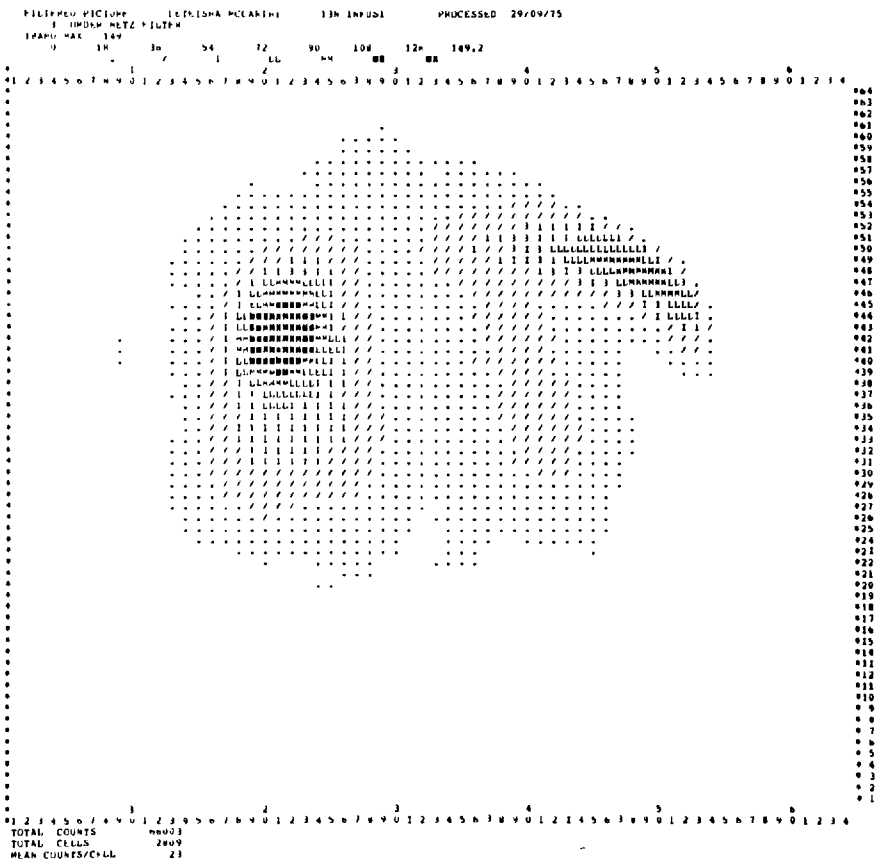

Fig. V N Case 5. Infusion study. Processed with 3rd order Metz filter.

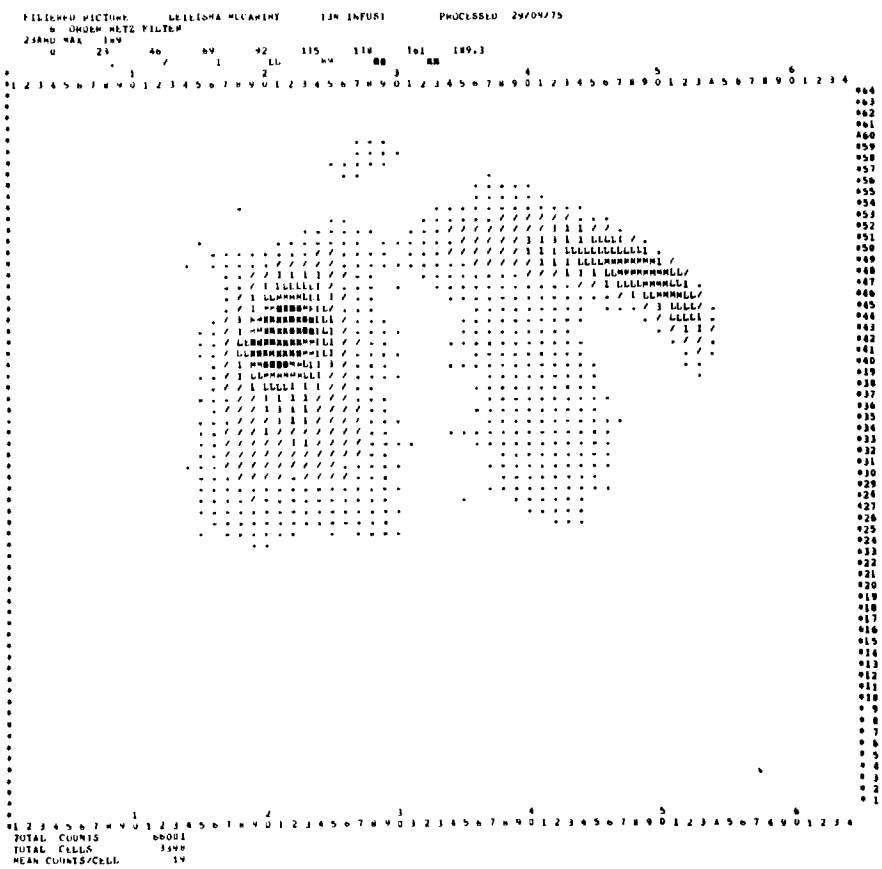

Fig. V 0 Case 5. Infusion study. Processed with 6th order Metz filter.

Fig. V P Case 5. Infusion study. Processed with 10th order Metz filter.

Figure V Q - Case 2 Infusion study - washout curves for 4 lung regions

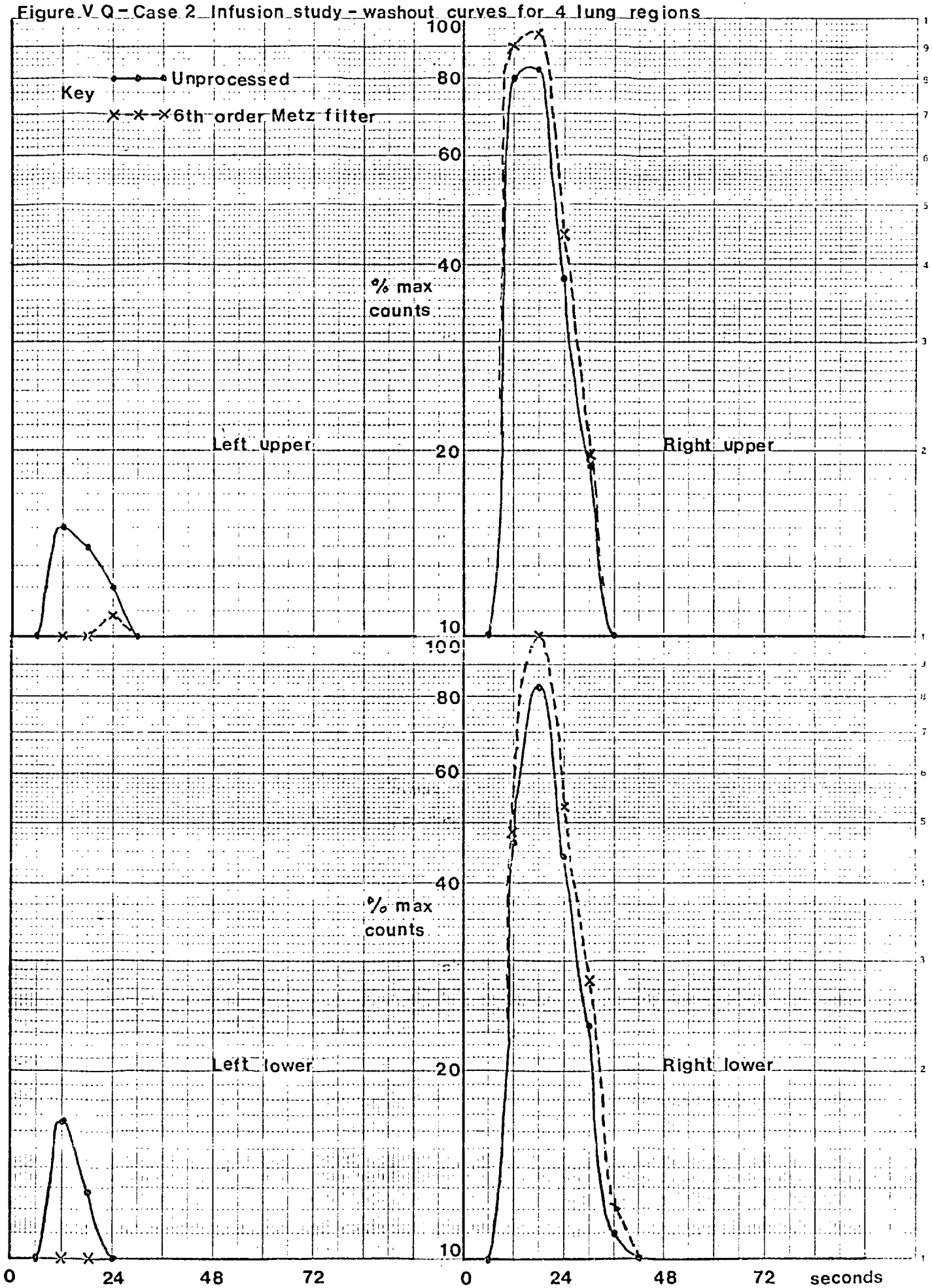

Chapter VI

Conclusions

Abstract

A summary is given of the work described in this thesis; the purposes of using an image processing method such as the Metz filter, the technique used here to apply it, choice of the optimum order of Metz filter, the success of the filter in clinical situations. Indications for future work arising from the findings of this thesis are then outlined too.

CHAPTER VI

Conclusions

(i) Performance of Metz filters

Clinical radioisotope studies using a gamma camera aim to obtain accurate representations of the radioisotope distribution in a living subject: in the case of dynamic studies the changes of the distribution with time are also followed. Image processing is carried out to extract more information from the degraded images which the gamma camera produces. Metz filtering is one of many methods (see Chapter I) used to improve resolution as well as reducing high frequency noise in the image. As it is applied here, Metz filtering attempts to correct some of the imperfections of the imaging system, but since these are partly governed by statistical factors, complete correction of the degraded image is never possible. However partial correction may be attempted. The Metz filter is a flexible method and use of different orders of the filter allows for varying degrees of correction as the circumstances demand. Higher orders of the filter result in a greater resolution enhancement.

The performance of the Metz filters in improving images of a known object, the Siemens' star phantom, under varying degrees of statistical variation due to noise was investigated (see Chapter III). Using the Siemens' star phantom it was possible to assess the effects on the image of Metz filtering from two points of view: (1) comparison of the general level of frequency response obtained with the theoretical one, and (2) the extent of fluctuations in frequency response resulting from image noise. Two quantitative indices were derived

to describe these two features in the performance of the filters. The results of this experiment indicated that even for images with very low count densities and correspondingly very low signal-to-noise ratios. processed images are more representative of the object than unprocessed ones. This remained true although, as expected, the higher the order of Metz filter used, i.e. the more ambitious the resolution enhancement attempted, the more slight image defects due to noise are exaggerated and may appear as artifacts in the image.

(ii) Criteria for selection of optimum order of Metz filters

For practical applications it would be useful to know not merely that Metz filtering improves images, but which is the optimum order of Metz filter at which a compromise is achieved between resolution recovery and amplification of noise to give image improvement and reliability. Ideally one would hope to find quantitative criteria for deciding on the optimum order of Metz filter for processing a given image. This would involve assessment of the noise level in the image and a knowledge of the performance of the Metz filters at that noise level for the radioisotope and scanning conditions used to obtain the image.

Unfortunately it was not possible to obtain exact criteria from the available data. but a rough criterion was obtained from observation of the behaviour of the index which described the extent of fluctuations in the frequency response resulting from noise. It was noted that the drop in this index was sharp initially but at higher count levels, only slight further fall was observed with increasing counts. The count level at which this transition was observed differs for each order of filter; it occurred at higher

count levels for higher orders. One could therefore decide which order of filter to apply to a given image under these conditions by selecting the highest order of filter for which the index curve is above its point of transition at the count level applicable to the image. This criterion was applied. using the average count density in the region of interest as a measure of the count level of the image.

(iii) Application of the Metz filters

Metz filters were applied to the images obtained in the clinical studies on bone metastases and on infants' lungs described in Chapters IV and V respectively. In both studies Metz filters were applied to all the "static" images, and in the dynamic study of infants' lungs, the filters were also applied to each of the sequence of images from which information about the change in the radioactivity distribution with time was obtained. The orders of Metz filter for the "static" images were selected by visual inspection, and also, for comparison. by applying the criterion described above. The validity of the criterion could not be tested accurately since different radioisotopes were used; however. approximate information could be obtained since under the conditions of the scans the observed point spread functions for these radioisotopes were similar to that for ^{133}Xe which was used in the Siemens' star phantom experiment. In these clinical studies, the criterion was seen to be a useful indicator for the choice of the optimum order of filter. giving agreement with selection based on visual inspection.

(iv) Indication for future work

A criterion for selecting the optimum order of Metz filter has

been found and tested, but it is only approximate, and more thorough investigation of the criterion itself and the way in which it is applied would be required to improve its reliability. The behaviour of the 'fluctuation' index used to derive the criterion could be determined more accurately if further calculations were performed and additional data obtained. Further examination of the second performance index might enable one to use the two indices in conjunction to give a more refined criterion. Greater accuracy might also be achieved through more detailed investigation of the method of assessment of image noise level used for application of the criterion.

Future work on such a criterion should also take into account the nature of image noise, since when an image is processed by filters such as Metz, the characteristics of image noise change from statistically random fluctuation to variations which show a spatial correlation[1].

In addition to this, it would of course be necessary to repeat all the measurements for other radioisotopes and imaging conditions as required. The Siemens' star phantom could be used for other cases where the point spread function is spherically symmetric, but for example with ^{13}N (as used in the study of infants' lungs) some other phantom would have to be used if accurate and meaningful measurements are to be made.

Much more work is also required in testing the filters and the criteria for applying them in clinical studies. Tests would have to be carried out on many more cases so that then in at least some of these cases verification could be obtained at surgery or post mortem. It would also be necessary to choose the cases carefully in order to avoid pitfalls such as that encountered in many of the ^{99m}Tc bone studies where the order of Metz filter was limited by edge

effects before the effects of noise became severe.

It would of course also be interesting to study the effects of Metz filtering on images produced by different systems, in particular by the newer type of gamma camera which has much higher resolution. Unprocessed images produced by these gamma cameras are therefore much less blurred, and due to better detection efficiency the signal-to-noise ratio in the image is generally higher, but the point spread function does have a finite width, and image processing should be able to improve the images here too.

(v) Conclusion

Thus a system was set up to calculate Metz filters from measured point spread functions, and apply them to images obtained in clinical studies. Metz filters were seen to facilitate the visual interpretation of scans, and there were also indications that the quantitative information obtained from processed images may be more accurate. A criterion was devised to assist in selecting the optimum order of Metz filter to use on a given image, and testing of this criterion indicated that while it is only approximate, it does seem to be useful. However, as a result of the limited amount of clinical data collected, the complexities of any clinical test situation and the difficulties of finding exact confirmation of results which are obtained, further study of the accuracy of the processed images and the reliability and the refinement of the criterion remains to be carried out.

Chapter I References

1. Metz C. E., A Mathematical Investigation of Radioisotope Scan Image Processing, Ph.D. Thesis University Microfilms, Ann Arbor, M.I., 1970, Page 54.
2. As 1 above.
3. Low F. H., Basic Considerations in Nuclear Instrumentation Chapter 3, pp. 29 - 55 in 'Instrumentation in Nuclear Medicine', Hine G. J. (Ed.), Volume 1, Academic Press Inc., 1967.
4. Pizer S. M., Digital Spatial Filtering and its Variations in 'Quantitative Organ Visualization in Nuclear Medicine', Kenny and Smith (Eds.), Coral Gables, Miami, 1971.
5. MacIntyre W. J., Christie J. H., A Comparison of Data Averaging of Radioisotope Scan Data by Photographic and Dimensional Computer Techniques in 'Medical Radioisotope Scintigraphy', Page 771, Proc. IAEA Symposium, Volume 1. Vienna, 1969.
6. Pizer, S. M., Vetter H. G., Processing Radioisotope Scans J. Nucl. Med., 150, 10, 1969.
7. Brown D. W., Kirch D. L. et al. Quantification of the Radionuclide Image, Seminars Nucl. Med., 311. 3, 1973
8. As Ref. 1 above, pp. 374 - 386.
9. Iinuma T. A., Nagai T., Image Restoration in Radioisotope Imaging Systems. Phys. Med. Biol., 501 - 509, 12, 1967.
10. As Ref. 1 above, pp. 358 - 361.
11. Nagai T., Fukuda N. et al. Computer Focusing Using an Appropriate Gaussian Function, J. Nucl. Med., 209 - 212. 10, 1969.
12. Pizer S. M., Vetter H. G., The Problem of Display in the Visualization of Radioisotope Distributions. J. Nucl. Med. 773 - 780, 7, 1966.

13. As Ref. 1 above. pp. 419 - 423.

14. IAEA Coordinated Research Programme on the Intercomparison of Computer-Assisted Scintigraphic Techniques. Progress Report in 'Medical Radioisotope Scintigraphy', Proc. IAEA Symposium, 727 - 743. Volume 1, Vienna 1972.

15. IAEA Coordinated Research Programme on the Intercomparison of Computer-Assisted Scintigraphic Techniques, Draft Report on Second Intercomparison. November 1974.

16. Kirch D. L., Brown D. W., Recent Advances in Digital Processing Static and Dynamic Scintigraphic Data, in 'Proc. 2nd Symposium on Sharing of Computer Programs and Technology in Nuclear Medicine', Oak Ridge, Tennessee. April 1972.

Chapter II References

1. Metz C. E.. A Mathematical Investigation of Radioisotope Scan Image Processing, Ph.D. Thesis, University Microfilms, Ann Arbor, M.I., 1970, pp. 374 - 386.

2. Mallard J., The Radionuclide Imaging Process and Factors Influencing the Choice of an Instrument for Brain Scanning, Prog. Nucl. Med. Vol. 1, pp. 1 - 114, Karger, Basel and University Park Press. Baltimore 1972.

3. Beck R. N., Zimmer L. T. et al. Advance in Fundamental Aspects of Imaging Systems and Techniques, in 'Medical Radioisotope Scintigraphy', Proc. IAEA Symposium, Vienna 1972.

4. Margenau H., Murphy G. M., The Mathematics of Physics and Chemistry, p. 252, 2nd Edition, Van Nostrand Co. Inc., 1967.

5. Low F. H., Basic Considerations in Nuclear Instrumentation, Chapter 3, pp. 29 - 55 in 'Instrumentation in Nuclear Medicine', Hine G. J. (Ed.), Volume 1, Academic Press Inc., 1967.

6. Pizer S. M., Digital Spatial Filtering and its Variations, in 'Quantitative Organ Visualization in Nuclear Medicine' Kenny & Smith(Eds.), Coral Gables, Miami, 1971.

7. Brown D. W., Kirch D. L. et al. Quantification of the Radionuclide Image, Seminars Nucl. Med., 311. 3, 1973.

8. As 1 above. pp. 377 - 378.

9. As 1 above, pp. 150 - 182.

Chapter III References

1. Scinticamera NE 8251 from Nuclear Enterprises.

2. Anger H. O., Radioisotope Cameras in 'Instrumentation in Nuclear Medicine'. Hine G. J. (Ed.), Volume 1, Academic Press Inc., 1967.

3. Mallard J., The Radionuclide Imaging Process and Factors Influencing the Choice of an Instrument for Brain Scanning Prog. Nucl. Med. Vol. 1. pp. 1 - 114. Karger, Basel, and University Park Press. Baltimore 1972.

4. Beck R. N.. Zimmer L. T. et al. Advance in Fundamental Aspects of Imaging Systems and Techniques. in 'Medical Radioisotope Scintigraphy'. Proc. IAEA Symposium, Vienna 1972.

5. Gottschalk A., Modulation Transfer Function Studies with the Gamma Scintillation Camera. in 'Fundamental Problems in Scanning', Gottschalk. Beck (Eds.), Chapter 27.

6. BMD07R, Nonlinear least squares pp. 387 - 396, Biomedical Computer Programs W. J. Dixon (Ed.), Univ. California Press, Berkeley, Los Angeles, London 1973.

Chapter IV References

1. Galasko C. S. B., Doyle F. H. The Response to Therapy of Skeletal Metastases from Mammary Cancer - Assessment by Scintigraphy Br. J. Surg. 85. 59, 1972.

2. Cox P. H. Abnormalities in Skeletal Uptake of $^{99}Tc^{M}$ Polyphosphate Complexes in Areas of Bone Associated with Tissues which have been Subjected to Radiation Therapy Br. J. Radiol. 851 - 6, 47, 1974.

3. Merrick M V. Review Article - Bone Scanning Br. J. Radiol. 327 - 351, 48. 1975.

4. Citrin D. L. Bessent R. G. et al Quantitative Bone Scanning. A Method for Assessing Response of Bone Metastases to Treatment Lancet 1132 - 3, 1, 1974.

Chapter V References

1. Ronchetti R., Stocks J. et al. Clinical Application of Regional Lung Function Studies in Infants and Small Children Using ^{13}N. Arch. Dis. Childhood 595 - 603, 50. 1975.
2. Godfrey S., Hambleton G. et al. Unilateral Lung Diseases Detected by Radioisotopic Scanning in Children Thought to have Asthma. Brit. J. Dis. Chest 7 - 18, 71(1). 1977.
3. Ball W. C., Stewart P. B. et al. Regional Pulmonary Function Studied with Xe^{133} J. Clin. Invest 519 - 531, 41, 1962.
4. Heckscher Th., Larsen D. A. et al. A Clinical Method for Determination of Regional Lung Function Using Intravenous Injection of Xe^{133}. Scand. J. Resp. Dis. Suppl. 31 - 39, 62, 1966.
5. Treves S., Ahnberg D. S. et al. Radionuclide Evaluation of Regional Lung Function in Children J. Nucl. Med. 582 - 587, 15, 1974.
6. Clark J. C., Buckingham P. D. Short-Lived Radioactive Gases for Clinical Use Chapter 6. Butterworth 1975.
7. Vernon P., Glass H. I. An Off-Line Digital System for Use With a Gamma Camera Phys.-Med. Biol. 405 - 415, 16, 1971.
8. West J. B. Ventilation/Blood Flow and Gas Exchange Blackwell Scientific Publications, Oxford-Edinburgh (2nd Edn.).
9. Winlove P., Freedman N. et al. The Quantitation of Regional Lung Function in Infants and Children Using Radioactive Nitrogen (^{13}N). To be published.

Chapter VI References

1. Metz C. E., Beck R. N. Quantitative Effects of Stationary Linear Image Processing on Noise and Resolution of Structure in Radionuclide Images J. Nucl. Med. 164 - 170, 15, 1974.

Acknowledgements

Firstly I must thank Dr. Harold Glass, since without his assistance, direction and encouragement this thesis would never have approached completion. In the first years that I was working on this thesis, the late Professor R. Oliver was also my supervisor, and his suggestions and advice were very helpful.

I am also grateful to many former and present members of the Medical Physics Department at Hammersmith Hospital for their useful comments, and to medical staff of the hospital, especially Dr. Simon Godfrey, with whom I was able to cooperate in the clinical applications described in this thesis.

Thanks are also due to Mrs. Heather Thomson and Mrs. Margaret Harrison for typing the manuscript.

Finally I must thank my husband, Laurence, for his patience and encouragement, and also his advice on statistical matters.